**Safety in Mines Research Advisory Committee**

**Final Report**

# Development of a method to estimate coal pillar loading

**DP Roberts, JN van der Merwe, I Canbulat**

**EJ Sellers and S Coetzer**

| | | |
|---|---|---|
| **Research Agency** | **:** | **CSIR Miningtek** |
| **Project No** | **:** | **COL 709** |
| **Date** | **:** | **September 2002** |
| **Report No** | **:** | **2001-0651** |

# Executive summary

The primary goal of this project was to determine the accuracy and validity of the Tributary Area Theory (TAT) and to provide better estimates of pillar load using numerical modelling and other tools.

Literature review highlighted that previous work concentrated on coal pillar strength formulae, and little effort went into investigation of loading environment. The few that focused on coal pillar loads mostly applied the tributary area method. Other methods that have been proposed for the determination of pillar loads included the application of beam theory, analytical methods and photo-elastic modelling. These methods have not found much application in coal pillar design. The literature review also highlighted that despite its limitations, the tributary area theory is the most widely used for determining coal pillar loads. The main limitations of the tributary area theory and the conditions under which the method is valid have been presented in the text. It has been deduced that in addition to the panel width to depth ratio, the percentage extraction and the stiffness of the surrounding strata influence the validity of the tributary area method.

An underground test was conducted to assess the magnitude of changes in pillar stress. Various stress measurement devices were installed in test pillars just prior to mining. The stress changes were monitored and compared with numerical modelling results. It was found that stresses increased by between 0.3 MPa and 0.5 MPa and that the stresses stabilised after the final splits were cut. The numerical modelling codes using different codes showed similar trends, with an increase of between 0.5 MPa and 1 MPa.

Numerical modelling was employed to determine the influence of mining parameters on pillar loads. The overburden stiffness and seam stiffness were varied using the LAMODEL boundary element code. It was found that pillar loads decreased with increasing overburden stiffness. It was observed that abutment loads increase as pillar loads decrease. The greatest deviations from TAT were observed at large depths, high extraction and low overburden stiffness. However, it was noted that, for typical mining parameters, the deviation from TAT was less than one per cent. This indicates that such a code is better suited to modelling irregular geometries, as the pillar loads are so close to TAT. The application of LAMODEL to irregular geometries was investigated. It was revealed that under-sizing of pillars may lead to a decrease of stress on that pillar and an increase on surrounding pillars, depending on the position of the pillar within the panel.

Finite element models were generated to assess the representivity of the LAMODEL boundary element code, which assumes no friction on stratigraphic parting. Friction was introduced in the overburden contacts in the Finite Element (FE) models, which resulted in APS's up to 21 per cent lower than estimated using LAMODEL, for a 50 per cent extraction. It was noted that contact conditions, both along seam contacts and into the roof, can greatly influence pillar loads and the confinement within the pillar.

A formula for calculating pillar load was determined through a numerical modelling procedure. The formula contains overburden stiffness and the panel width-to-depth ratio as parameters.

In light of the observed over-estimation of pillar loads using TAT, the implications for the Salamon safety factor formula were examined. Analysis of the roof showed that failure of the immediate roof beam occurred in nearly all failed cases in the database. The resulting discontinuous beam results in full load distribution to individual pillars, exactly the conditions required by tributary area theory. This implies that pillar load estimations were accurate and that the safety factor formula, as it stands, is valid.

# Acknowledgements

The authors gratefully acknowledge funding from SIMRAC. The staff of the Gloria Section of Koornfontein Mine has been extremely helpful. Mr Lazar rescheduled production sequence in order to accommodate the instrumentation. The staff of Wilmansrust shaft including Mr de Vlies, Mr Du Preez, Mr van der Colff, have accommodated us with provision of services and the interruption of their production. Numerous mine staff members assisted with transport, provision of electricity and water. Special mention must be made of the AMCO drivers and shaft operators who worked overtime in order for us to complete the project. Thanks are also due to the Rock Engineering staff, particularly Mr Dave Neal and Mr Johann van Wyk who facilitated the project and assisted with site selection. Their interest in the project was a great driving force for the successful installation.

# Table of Contents

# List of Figures

# List of Tables

# List of contracted Enabling Outputs

# 1.0 Introduction

The so-called “Tributary Area Theory’ is commonly used in South Africa to calculate pillar loads in the safety factor calculation for coal pillars. The fundamental basis of the theory is that each pillar is assumed to bear the full load of the overburden strata directly above the pillar and half of the surrounding roadway. The current criterion for applicability of the theory is that it is assumed to be valid for situations where the panel width to depth ratio exceeds unity.

Recent studies into the pillar loading environment showed that the panel width to depth ratio is not the only parameter that influences pillar loading. The percentage extraction and the stiffness of the overburden may also play a role in determining the load acting on pillars. The significance of the influence of the percentage extraction is that the real load on the pillars inside the panel is less than assumed. This is compensated for by an increased but unknown real load on the inter panel pillars. At increased depth of mining, this effect could lead to the destruction of inter panel pillars directly or by roof or foundation failure. This may in turn result in dynamic loading of the pillars inside the panel. Therefore, while the application of the theory is conservative from the point of view of the evaluation of stability of pillars inside the panel, it results in an over optimistic view of the load on the inter panel pillars.

Another implication of this effect is that the current method of calculating pillar strength may be incorrect. The method was derived empirically, using the tributary area theory to calculate the loads on the pillars that had failed. Using the tributary area theory results in the maximum load that a pillar inside a panel is assumed to bear. The derived pillar strengths depend on the calculation of the pillar loads — therefore, if those calculations predicted greater loads than the actual loads acting on the pillars, the derived pillar strengths will also be greater than the real strengths.

If the tributary area theory is used consistently in all calculations of safety factors, this argument is not important because the lower real strength of the pillars is compensated for by the lower real loads acting on the pillars and the ratio between the two (which is the safety factor) remains the same. There are thus compensating “errors” in the calculation procedure.

However, a problem arises at increased depth or reduced panel widths where computer methods may be used to calculate pillar loads. If these numerically estimated loads are used in conjunction with the over-estimated strength formula, an optimistic value of the safety factor will be the result, which in turn implies that the probability of failure will be greater than that calculated.

This investigation entailed the development of a method to estimate loads using numerical modelling techniques and an effort to verify the predicted pillar loads by underground measurement. The results of the numerical model loads are discussed against the background of the implications for the pillar strengths that were determined using empirical methods. A number of available numerical methods are discussed and compared.

# 2.0 Literature review

## 2.1 Introduction

Two of the most important parameters in coal pillar design are the coal pillar strength and the pillar load. The ratio of the pillar strength to the pillar load gives the safety factor. During the second half of the last century more time and effort was spent on developing appropriate formulae for the determination of coal pillar strength than on determining the loads acting on pillars. The pillar load is actually determined by using the tributary area theory, which is known to have several limitations.

Given that pillar load is as important as the pillar strength, it is expected that comparable expenditure and effort would have been made in developing accurate methods of calculating pillar load. The purpose of this literature review was to identify the various methods that are used for determining pillar load and their respective limitations. The insight gained would guide subsequent attempts to develop an accurate method to estimate coal pillar load in areas where the tributary area theory is inappropriate.

## 2.2 Determination of the load on panel pillars

The determination of the load imposed on a coal pillar is important for safety factor calculation purposes. For a given seam height and required factor of safety, a knowledge of the prevailing pillar load will enable appropriate pillar widths to be determined which in turn will optimise percentage extraction. Surprisingly, the body of work done to develop accurate methods of determining coal pillar loads is somewhat limited. After a thorough review of many coal research reports, it was found that efforts made to determine coal pillar loads included the application of analytical and numerical methods, the Tributary Area method, beam deflection, and photo-elastic analyses. Each of these approaches is briefly discussed in the following subsections.

### 2.2.1 Analytical method

According to Salamon and Oravecz (1976) there is no simple method of estimating the load acting on individual panel pillars. The difficulties arise from the fact that individual pillar loads depend on the deformation characteristics of both the surrounding strata and the pillars themselves.

Salamon and Oravecz (1976) used a mechanical model of an elastic beam with three supports, the ends being rigid and an elastic spring acting at the centre. The centre support provides resistance only if the spring is compressed. By using several springs the mechanical model could be used to simulate a bord-and-pillar configuration, where the beam represents rock strata and the springs correspond to the pillars. In order to estimate pillar load, it is necessary to determine the deformation characteristics of both the roof strata and the pillar. The development of an electric analogue permitted the determination of pillar load in the general situation, by means of electric resistance (Salamon and Oravecz, 1976).

The electrical analogue model was used to produce diagrams of maximum loads in a panel of pillars, as a function of extraction ratio and overburden load, Figure 2–1. Commonly used geometries were represented. According to Salamon and Oravecz, Figure 2–1 gives a reliable estimate of pillar load, but only if the mining depth does not greatly exceed panel width.

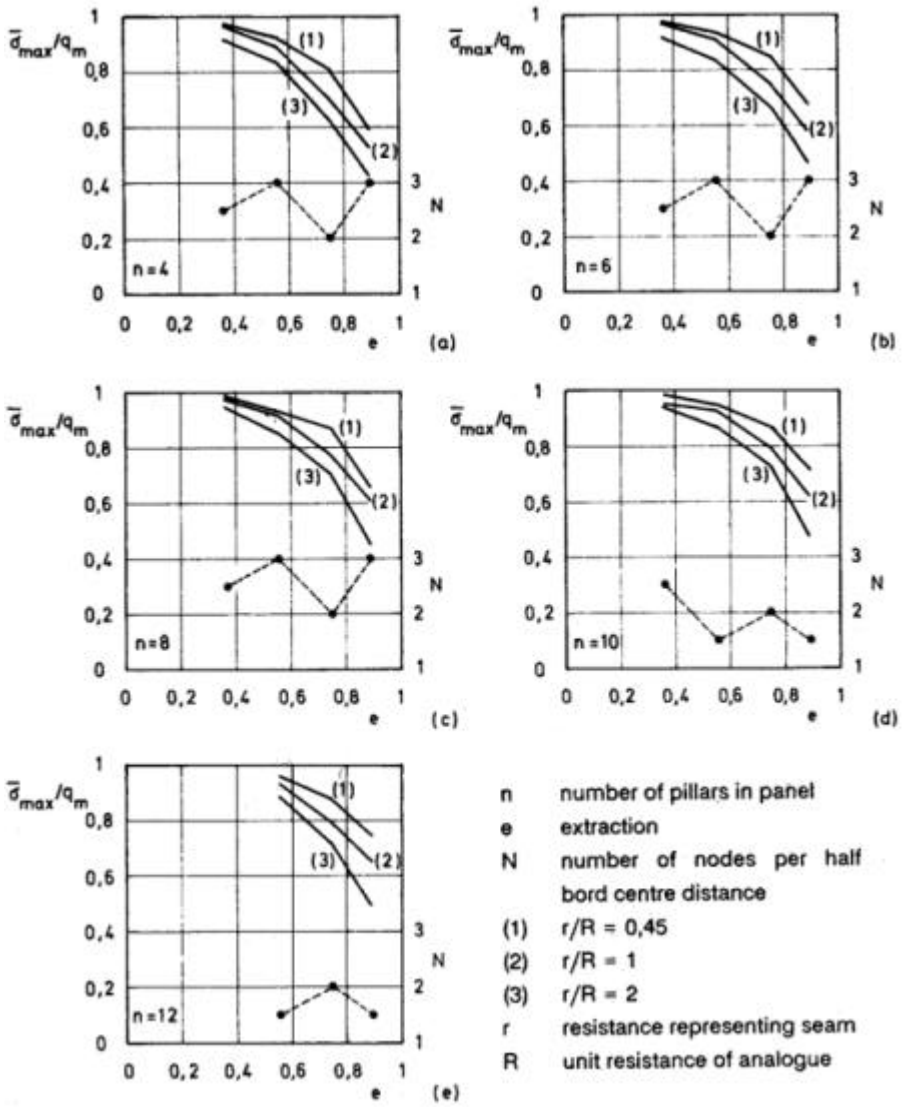


***Figure 2–1 Maximum pillar load in a panel of pillars calculated using electrical analogue (After Salamon and Oravecz, 1976) where e is extraction ratio and $\bar{s}/q_m$ is maximum pillar load relative to the modified cover load.***

## 2.2.2 Tributary Area Theory

For a simple layout with a reasonably uniform pattern of pillars and a panel width at least as large as the depth, the average pillar load can be estimated by using the tributary area theory.

The theory assumes that each pillar carries a proportionate share of the full overburden load. Figure 2–2 illustrates a simplified layout for tributary area analysis of rectangular shaped pillars in uniaxial loading. Assuming H is the depth to the seam floor, B is bord width, $w_1$ and $w_2$ are pillar dimensions, and $C_1$ and $C_2$ are pillar-centre distances, then for a regular pillar layout the pillar load (L) can be estimated as:

$$L = \frac{0.025HC_1C_2}{w_1w_2} \tag{2-1}$$

For square shaped pillars, the above Equation simplifies to:

$$L = \frac{0.025HC^2}{w^2} \tag{2-2}$$

$$C = w + B \tag{2-3}$$

The above equations indicate that the factors influencing pillar load are:

- depth – the deeper the mining, the higher the load,
- pillar width – the smaller the pillar, the higher the load,
- bord width – the wider the bord, the higher the load, and
- extraction ratio. A function of the relative sizes of the bords and pillars. The higher the extraction, the higher the pillar load.

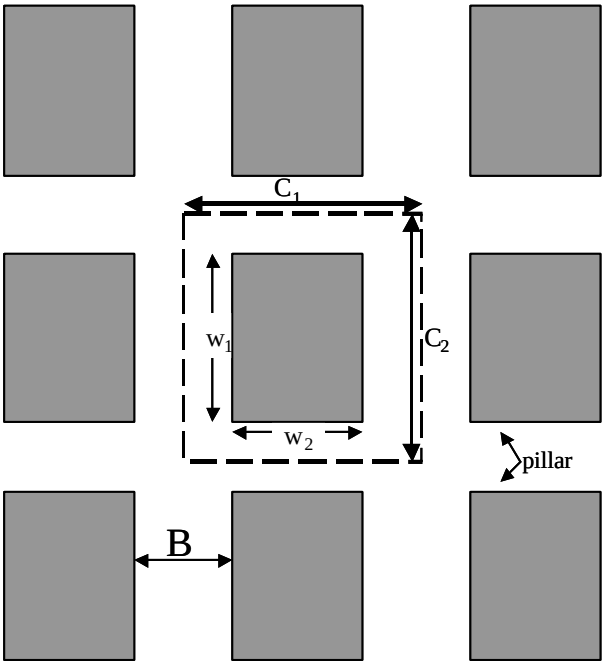


***Figure 2–2 Geometry for tributary area analysis of pillars in uniaxial loading***

Brady and Brown (1993) explain that in mining a mineral deposit of uniform thickness, a quantity of practical interest is the area extraction ratio (e), which can be calculated by:

$$e = \frac{B}{w + B} \tag{2-4}$$

The extraction ratio is related to the pillar load as follows:

$$s = \frac{0.025H}{1 - e} \tag{2-5}$$

By substituting the vertical normal component of the pre-mining stress field, $P_{zz}$ for 0.025H, Equation (2-5) can be written as:

$$\frac{s_p}{P_{zz}} = \frac{1}{1 - e} \tag{2-6}$$

Where the ratio $s_p/p_{zz}$ is a pillar stress concentration factor. Equation (2-6) can be represented graphically as shown in Figure 2–3.

It can be observed from Figure 2–3 that above an extraction ratio of about 0.75, the stress concentration factor increases rapidly. For example, a slight increase in extraction ratio, say from 0.9 to 0.91, changes the pillar stress concentration factor from 10 to 11.11. In areas where in-panel pillars alone are used to support the workings, the percentage extraction that can be achieved in practice is therefore limited.

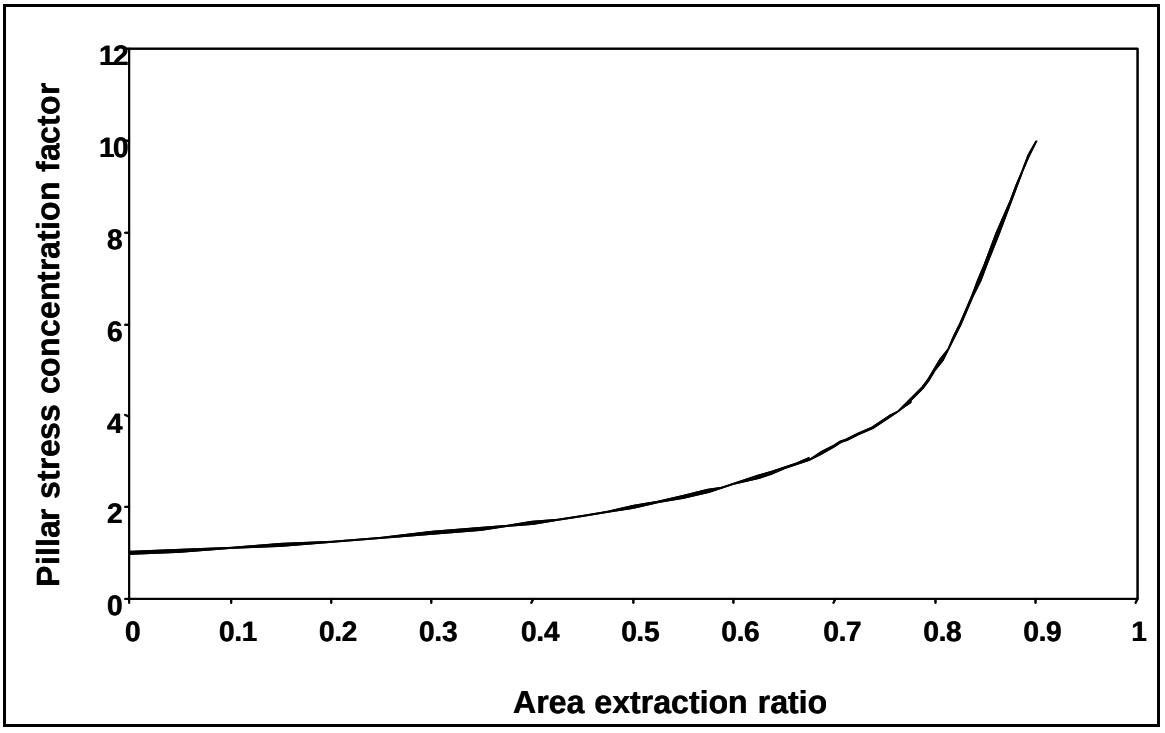


***Figure 2–3 Variation of pillar stress concentration factor with area extraction ratio***

### 2.2.3 Limitations of the tributary area theory

While the tributary area theory provides a simple method of determining the average state of axial stress in a pillar, it has implicit limitations which must be borne in mind. Average pillar stress is calculated by assuming that pillars uniformly support the entire load overlying both the pillars and the mined-out areas. Tributary area theory assumes regular geometry and ignores the presence of abutments. The effects of deformation and failure in the roof strata resulting from the mining operation are disregarded.

According to Jeremic (1985) the evaluation of average pillar stresses of flat or gently dipping coal seams by the tributary area theory is over-simplified. The concept does not take into account abutment stress distributions and deformation or failure of the pillar. Also, if there is displacement interaction between the surrounding strata and the pillar itself, stress may be redistributed within the system, resulting in a stress state considerably different to the theoretical state.

Brady and Brown (1993) argue that the average pillar stress is purely a convenient quantity representing the state of loading of a pillar in a direction parallel to the principal direction of confinement. It is not simply or readily related to the state of stress in a pillar that could be determined by a complete analysis of stress.

Brady and Brown are also of the view that the tributary area analysis restricts attention to the pre-mining normal stress component directed parallel to the principal axis of the pillar support system. They argue that the implicit assumption that the other components of the pre-mining stress field have no effect on pillar performance is not generally tenable. Furthermore Brady and Brown highlight the fact that the tributary area theory ignores the effect of the location of the pillar within a mine panel.

It has also been mentioned by Van der Merwe (1998) that the tributary area theory is only valid for cases where the width of the panel is as great as or greater than the depth and where the pillars in a panel are of the same size. Other factors that have been found by Van der Merwe to influence the validity of the tributary area theory include the percentage extraction and the stiffness of the overburden.

For practical design purposes however, the suggested equations for average stress calculations are acceptable if the designer appreciates the limitations.

### 2.2.4 Beam deflection

Sheory and Singh (1974) suggested the concept of beam deflection for the estimation of average pillar stress. The method is primarily for narrow workings, where loads are transferred on to pillars due to deflections of the overburden strata. Jeremic (1985) explained that under these circumstances the rock beam deflections are a function of the flexural rigidity of the strata and the compressibility of pillars.

The approach for calculation of coal pillar loads is based on the theory of thick beams on elastic support. A thick beam is considered to be one where thickness is greater than five times the distance between the supports (roof span). The evaluation of average pillar stress is convenient for narrow workings or mining configurations where the tributary area concept does not apply.

### 2.2.5 Numerical analysis

Recent work by van der Merwe has also shown that the panel width to depth ratio is not the only parameter that influences the validity of the tributary area theory; that in fact the percentage extraction and the stiffness of the overburden each play a role. The significance of the influence of the percentage extraction is that the real load on the pillars inside the panel is less than assumed at relatively high extraction ratios. This is however compensated for by an increased but unknown real load on the inter panel pillars. His preliminary work suggests that the effect of the increased load on the inter panel pillars is significant, and could result in overloading of the inter panel pillars. At increased depth of mining, this effect could lead to the destruction of the inter panel pillars either by direct failure or roof or foundation failure. This may in turn result in dynamic loading of the pillars inside the panels.

Van der Merwe therefore concludes that while the application of the tributary area theory is conservative from the point of view of the evaluation of the stability of pillars inside the panel, it results in an over optimistic view of the load on the inter panel pillars.

### 2.2.6 Internal stress distributions in panel pillars

Jeremic (1985) reported that the internal stress distribution of a single pillar in the mining of relatively flat and shallow coal seams has been a matter of consideration for many European investigators. Internal stresses within a pillar can be analysed by using two or three-dimensional photo-elastic modelling.

The two-dimensional analysis is carried out on optically sensitive plates usually of the size 250 x 250 x 20 mm and tested for loading conditions, which corresponded to the mining

conditions. Various aspects of interaction between room-and-pillar structures have been investigated. Jeremic (1985) reported some of the earlier results obtained from two-dimensional analyses as follows:

a) For the case where the pillar width is twice the pillar height, it was found that the vertical stress is more than double the horizontal stress (under gravity loading only), Figure 2–4. It was also noted that there is a difference in the distribution of the vertical and horizontal stresses. For example, the horizontal stress is greatest at the contact between pillar and roof and floor strata. Maximum vertical stress concentration tends to be at the corners of the pillar.

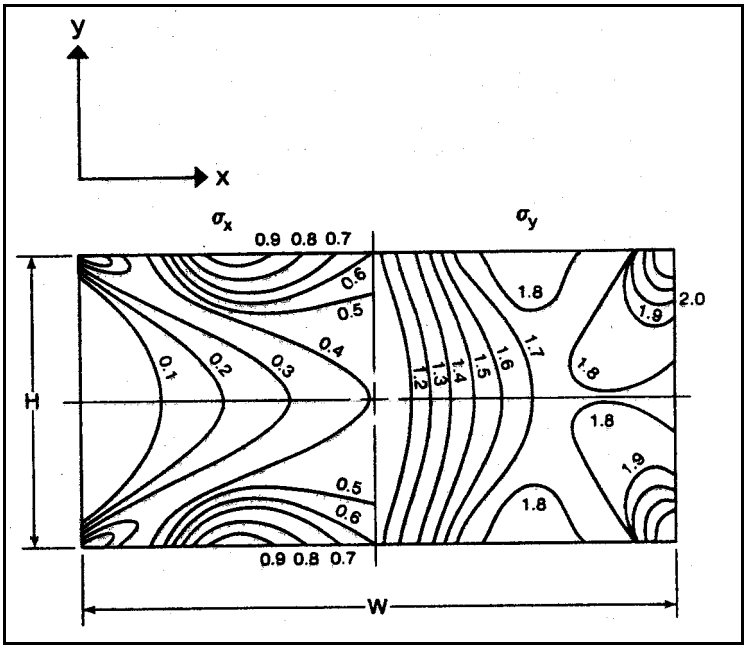


***Figure 2–4 Vertical and horizontal stress distribution in the mine pillar model, w/h=2 (After Jeremic, 1985)***

b) It was also found that the stress concentration over the plane cutting the pillars at mid height varies with width to height ratio as follows:

w/h < 1 high pillar stress ($\cong 3\rho H$)
w/h = 1 – 2 rapid decrease of pillar stresses ($\cong 2\rho H$)
w/h > 2 the pillar stresses became constant ($\cong 1.2\rho H$)

where $\rho H$ = overburden pressure, $\rho$ = unit weight of rock and H is the overburden height

c) In addition, it was found that the stress concentration at the base of the pillar also varies with pillar width to height ratio as given below:

w/h < 2 gradual increase of stress (> 1.0ρH)

w/h > 2 pillar stress became constant (0.5ρH)

d) Of particular interest from the research were studies of stress concentration in pillar corners for different loading conditions. The high stress concentration in the corners of the pillars was found to a function of the radius of curvature. For example, where curvature is zero, stress concentration is unlimited. It is a well-known fact that the corners of the rooms are the most critical part of a pillar-stope structure, where instability increases with increasing room width and pillar height.

Jeremic (1985) mentioned that the two-dimensional photo elastic stress analysis have had greater success in the control of mine stability in metal mines than in coal mining, because the properties and behaviour of the hard rock structure are closer to model test conditions of linear elasticity. Jeremic however, suggested photo-elastic model investigations should be considered a useful tool for investigation of internal stress distribution in pillar-stope structures, particularly in the case where a room-and-pillar mining method is used to exploit horizontal or gently dipping deposits.

## 2.3 Summary and conclusions

Various reports on coal pillar design were identified and reviewed. Most of these reports concentrated on coal pillar strength formulae. The few that focused on coal pillar loads mostly applied the tributary area method. Other methods that have been proposed for the determination of pillar loads included the application of beam theory, analytical methods and photo-elastic modelling. These methods have not found much application in coal pillar design.

Despite its limitations, the tributary area theory is the most widely used for determining coal pillar loads. The main limitations of the tributary area theory and the conditions under which the method is valid have been presented in the text. It has been deduced that in addition to the panel width to depth ratio, the percentage extraction and the stiffness of the surrounding strata influence the validity of the tributary area method.

It is therefore essential that any attempts of developing a suitable method for determining coal pillar load must take cognisance of the limitations of the tributary area theory and incorporate the percentage extraction and the stiffness of the surrounding strata.

# 3.0 Expression for pillar load as function of width to depth ratio, stiffness and percentage extraction

A series of simulations of bord and pillar workings were performed using a pseudo three-dimensional boundary element code, MINLAY. Due to the subsequent unavailability of MINLAY, the results were compared with the similar LAMODEL code. The results were found to correlate well. In successive simulations the percentage extraction (e), overburden Modulus of Elasticity ($E_o$) and the panel width to mining depth ratio (W/H) were varied. The Modulus of Elasticity of the coal was kept constant at 4 GPa, which appears to be an acceptable value in the literature. It was remarked by Wagner (1980) that the modulus appears to be the only real constant of coal, as it is not influenced by size or shape.

Each of the simulations consisted of a single bord and pillar panel with length equal to four times the width of the panel, in the centre of an unmined block. The widths of the unmined coal on either side of the panel was equal to the width of the panel to ensure that results would not be affected by edge effects of the model.

The ranges of variables that were investigated were as follows:

W/H: 0.25 to 4.0
$E_o$: 1.5 GPa and 15 GPa
e: 0.19 to 0.91.

The average pillar load on a pillar in the centre of the panel was determined from the model results and the ratio of the model stress to the stress calculated by the tributary area theory was calculated. This ratio was called the Load Ratio ($R_L$). Therefore, a $R_L$ of less than unity would indicate that the model load was less that the load calculated by tributary area theory and vice versa.

It was found that the $R_L$ only started leveling out at a W/H ratio of greater that 2.0, but that varying the W/H ratio between 0.25 and 4.0 only resulted in a maximum 6.0 per cent difference in $R_L$ for a very soft overburden of 1.5 GPa and percentage extraction of 50 per cent, see Figure 3–1. While it thus appears that the commonly applied criterion that the W/H must be greater than unity to apply the tributary area theory is not strictly valid, however, it is compensated for by the fact that the error is small, only 4.5 per cent as W/H changed from 1.0 to 2.0, but increases to 15 per cent at an extraction ratio of 91 per cent, Figure 3–2

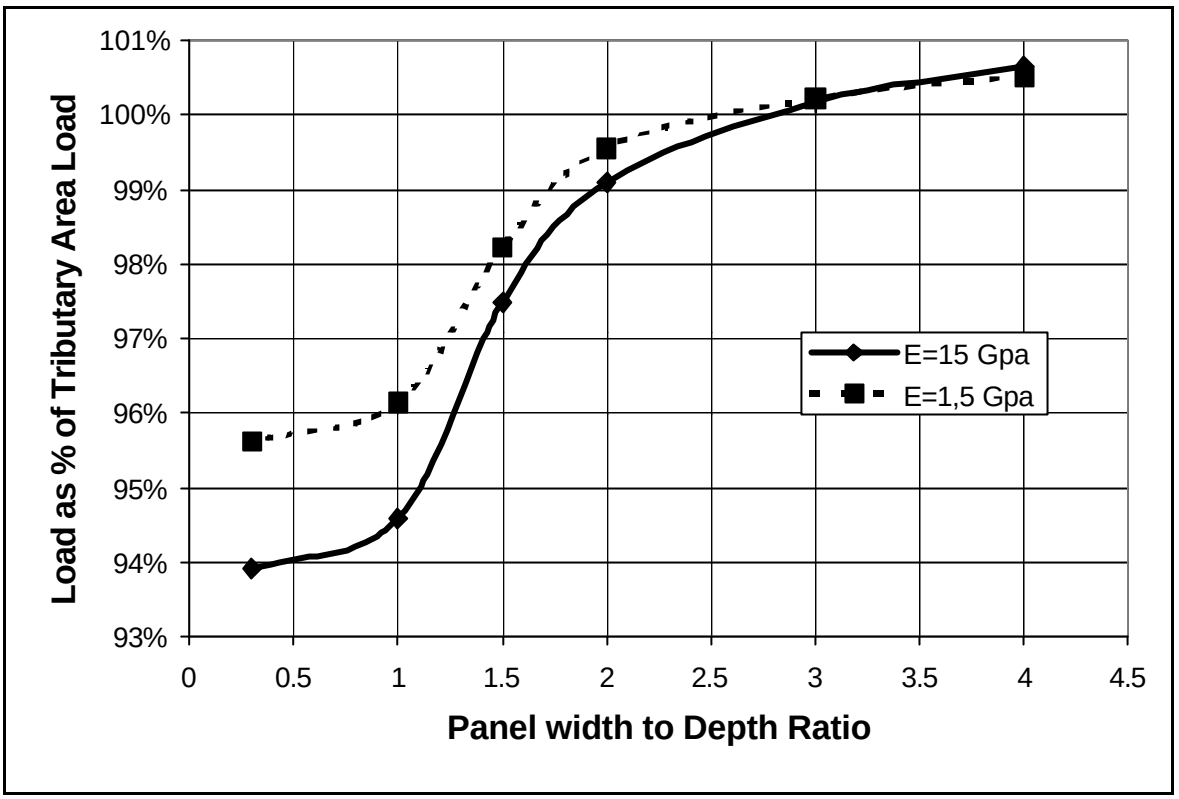


***Figure 3–1 Variation of $R_L$ with W/H for different overburden moduli, 50% extraction***

The influences of all the investigated variables are demonstrated in Figure 3–2, which summarises the effects of W/H, overburden Modulus and percentage extraction on the $R_L$.

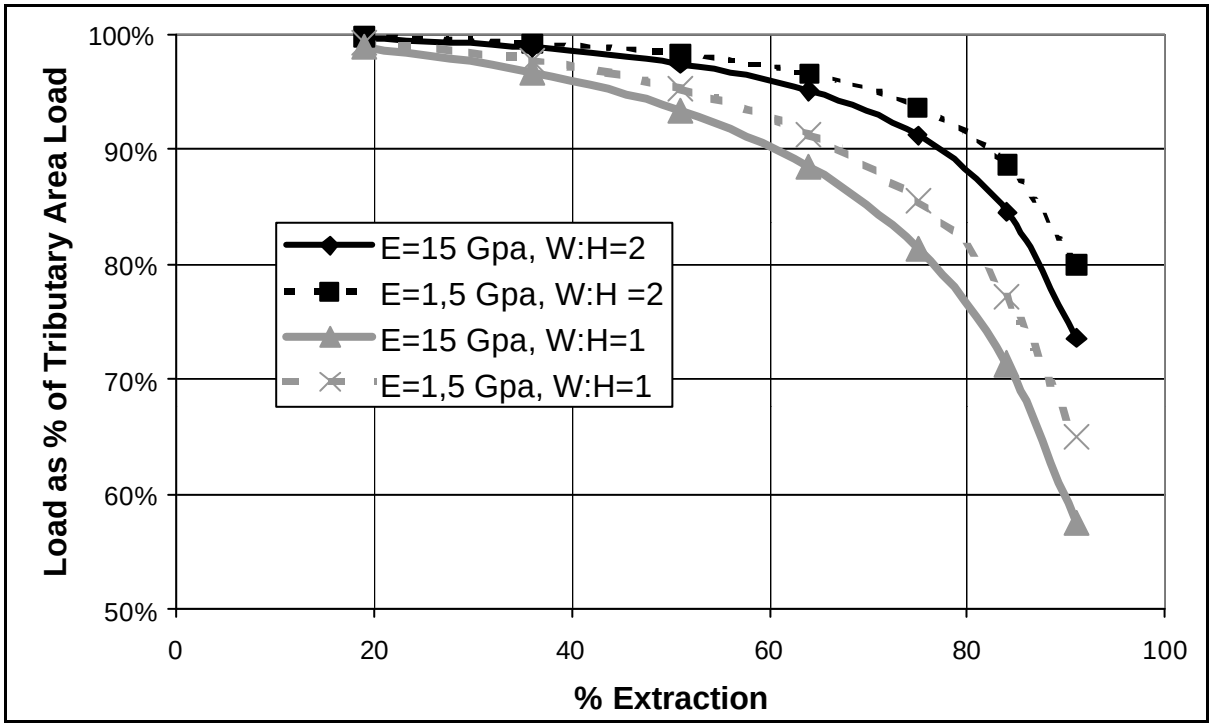


***Figure 3–2 The ratio of model load to tributary area load for different W/H ratio's and overburden moduli as a function of percentage extraction.***

In the interests of clarity, the figure does not show all the results. However, the following trends can be seen:

- For a tenfold difference in overburden modulus, the $R_L$ only differs by a few percentage points;
- Doubling the W/H ratio does not have the same relative effect on the $R_L$, and
- Increasing the percentage extraction has the greatest effect on $R_L$ and the effects of the other variables are more pronounced with increasing Percentage Extraction.

The following expression was then found that describes the influence of the variables on $R_L$:

$$R_L = 0{,}99\left(1 - e^{a}\right)^{b}$$

where

$$a = 2{,}2 + 1{,}4\,W/H$$

and

$$b = \frac{0{,}667}{1 + W/H} + 0{,}0067(E_o - 1{,}5)$$

In order to determine the relative influence of the variables on $R_L$, a sensitivity analysis was done. The results are shown in Figure 3–3.

The following can be concluded from the Figure:

- The $R_L$ is relatively insensitive to the overburden modulus;
- The W/H only has a meaningful effect on $R_L$ at values less than 1.25 (0.5 times 2.5)
- The greatest influence on $R_L$ is from the percentage extraction, *e*. As e exceeds 50 per cent, the reduction in $R_L$ is progressively greater.

Overall, it can be concluded that the tributary area theory is less valid at W/H less that 1.25 and especially for extraction ratio's greater than 65 per cent. Beyond those limits, the "error" is greater than 5.0 per cent. At extraction ratios exceeding 75%, the "error" for higher extraction ratios is greater than 10 per cent and it increases rapidly.

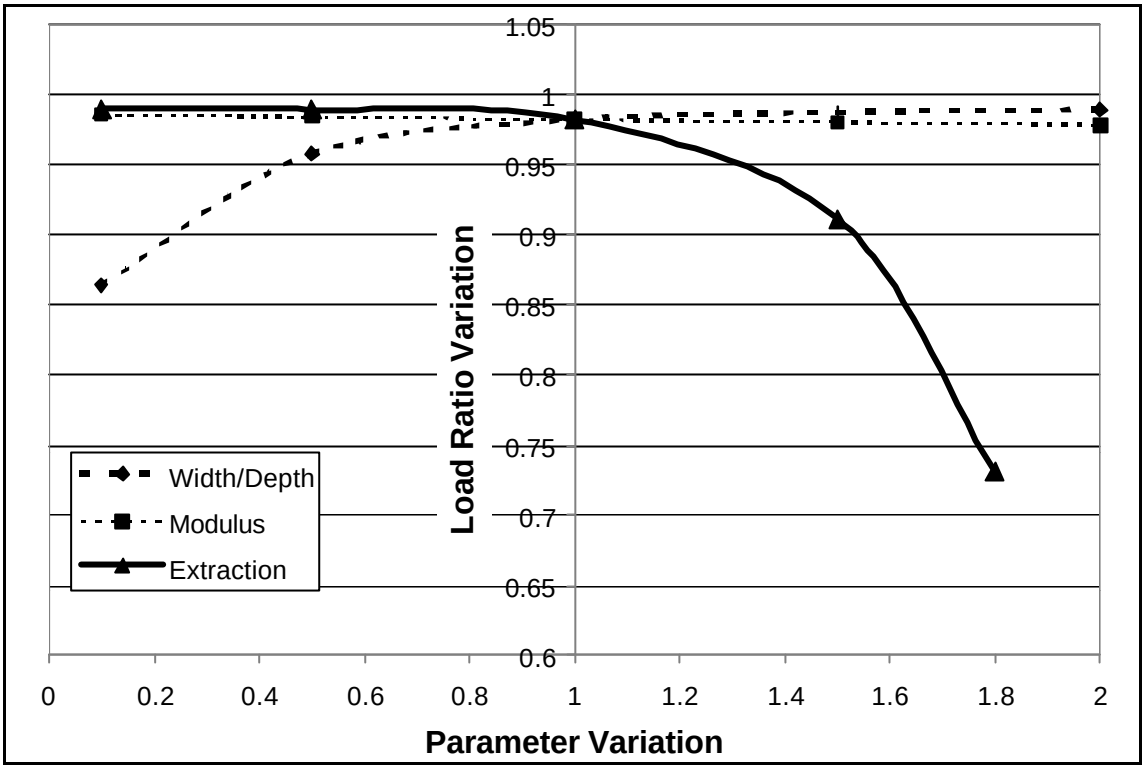


***Figure 3–3 Sensitivity analysis showing the effects of W/H, overburden modulus and percentage extraction on the load ratio. The bases were chosen as follows: e = 50%, $E_o$=30 GPa and W/H = 2.5.***

# 4.0 Underground stress measurements

## 4.1 Objectives

The aim of the underground instrumentation work was to determine the change of stress on a coal pillar as the mining progressed. A site was selected on Gloria section of Koornfontein Coal Mine. The mine offered to stop mining the active face in order that the instrumentation could be installed. The instrumentation could then be monitored once the mining moved past the instrumented pillars.

## 4.2 Description of underground site

The site selected was in Section 9 at the Wilmansrust shaft of Gloria shaft on Koornfontein mine. Bord and pillar mining is carried out in this section and the mine layout is shown in Figure 4–1. A chequerboard mine layout was initially considered due to the potential for considerable stress increase on the retreat mining sequence. This site was however not used due to problems with scheduling production and instrumentation installation within the time assigned for the research project. Therefore, a primary production section was chosen for the experiment.

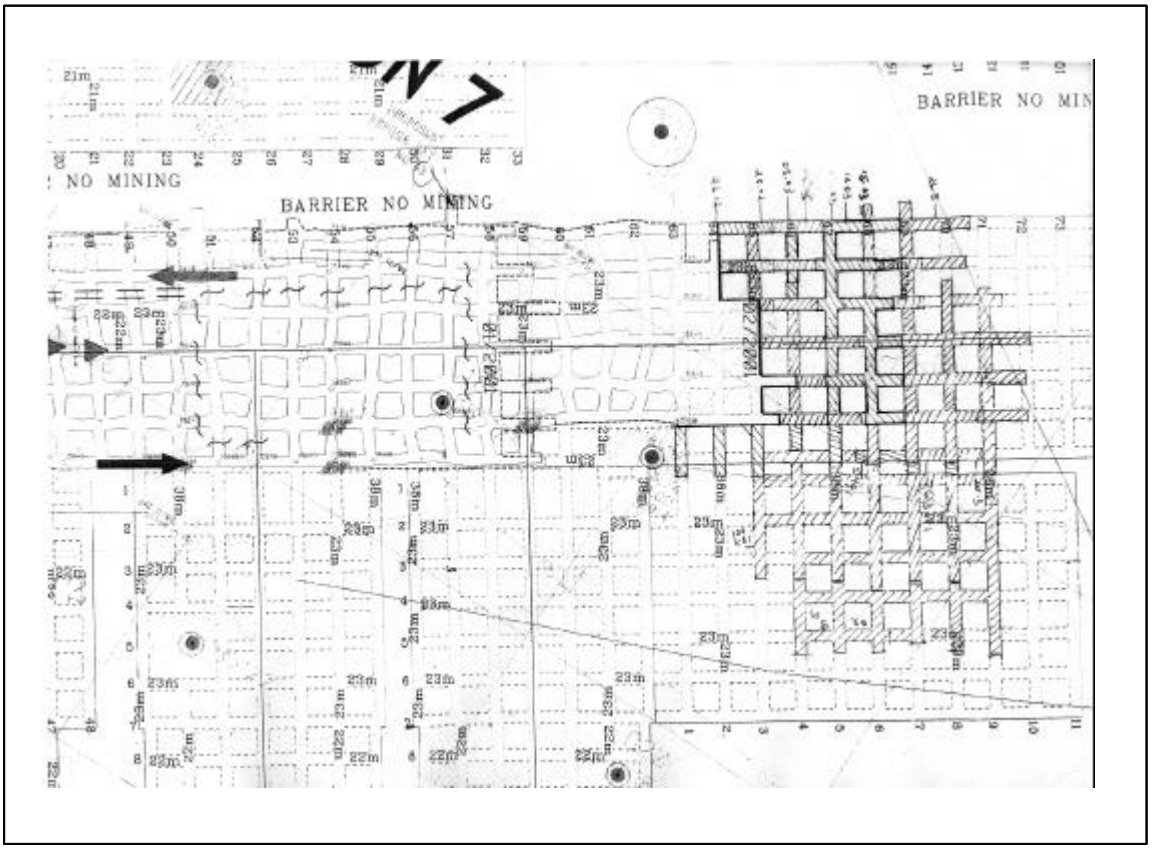


***Figure 4–1 Plan of site***

Geological logs from boreholes in the vicinity of the site were studied to make certain that there were no dolerite sills overlying the site. The borehole logs supplied by the mine indicate that the site is on the No. 2 Seam at a depth of 105 m. The roof is a laminated, carbonaceous shale. Above the shale layer, the roof consists of a number of layers of mudstone, shale, sandstone and coal. The seam is underlain by a narrow layer of gritty sandstone, below which are further layers of sandstone, gravels and mudstones.

## 4.3 Instrumentation design and installation

### 4.3.1 Planning and installation of instrumentation

The measurement of stress changes in coal pillars has been previously performed using uniaxial vibrating wire stress meters for a rib pillar extraction sequence (Wardle and Mc Nabb, 1985). Stress changes of up to 10 MPa were measured. Solid inclusion cells gauges were used in 38mm boreholes. They noted a number of sources of error in using such gauges. These include the difference between individual gauges resulting from the manufacturing process, the amount of preload stress applied by the gauge, and the possibility of crushing of the coal around the gauge. Rigid stressmeter cells can also induce tension at the borehole wall in soft rocks causing measurement errors (Mills, 1997).

A single stress meter does not provide a uniaxial stress change measurement as the gauge is affected by the complete 2D stress state. Wardle and Mc Nabb (1985) however noted that the horizontal component produced only a small effect on the vertical stresses and considered that the uniaxial stresses measured were equal to the vertical stress changes. Dunnicliff (1993) noted that early studies suggested that the vibrating wire stress cells were not suited for rock with a stiffness of less than 20 GPa, but that later studies found that it is possible to use these gauges in less stiff rocks. Vibrating wire gauges grouted into boreholes were used to measure small stress changes. Grouting of vibrating wire gauges into the borehole produced a solid inclusion cell with a modulus that has a very similar stiffness to the rock stiffness. This method is more economical and removes the problems of debonding of the hard inclusion or crushing of the rock near the cell.

Borehole pressure cells (e.g. Glotzl cells) have also been used to measure stresses. Strain gauge overcoring methods have been used to measure absolute stresses in coal mines (e.g van Heerden, 1969, Mills, 1997). CSIRO cells used for long term monitoring should be installed at least 1 month prior to the commencement of the monitoring period to allow for stabilization of the glue (Dunnicliff, 1993). Long term measurements may be affected by creep of the glue. The

USBM borehole deformation gauge can also be used to measure stresses in coal, however this is not recommended for measuring stress changes (Dunnicliff, 1993) due to unstable instrumentation readings, the possibility of movement and the effects of moisture ingress. CSIRO Yoke gauges were developed specifically for stress change monitoring and to measure the change of borehole diameter. The gauge has three semi-circular yokes that are arranged so that the ends press against the borehole sides. The yokes are strain gauged to measure the change in borehole diameter.

The instrumentation for this project was designed to have redundancy by using a number of different types of instruments, because of the number of different possibilities for stress change measurements, and the possible errors associated with each. The planned set up of instrumentation is shown in Figure 4–2. The objectives were to have;

- three different pillars in the same panel
- four types of gauges to cross check values
- a number of each type of gauge to guard against installation defects, breakages and loss of cable
- Gauges in different parts of the pillar to obtain some idea of the difference in stress change

The number of different instruments could pose a problem in determining which of the readings were correct if some produced significantly different results. This was seen as a minor problem compared to the possibility of not obtaining any information if only one pillar was instrumented with one gauge at a single site. The cost and time for the drillers to set up and drill holes and the requirement for the mine to stop production imposed a responsibility to produce results that necessitated the installation of possibly redundant gauges. The planned instrumentation scheme used vibrating wire gauges (Geokon, 2000) grouted into the rock to measure the vertical and horizontal stress changes, CSIRO cells, Glotzl borehole pressure cells and CSIRO yoke gauges (Mindata, 2001). Most of the instrument locations were selected to measure stress changes at the centre of the pillar, but some would be installed at quarter distances across the pillar.

As shown in Figure 4–2, pillar 1 was planned to have a Glotzl cell and a vertical vibrating wire gauge installed near the centre of the pillar. Pillar 2 would have a Glotzl cell and a vertical vibrating wire gauge to verify the changes measured in pillar 1, as well as a CSIRO cell. Pillar 3 would be used to determine the way that the stress change varied throughout a pillar. Vertical and horizontal vibrating wire gauges were planned for the centre of the pillar. Vertical vibrating wire gauges would be installed at opposite quarter points of the pillar. A Yoke gauge would be

installed at another quarter point. The diamond drilled holes were required to be different for various instruments. The diameter for the Glotzl cells was 146mm, the vibrating wire and yoke gauges were installed in a BX hole (60mm diameter). The CSIRO cells require an NXCU hole with an EX hole drilled 500 mm past the end of the NXCU hole. Thus, a range of drilling equipment was required and transported to site. The vibrating wire gauges and the Glotzl cell had to be grouted into place and a Conbextra grout was used for this purpose. Tests were performed on the grout in the laboratory to determine the strength and modulus.

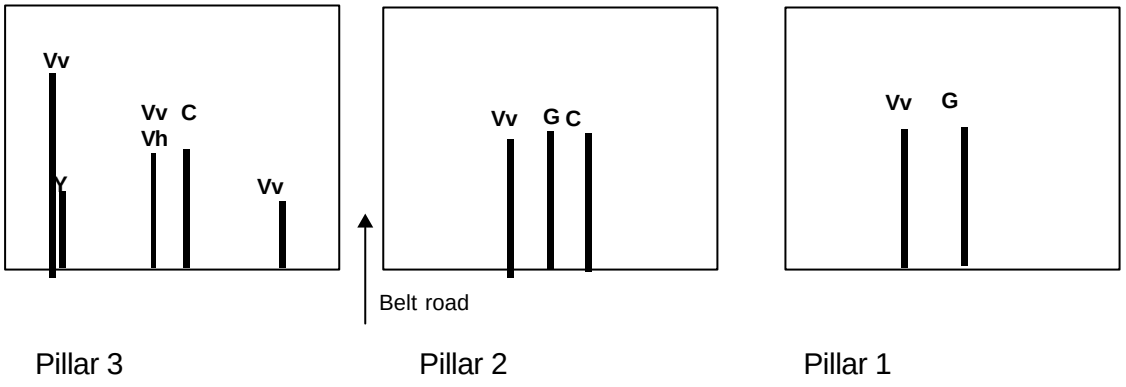


***Figure 4–2 Schematic of planned instrumentation (Vv denotes vertical vibrating wire gauge, Vh denotes horizontal vibrating wire gauge, C denotes CSIRO cell, G denotes Glotzl cell and Y denotes Yoke gauge)***

The drill team went through mine induction and safety training processes during the week from 12 February 2001 to 16 February 2001. The mine stopped production at the site on Wednesday 21 February, during night shift and drilling commenced immediately. Figure 4–3 shows the drill rig set up on site. The drilling was interrupted by a number of power and water cuts. The pay weekend on the mine meant that there were few staff at the mine and solving the water and power problems took longer than anticipated. Due to these problems, fewer holes were drilled than was planned. The mine permitted the CSIR to work over the weekend and so the instruments were installed from Friday 22 February 2001 to Sunday 25 February 2001. Fewer instruments could be installed than planned, as it was not possible to delay production any longer.

The reduction in the number of holes to be drilled meant that some vibrating wire gauges were not installed. The cages holding the vibrating wire gauges were modified underground to accommodate more gauges so that as many readings as possible could be obtained. Thus, more instruments were installed, where possible, to provide some additional redundancy. A vibrating wire cage with four gauges is shown in Figure 4–4. The CSIRO cells were not installed due to the more complex drilling requirements. The yoke gauge position was moved to save time in not having to move the drilling rig again.

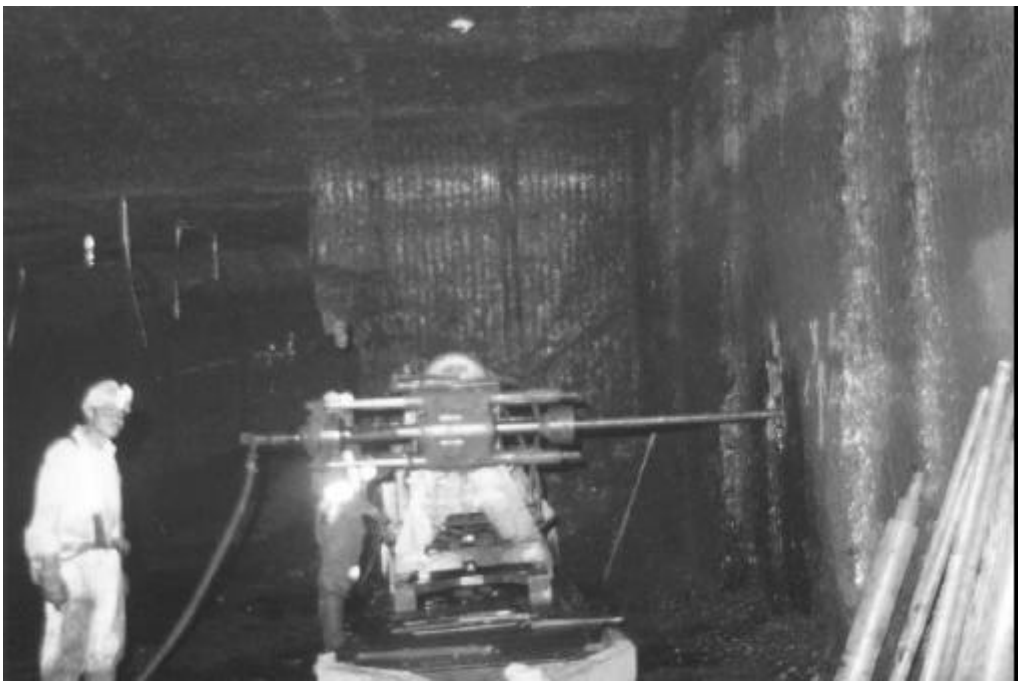

***Figure 4–3 Photograph of site with drill rig in place at pillar 3.***

The delay in installing instruments meant that the grout would not have set by the first shift on Monday. The mine kindly agreed to reschedule production again so that mining only started again on the nightshift of Tuesday 27 February. This additional time was sufficient for the grout to set.

The final instrumentation layout is shown in Figure 4–5. The instrumentation was installed in pillar 1 as planned comprising one vertical vibrating wire gauge and one Glotzl cell. The mine had to cut the roadways some distance across pillar 1 for production reasons and to allow vehicles to turn. Thus, both pillar 1 and pillar 2 would have experienced some stress increase and so the instrumentation in pillar 2 was considered to be less important than that in pillar 3, which had not been cut at all. The layout of the instruments in pillar 3 was however altered to reduce the amount of drilling. The final layout included two vertical and one horizontal vibrating wire gauge at the centre of the pillar and a cage with two vertical and two horizontal gauges placed halfway through the thickness of pillar 3, and 4m in from the planned roadway. In addition a Yoke gauge was installed 2,5 m into the pillar.

***Figure 4–4 Vibrating wire cage with four vibrating wire gauges ready to be installed and grouted into the hole.***

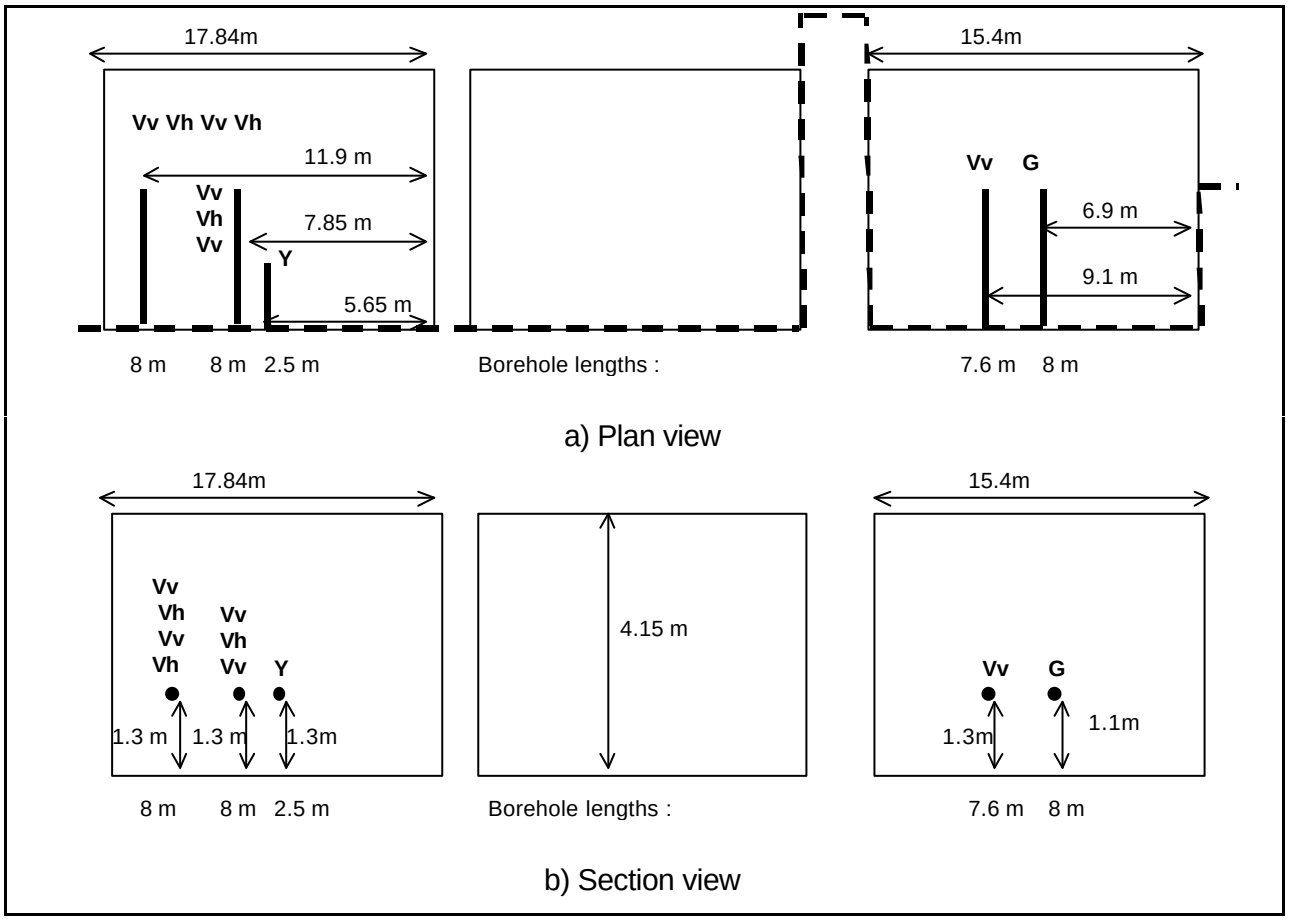


***Figure 4–5 Schematic of positions of actual instrumentation installed (not to scale) with approximate dimensions. a) plan view (dotted line indicates the face position during installation) b) section view***

## 4.3.2 Data analysis methodologies

The readings taken in the mine consisted of voltage outputs from the transducers and needed to be calibrated to determine the stress change. All transducers were calibrated using the standard procedures as recommended by the manufacturers.

A vibrating wire readout unit was used to read the vibrating wire gauges. This unit enables the reading of the change in gauge length to be read directly in microstrain (Geokon, 2000). The stress state in the direction of the gauge is assumed to be uniaxial (e.g. Wardle and McNabb, 1985) and thus, the stress change can be determined from Hook's law as:

$$\Delta \sigma = E \Delta \varepsilon \tag{4-1}$$

where $E$ is the Young's modulus of the grout and $\Delta \varepsilon$ is the strain change, read in microstrain. The stress change depends on the modulus of the grout. A special grout mix was obtained from Fosroc Conbextra that was designed to have a modulus that only slightly exceeded the modulus of the coal. The grouted borehole would act as a hard inclusion, but remain sufficiently soft to be able to deform and register the small strain changes that were expected. The modulus was expected to increase during the setting of the grout and so laboratory tests were performed to determine the grout modulus. It was found that the modulus was 2.3 GPa after 4 days as shown in Table 4–1. The elastic properties of the grout vary considerably and must therefore be sensitive to the mixture. The average modulus was found to be 4.3 and the average Poisson's ratio is 0.16.

Once the stress has been calculated in each direction, the values are reduced by a factor related to the difference between the stress in the solid inclusion and the applied external stress. This factor can be determined from the elastic solution for the stresses in a solid elastic inclusion, assuming that the inclusion remains bonded to the surrounding coal. This is expected to be the case as the modulus of the inclusion was designed to be only slightly higher than that of the coal. The coal modulus was determined in the laboratory to be 3.3 GPa on average, at a uniaxial stress of 5 MPa (see Table 4–2).

The principal stresses in the rock mass can be determined from the relationship

$$\begin{aligned} \sigma_1 &= \frac{k(x+2)+x_0}{2k(x+1)}\sigma_{10} + \frac{x_o-2-k(x-2)}{2k(x+1)}\sigma_{20} \\ \sigma_2 &= \frac{x_o-2-k(x-2)}{2k(x+1)}\sigma_{10} + \frac{k(x+2)+x_0}{2k(x+1)}\sigma_{20} \end{aligned} \tag{4-2}$$

where $\sigma_{10}$ is the major principal stress and $\sigma_{20}$ is the minor principal stress (Jaeger and Cook, 1979). For plane strain, $x = 3 - 4\nu$, where $\nu$ is the Poisson's ratio of the rock mass, $x_o = 3 - 4\nu_o$ and $\nu_o$ is the Poisson's ratio of the inclusion. The factor $k = G_o / G$ is the ratio of

the shear modulus in the inclusion to that of the surrounding rock mass. The effect of different shear modulus ratios, with equal Poisson's ratios, on the factors in Equation (4-2) can be seen in Figure 4–6. The value of k in this study is estimated to range between 1.2 and 1.7. The value of k, however, could be less than 1.0 depending on the grout mix and the stress in the coal. Considering the gauges independently, i.e. by neglecting the off-diagonal terms in (4-2), the stress can be calculated as:

$$\begin{aligned} \sigma_1 &= \frac{k(x+2)+x_0}{2k(x+1)}\sigma_{10} \\ \sigma_2 &= \frac{k(x+2)+x_0}{2k(x+1)}\sigma_{20} \end{aligned} \qquad (4\text{-}3)$$

with an error that depends on the differences in shear moduli and Poisson's ratio. For the range of shear moduli and Poisson's ratios in this study, the difference is estimated to be less than seven per cent.

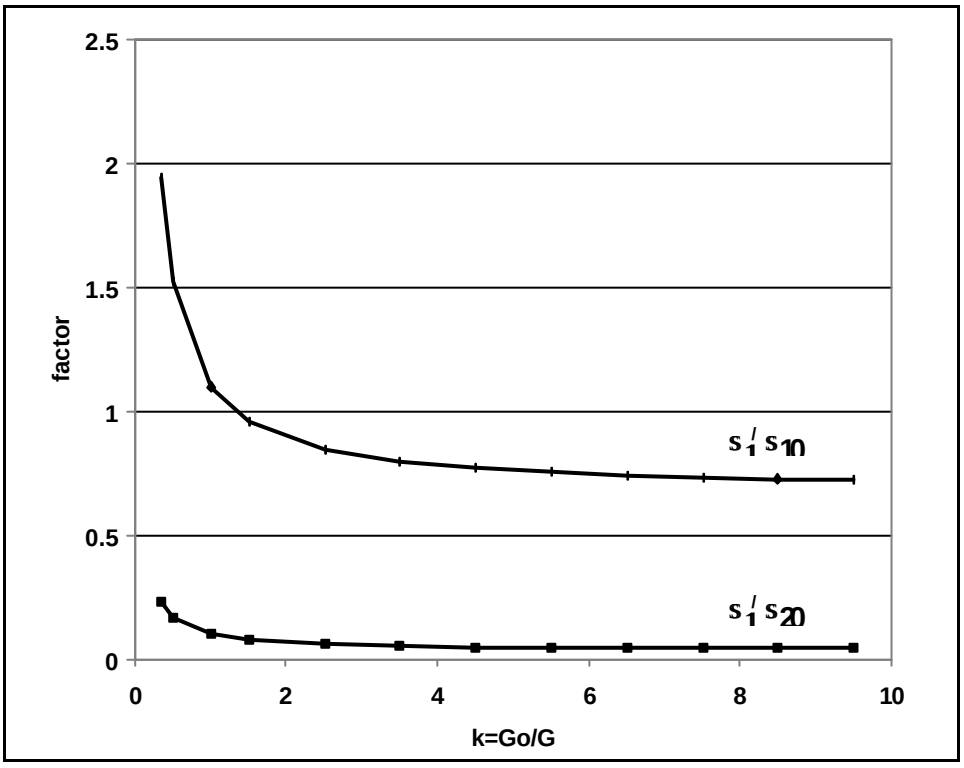


***Figure 4–6 The effect of different shear modulus ratios, with equal Poisson's ratios, on the factors in Equation (4-2)***

The Glotzl cell that was used is of type EBKO 10/20 K100 Z4 and has a measuring range of 0 to 10 MPa. The Glotzl cell is read using a current loop readout unit. A constant voltage equal to 24 volts is applied as input to the gauge. The output current can be directly related to the stress acting perpendicular to the gauge using a calibration factor supplied by the manufacturer. The change in stress $\Delta\sigma$ (in MPa) between two readings is calculated using the Equation

$$\Delta\sigma = \Delta A / 1.6 \qquad (4\text{-}4)$$

Where $\Delta A$ is the change in current (in milliAmps). The stress needs to be related to the stress in the rock mass using the equations given in (4-2) and (4-3).

The calibration of the yoke gauges is described in the manual (Mindata, 2001). A program (yoke.exe) is supplied to perform the data analysis. The program requires the inputs of the calibration factors of the particular yoke gauges, the Young's modulus and Poisson's ratio of the coal and the voltage readings. An assumption is made regarding the out of plane stress or strain conditions and the program calculates the stress state. In this case, plane strain was assumed (i.e. zero out of plane strain). The calibration factors obtained for the Yokes used in this project are K1 = 12.02 mV/mm, K2 = 18.98 mV/mm and K3 = 18.90. In this installation, yoke K1 is 45 degrees clockwise from vertical, K2 is vertical and K3 is 45 degrees anti-clockwise from vertical.

***Table 4–1 Measured elastic properties of grout related to time after preparation***

| Time (Days) | 4 | 9 | 17 | 17 | 110 | 110 |
|---|---|---|---|---|---|---|
| Modulus (GPa) | 2.3 | 1.3 | 9 | 4.6 | 1.3 | 7.2 |
| Poisson's Ratio | 0.17 | 0.18 | 0.078 | 0.15 | 0.18 | 0.18 |

***Table 4–2 Elastic properties of coal at 5 MPa uniaxial compression***

| TEST | 1 | 2 | 3 | 4 | 5 | 6 |
|---|---|---|---|---|---|---|
| Modulus (GPa) | 4 | 2.5 | 4.5 | 5 | 1 | 3 |
| Poisson's Ratio | 0.32 | 0.15 | 0.39 | 0.20 | 0.25 | n/a |

## 4.4 Underground observations

Underground observations were made after each significant change in mining geometry. The dates of the readings are given in Table 4–3, along with the relative number of days. Relative timing is calculated from the day after the installation was completed (i.e. 26 February). All of the stress change measurements were calculated from the difference between any reading and the base values taken on the 26 February. The interpretation of stress change measurements is always very sensitive to the quality of the initial readings. For best results, the instruments should be installed a considerable time prior to the start of stress changes so that a good, stable baseline reading can be obtained. This was not possible at this site due to the need to stop production. Interpretation of the stress change also requires care to correctly relate the readings to the mining sequence. On each site visit, the mine plan was updated based on the stope plan obtained from the miner, and was checked by visual observation of the opening.

***Table 4–3 Dates and relative timing of the readings.***

| Reading | 1 | 2 | 3 | 4 | 5 | 6 | 7 | 8 | 9 | 10 | 11 | 12 |
|---|---|---|---|---|---|---|---|---|---|---|---|---|
| Date | 26-Feb | 28-Feb | 05-Mar | 07-Mar | 12-Mar | 15-Mar | 20-Mar | 26-Mar | 30-Mar | 05-Apr | 18-Apr | 02-May |
| Days | 0 | 2 | 7 | 9 | 14 | 17 | 22 | 28 | 32 | 37 | 51 | 65 |

The mine plan is shown in Figure 4–7. The instrument pillars are marked as P1 and P3. Areas mined in the interval between readings are shaded in different grey scales. The relative timing of the different stages is indicated in Figure 4–7. Readings were initially taken at 2 to 5 day intervals. To reduce costs, the interval was increased as the readings were observed to stabilize.

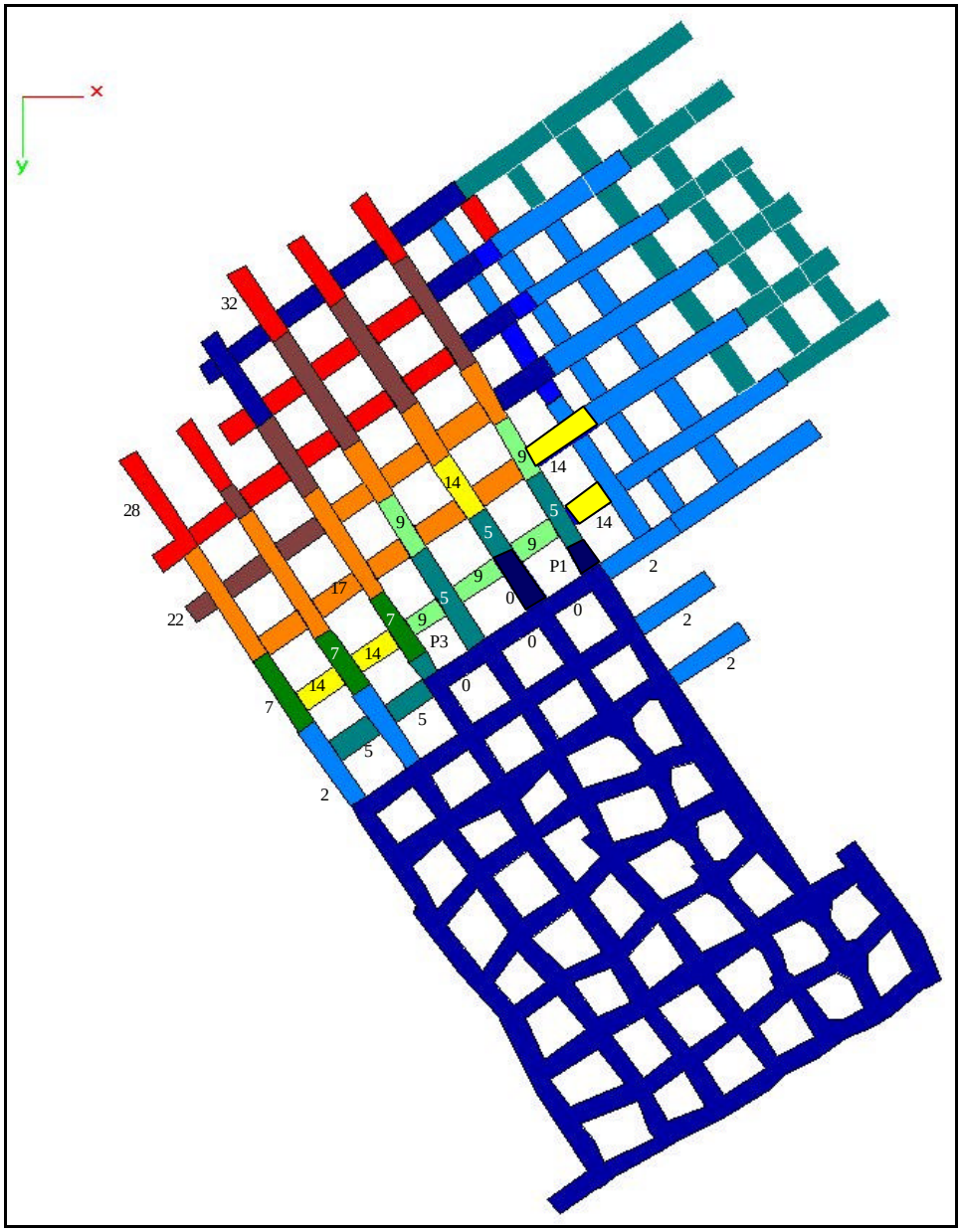


***Figure 4–7 Mine plan showing amount of mining during each observation period. Shaded regions indicate the mining in a certain time period and the numbers indicate the number of days after 26 Feb 2001.***

The stress changes at the centre of the pillars, measured by the vibrating wire gauges, are shown in Figure 4–8. The final magnitudes of the vertical stress change in both pillars, using the vibrating wire gauges, are very similar. The stress becomes more compressive in both cases. The final stress depends on the moduli selected for the grout and the coal. Using the values from laboratory tests, as described in Section 4.3, the stress change of 0.44 MPa is observed at the centre of pillar 1 and 0.55 MPa stress increase is observed at the centre of pillar 3. The stress increase in pillar 1 is less than the increase observed for pillar 3. This is expected as the roadways were cut most of the length of pillar 1 prior to installation of the gauges, whereas no roadways had been cut alongside pillar 3. Most of the stress change occurred up to the ninth day when the splits were cut behind the pillars. Subsequent mining of the panel away from the pillars caused an increase of stress that was less than 0.1 MPa.

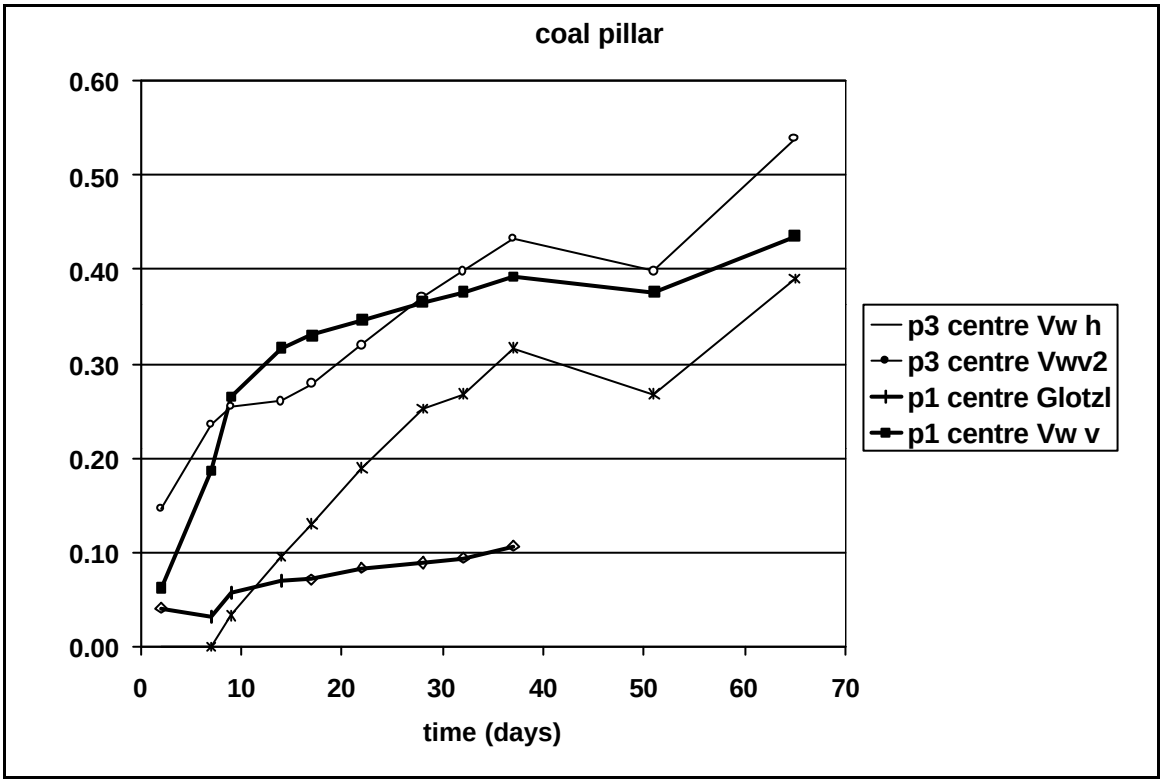


***Figure 4–8 Stress change measured in the centre of the pillars, assuming a hard inclusion***

The Glotzl cell in pillar 1 showed a similar trend in stress increase. Most of the stress increased occurred within 16 days. The stress subsequently changed very little. The magnitude of the stress change reported by the Glotzl cell is about 20 percent of the stress reported by the vibrating wire gauges. There are two alternative explanations for this trend. Firstly, the total stress change is less than 10 percent of the range of the Glotzl cell, and so it may be assumed that the gauge was not sensitive enough. Slight calibration differences could alter the stress change, but possibly not enough to cause a fourfold increase in stress. Secondly, it is possible

that the grout stiffness did not increase underground as much as it did in the laboratory. In this case, it is possible that the grouted borehole acts as a soft inclusion. From Figure 4–6, it can be seen that the stress factor increases above 1.0 for soft inclusions. Assuming that the modulus of the grout remained at 1 GPa, and the coal has a modulus of 3 GPa, the inclusion factor becomes 1.9. In this case, the stress changes can be seen in Figure 4–9 where the Glotzl cell agrees well with the results from the vibrating wire gauges. When the Glotzl cell stopped working after 38 days, the stress increase is calculated to be 0.22 MPa, using the Goltzl cell, and 0.27 MPa, using the vibrating wire gauge. Thus, the difference between the two gauges is reduced to 0.05 MPa.

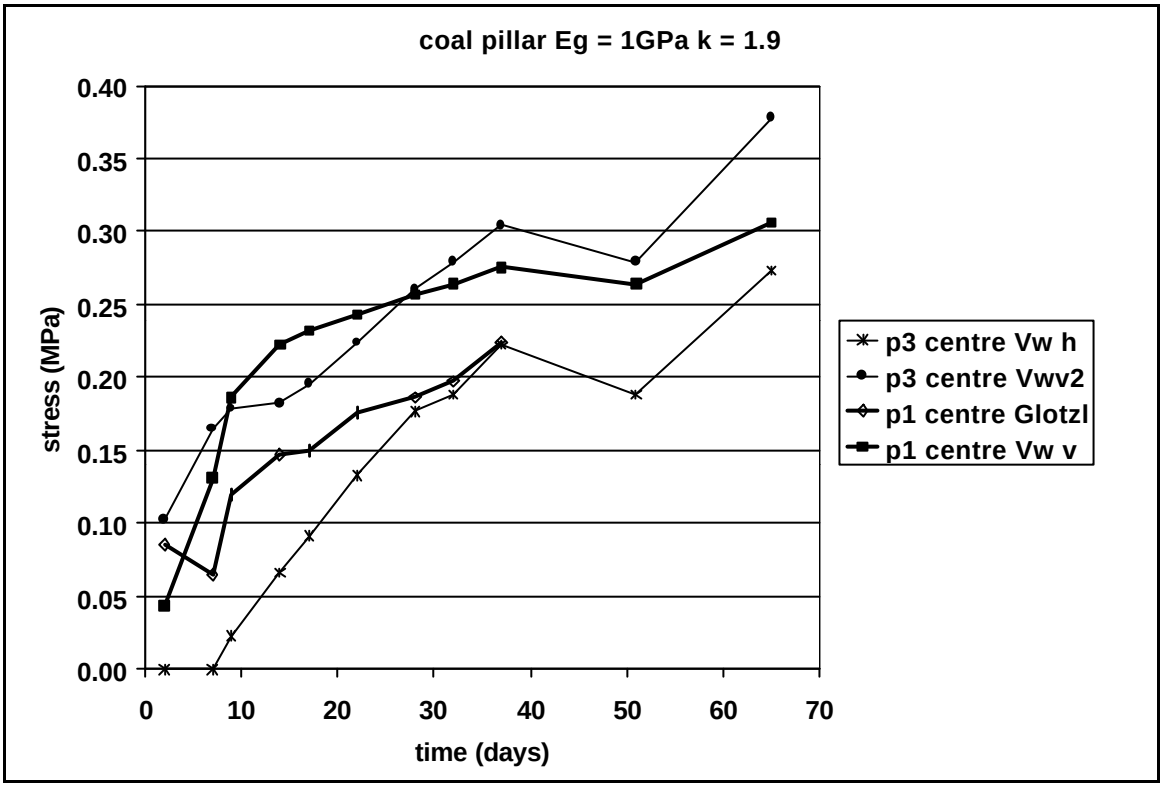


***Figure 4–9 Stress change measured in the centre of the pillars, assuming a soft inclusion***

Only the data from the second vertical vibrating wire gauges in pillar 3 is shown, because gauge 1 was faulty and provided no readings. The horizontal stress at the centre of pillar 3 also became more compressive. The start of increasing horizontal compression was delayed until the ninth day. This indicates that the cutting of splits and roadways in the regions surrounding the pillars increased the vertical stress. The horizontal stress only changed once the roadways were cut alongside the pillar itself.

The stress changes at the edge of pillar 3, at a distance of 4m in from the roadway, are shown in Figure 4–10 and Figure 4–11 for the assumptions of hard and soft inclusions, respectively. The vertical stress is shown to become less compressive with time. The horizontal stresses increase slightly. Most of the stress change occurs before the 17$^{th}$ day and is therefore

associated with the cutting of the splits and roadways around the pillar. The stress changes are not as expected and would appear to be rotated by 90 degrees. Thus it would be expected that the horizontal stress decreases and the vertical stress increases. It is impossible to determine if the cage was inadvertently rotated during installation or if the wiring was labelled incorrectly when the cage was modified to accommodate more gauges.

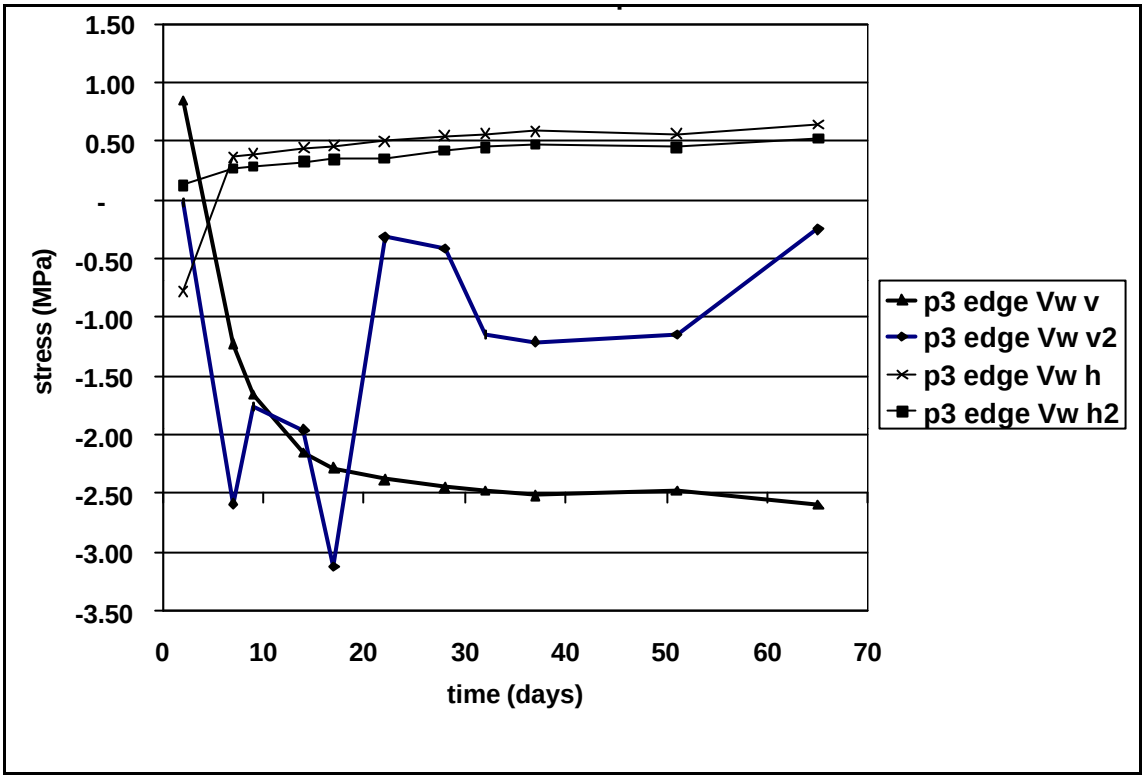


***Figure 4–10 Stress change measured at the edge of pillar 3, assuming a hard inclusion***

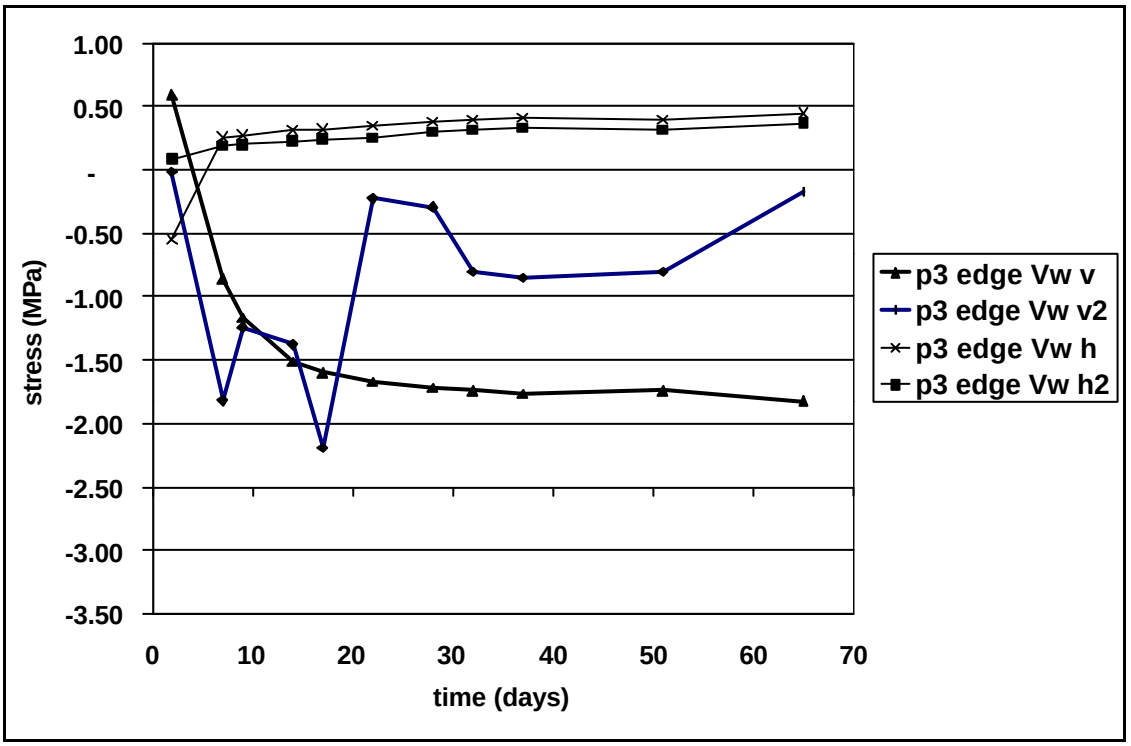

***Figure 4–11 Stress change measured at the edge of pillar 3, assuming a soft inclusion***

The stress increases measured by the Yoke gauge are shown in Figure 4–12. The results indicate that the stresses increased considerably throughout the mining period. The major principal stress is orientated at an angle of 45 to 50 degrees clockwise from vertical. There is a considerable difference, of about 4 MPa, between the magnitudes of the major and minor principal stresses. The magnitudes of the stresses are sensitive to the choice of Young's modulus of the coal, but not very sensitive to the Poisson's ratio. However, the ratio of the principal stresses in not sensitive to the choice of elastic properties.

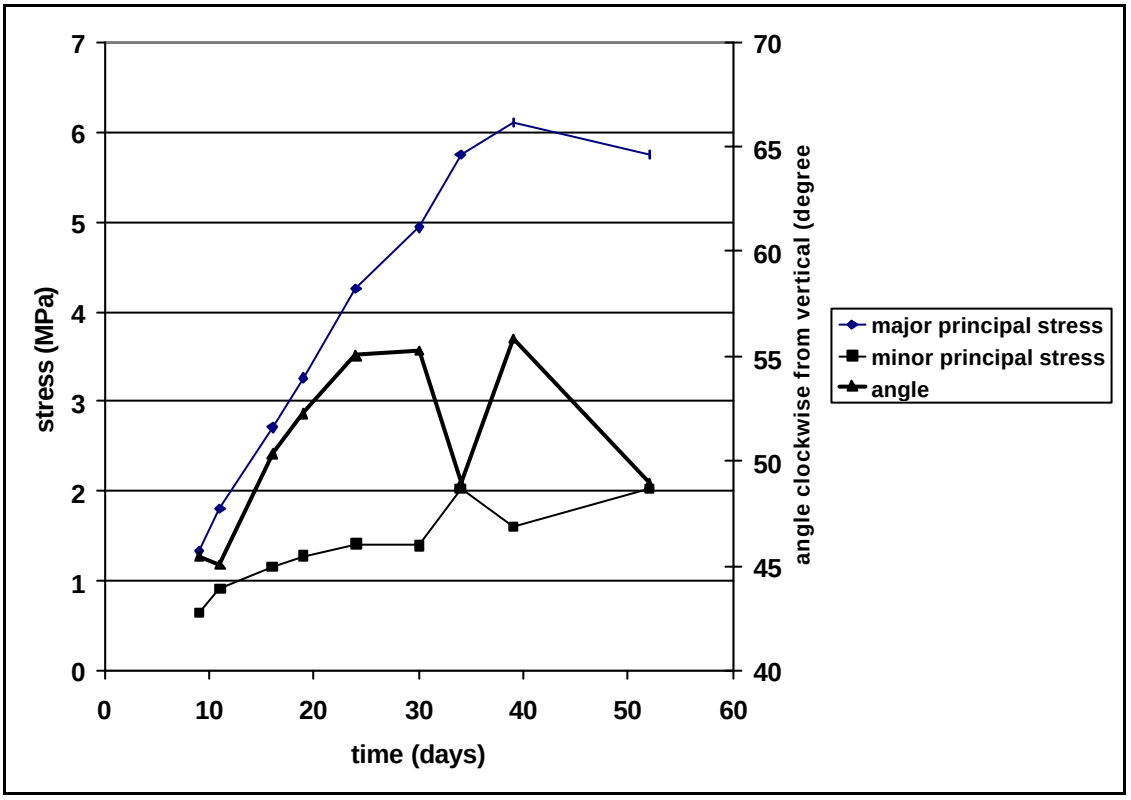


***Figure 4–12 Principal stress changes measured using the yoke gauge. (positive stress implies increasing compression)***

## 4.5 Comparison of modelling and underground observations

Two different numerical models were constructed in order to determine the predicted stress changes due to the mining sequence that had occurred at the observation site. A MINSIM 2000 model was built from a digitised mine plan. This model can provide an indication of the changes in the vertical stress in the pillars with the progression of the mining. A two-dimensional ELFEN

model was set up to determine how the vertical and horizontal stresses would change through the section of the pillar.

The MINSIM 2000 model assumed that the rock mass was infinite in extent with a Young's modulus of 30 GPa and a Poisson's ratio of 0.3. The mine layout and mining sequence was digitised from the mine plan. The sequence is shown in Figure 4–13. The stress states, for different stages of mining, at positions though the centreline of the pillars, parallel to a split are shown in Figure 4–14. Only certain points are shown and different points are selected for each pillar due to the way in which the selection and interpolation of stress points is done in the program. The stress does not increase very much at the centre of the pillar. Higher stresses are evident at the edges of the pillar. However, once the initial stress change has occurred, there is very little further influence from additional mining. The stress changes with time can be seen in Figure 4–15. The stress at the centre of the first pillar increased by about 0.5 MPa. The stress in the third pillar increased by about 1 MPa. This is greater as the first pillar was partially excavated prior to the installation of the gauges. These stress changes are similar in magnitude to those measured underground, see Figure 4–10 and Figure 4–11. A higher stress change was observed near the edge of the pillar in the model, but the magnitude of this stress is significantly influenced by the boundary element formulation for constant stress elements and the element size. The value of the change in stress will depend strongly on the position within the pillar and cannot be used for direct comparison with the results of the measurements

A finite element model was set up to investigate the stress transfer through the vertical section of the mine as the roadways were extracted. The model is shown in Figure 4–16. In the model, the stope is assumed to be at a depth of 100m. The roof is divided into five layers consisting of a soil layer at surface, three sandstone layers and a shale/mudstone layer above the coal seam. The floor is assumed to consist of sandstone. The choice of stratigraphic layers was based on geological reports provided by the mine, but is an approximation that is required in order to construct the model in a reasonable time. The moduli of the layers are selected to be approximately those expected for the equivalent strata within the 20 m thickness into the roof in the model. An initial stress state is obtain by applying a gravitational loading in the vertical direction. Two cases were analysed, with horizontal stresses twice the vertical stresses (k-ratio = 2) and half the vertical stresses (k-ratio = 0.5). The horizontal stresses were included by displacing the right hand edge of the layers an amount that was calculated to induce a stress that is equal to the required horizontal stress at the centre of the layer. The friction angle on the layers was set to zero during the stress equilibrium stage then increased to 30 degrees when the required stress state was attained.

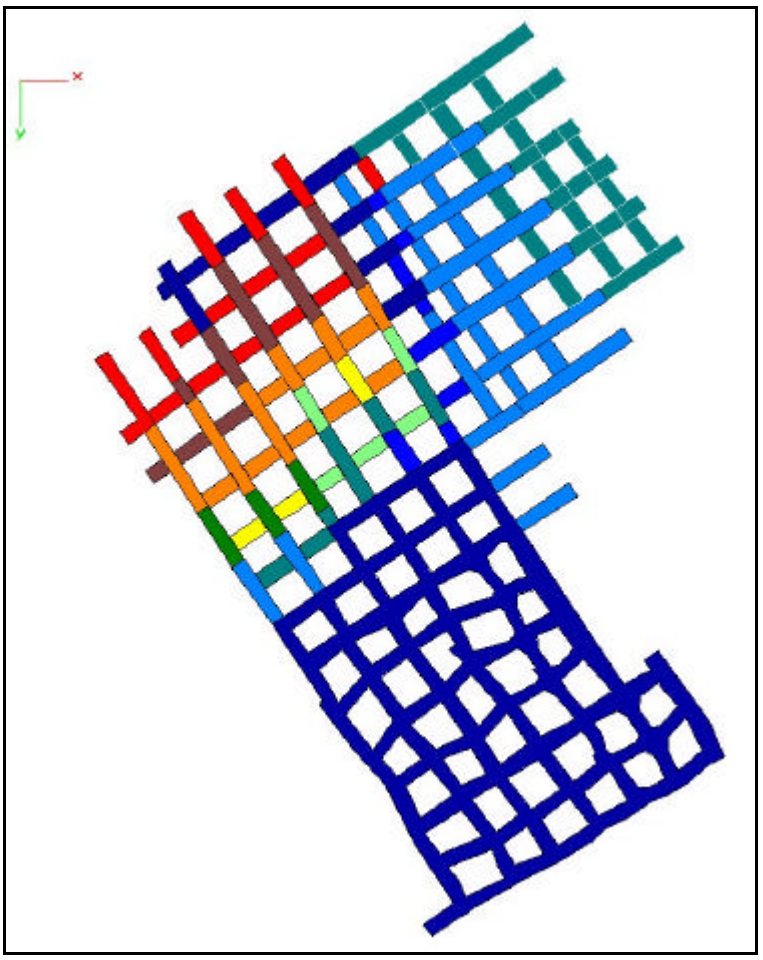

*Figure 4–13 Mine plan showing mining steps taken in MINSIM 2000 model*

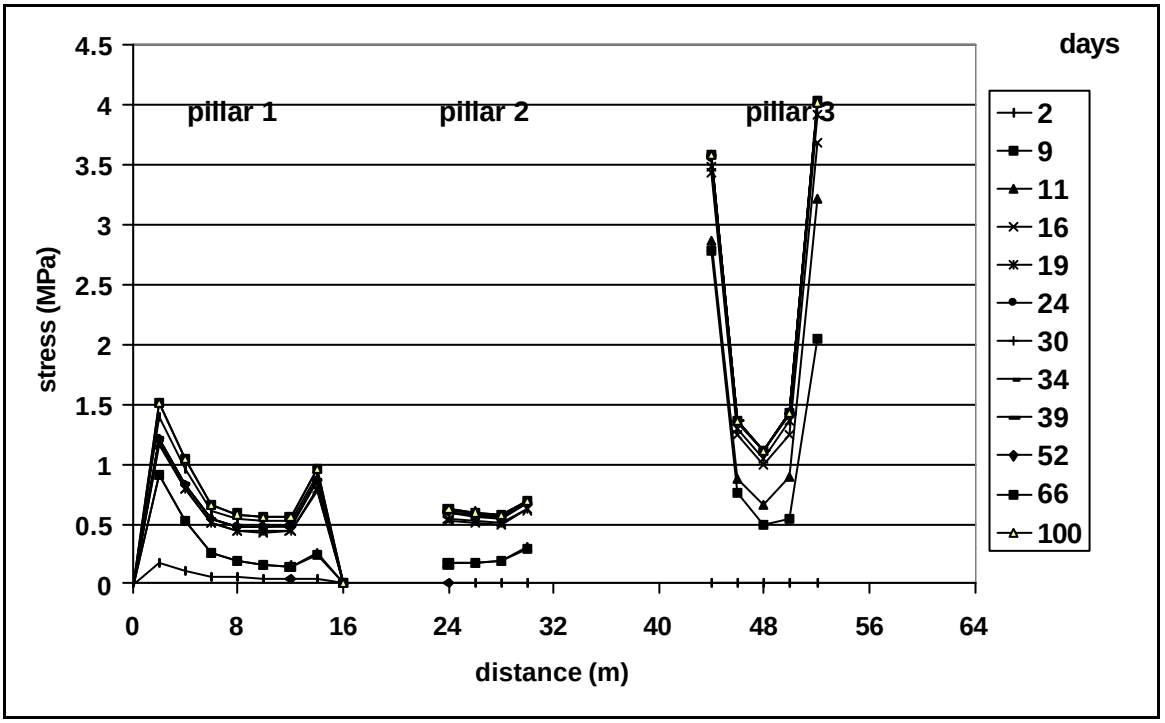


*Figure 4–14 MINSIM 2000 predictions of pillar stress distribution (increasing compression is positive)*

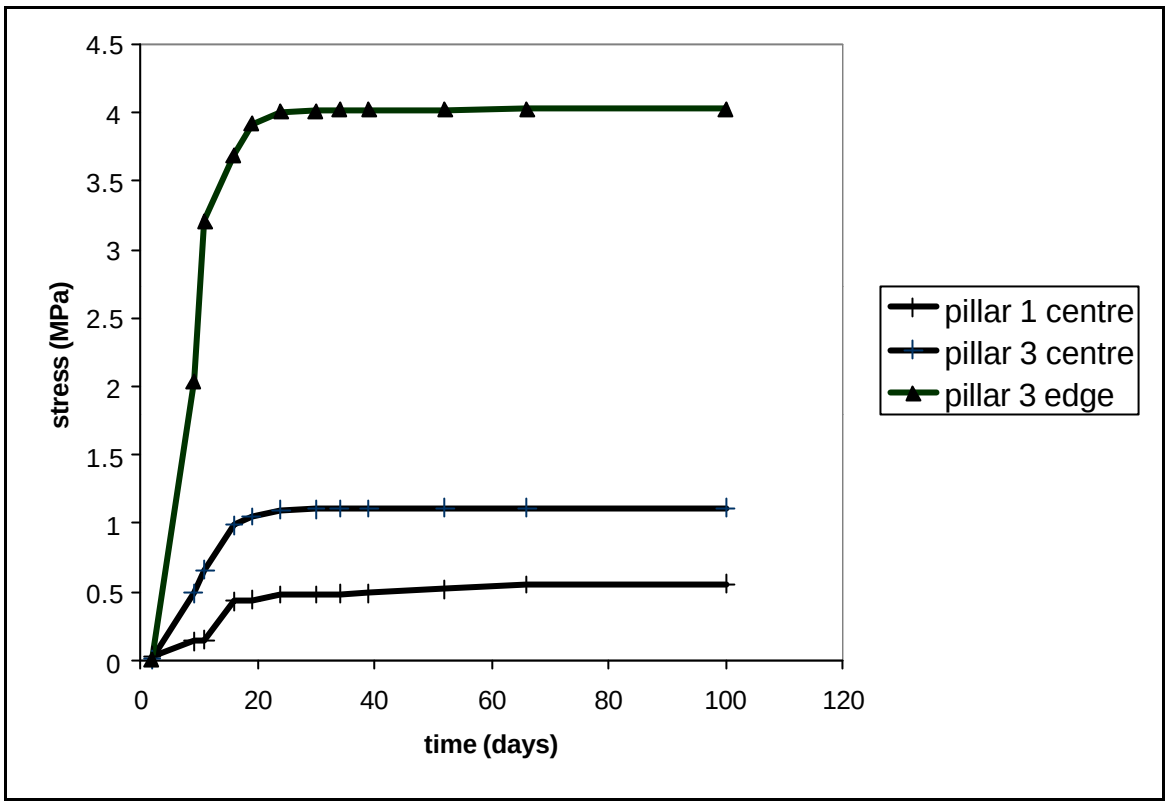


***Figure 4–15 MINSIM 2000 predictions of pillar stress change with mining (increasing compression is positive)***

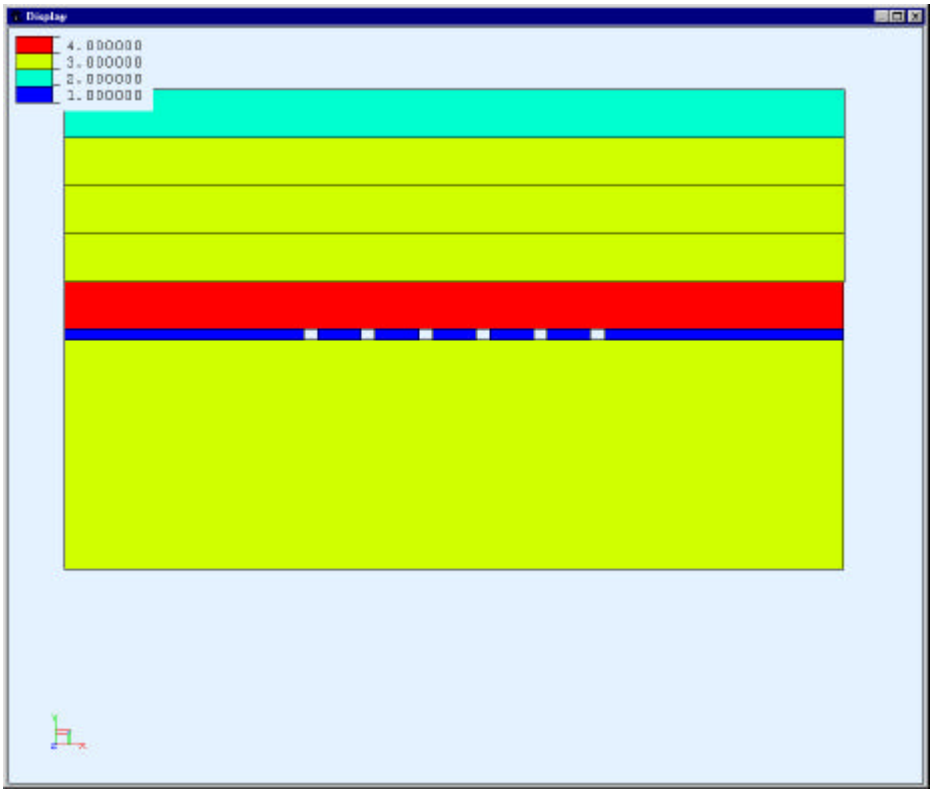

***Figure 4–16 ELFEN 2-D model of section of mine***

The vertical stress distribution after extraction of all roadways, from right to left, is shown in Figure 4–17, for the case of a k-ratio equal to 2.0. Figure 4–18 shows detail of the finite element mesh and indicates the points where stress changes were calculated. The stress change results, shown in Figure 4–19 (with a k-ratio of 2), show that the predicted stress change agrees with the MINSIM results in that pillar 1 should experience a stress increase of 0.5 MPa. Pillar 3 experiences a stress increase of 1 MPa. The horizontal stress decreases considerably and reduces from the in situ stress level when the roadways are excavated. The horizontal stress depends strongly on the position within the pillar. At the centre, the stress decreases less than the stress nearer the edge of the pillar. Figure 4–20 shows the stress changes for the case with a k-ratio equal to 0.5. The stress changes are similar, except for the horizontal stress, which decreases much less than for the case of k=2, as a result of the lower initial horizontal stress.

Figure 4–21 shows the vectors of principal stress in pillar 3 predicted by the ELFEN model with a k-ratio equal to 2.0. The stresses at the position of the yoke gauge confirm the observations from the yoke gauge that the major principal stress is rotated at an angle of about 45 to 50 degrees clockwise from vertical. However, the model predicts a much smaller difference in magnitudes between the major and minor principal stresses. This ratio is sensitive to distance from the edge of the pillar.

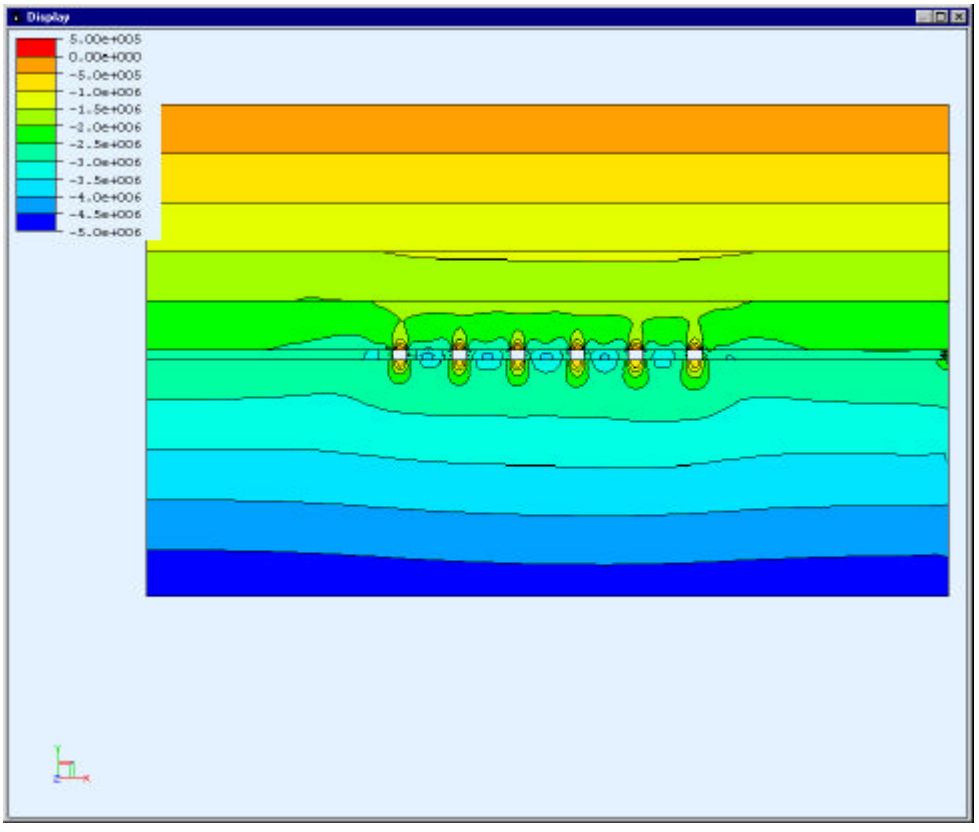


***Figure 4–17 ELFEN 2-D model of section of mine***

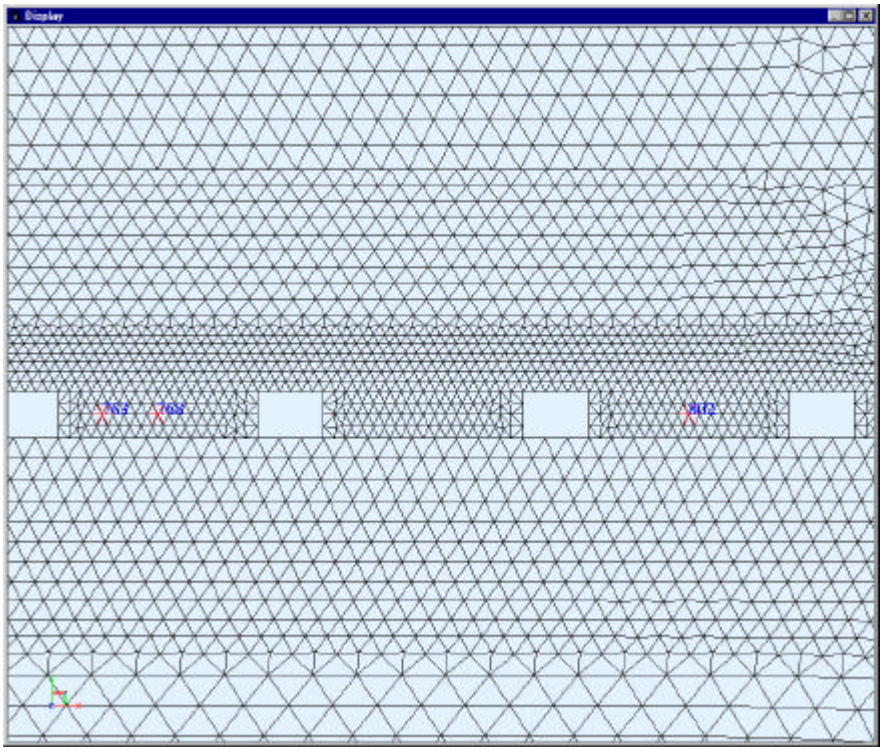

*Figure 4–18 Detail of ELFEN mesh showing points where stress change data is obtained*

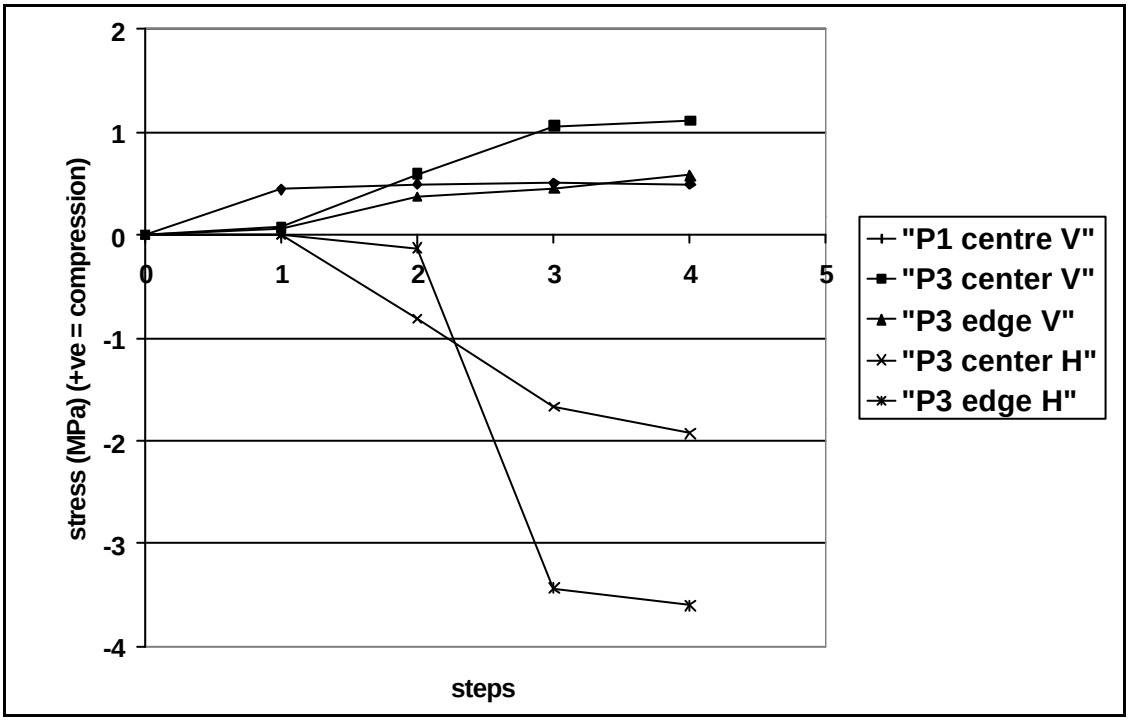


*Figure 4–19 Stress changes predicted by ELFEN for k-ratio of 2 (increasing compression is positive)*

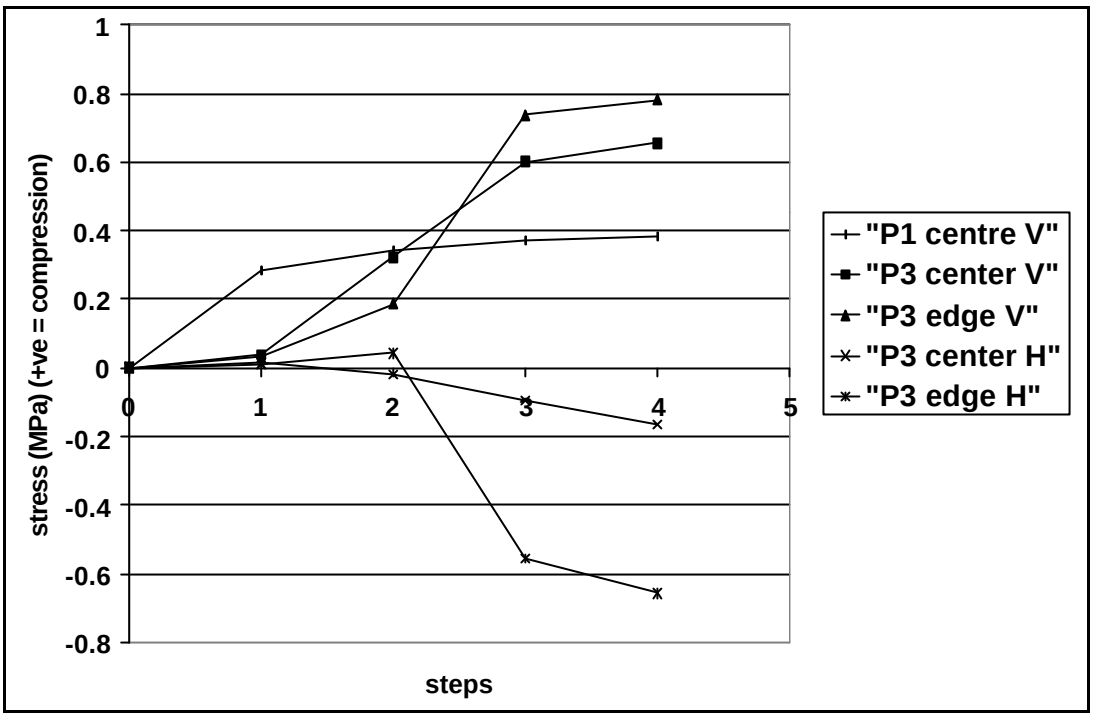


***Figure 4–20 Stress changes predicted by ELFEN for k-ratio of 0.5 (increasing compression is positive)***

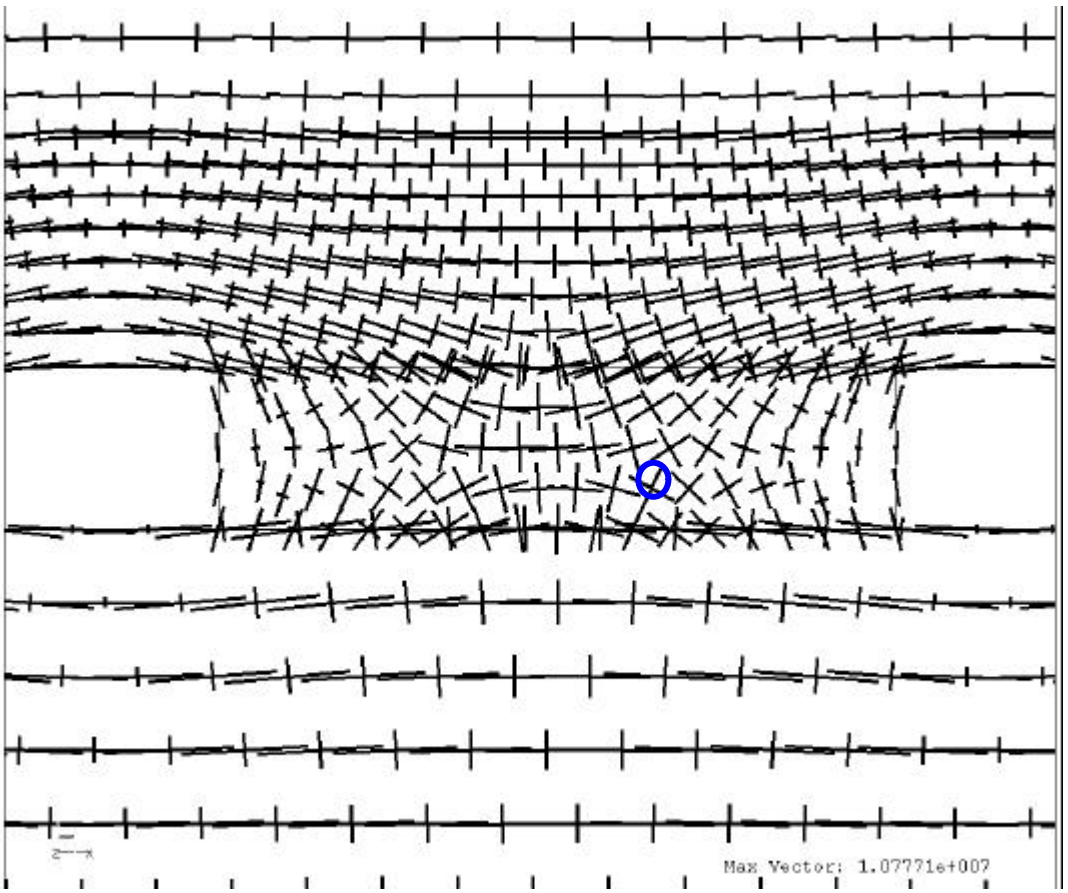


***Figure 4–21 Stress vectors in pillar 3 predicted by ELFEN for k-ratio of 2.0. Circle marks approximate position of the yoke gauge.***

## 4.6 Conclusions

Stress changes were measured in a pillar at Wilmansrust Shaft, Gloria Section of Koornfontein mine. The project involved the installation of stress change meters in a bord and pillar mining section. The mining was stopped so that the instrumentation could be installed into the face. The instrumentation took five days to install and mining was started on the seventh day. Some modifications to the planned instrumentation layout were made on site. Vibrating wire gauges were grouted into the centre of two pillars, and the edge of the second pillar. A yoke gauge was installed into one pillar. A Glotzl pressure cell was installed into the first pillar.

Readings were taken as the mining progressed. Initially readings were taken every two days and the reading intervals were extended as the readings were observed to stabilize. In total, the cells were monitored for 65 days. The stress changes measured at the centre of the pillar varied between about 0.3 MPa and 0.5 MPa in magnitude. The first pillar showed less stress increase as the roadway had been extended part of the way past the pillar when the instruments were installed. The stress increase is greatest during cutting of the roadways between the pillars and the first split that defines the pillars. The stress increases slightly as mining moves away from the pillars under consideration, but is essentially stable after the 2$^{nd}$ split has been cut.

A three dimensional model of the mining was analysed using MINSIM 2000 to compare the modelled and observed stress changes. MINSIM predicts slightly larger stress changes (0.5 to 1.0 MPa) than measured underground. The modelled values will depend on the material parameters. A two dimensional model was developed using the ELFEN finite element program. The results compare well with the underground observations and indicate that most of the stress will be transferred during cutting of the adjacent roadways. The models also indicate that there can be a considerable variation in the magnitudes and directions of the principal stresses within the pillar. The model parameters such as layer stiffness, in situ stress and layer friction will strongly influence the stress changes observed at different points within the pillar.

This work was conducted on 2 seam at a depth of 105 m. The applicability of these results at different depths (for example, on 4 seam at an average depth of 50 m to 60 m) should consider the results from the numerical modeling analyses conducted in section 5.0. These results indicate that stresses relative to tributary area decrease with increasing depth. It may be expected, therefore, that the stress changes will be higher (relative to virgin stress) on a shallower seam. The magnitude of this difference for the extraction ratio of the instrumented section (58 per cent) will be very small however. Figure 5–9 indicates that the difference in stresses for this extraction ratio will be less than 0.1 per cent.

# 5.0 Numerical analyses

## 5.1 Introduction

The fact that pillars with very low safety factors (sometimes less than one) have been observed in a stable condition implies that either the pillar strength or pillar load estimation is inaccurate. This investigation concentrates on the pillar loading aspect and attempts to determine the accuracy and applicability of the tributary area method.

It is well known that tributary area theory (TAT) slightly over-estimates pillar loads in general. It has been suggested (van der Merwe, 2000) that this discrepancy can become significant, particularly where the overburden strata are stiff and the workings are relatively deep with a high extraction ratio. In this project numerical modelling is employed to determine pillar loads under a variety of conditions, hence evaluating where TAT is, or is not applicable.

This report describes an evaluation of the LAMODEL (Heasley, 1997) boundary element program. LAMODEL differs from most boundary element codes in that the overburden is treated as laminated, thus introducing flexural rigidity into the analysis as a parameter. Sensitivity analyses are undertaken to assess how the flexural rigidity and other parameters influence the results. The results from the code are then compared with those obtained with plane strain finite/discrete element models. Trends and insights from these analyses are presented in terms of their relation to tributary area theory.

## 5.2 Initial investigations

The main focus of the preliminary investigations was to establish an expression for pillar load as a function of panel width to depth ratio, strata stiffness and percent extraction. The analyses were carried out by using the 2D boundary element programs, MINLAY and BEPIL. Both of these programs were used with the finite depth options activated. A panel width of 100 m at depths of 50 m, 100 m, and 200 m was modelled at various extraction ratios using these programs. Regular layouts with 20 m centre-to-centre distances were analysed with different pillar sizes. Variation of the pillar size allowed for the extraction ratio to be adjusted. For each set of runs the elastic modulus of the seam was assumed to be 3.5 GPa with that of the roof strata being kept constant at 14 GPa.

The average pillar stress was calculated for the central pillar for each run. For the specific conditions modelled, the tributary area theory (TAT) was also used to calculate the theoretical

pillar stress. The resulting value was used to normalize the modelled pillar stress so as to the obtain an average pillar stress ratio. The average pillar stress ratios obtained are plotted against the corresponding extraction ratios for panel width to depth ratios of 1:1 and 2:1 in Figure 5–1 and Figure 5–2 respectively.

The BEPIL and MINLAY programs produced very similar results. The results shown in Figure 5–1 give an indication that from 0.2 to 0.75 extraction ratio the model stresses are lower than the tributary area calculation by up to 17 per cent. From 75 per cent extraction to 90 per cent there is a further, sharp decrease to about 27 per cent less than tributary area. Therefore, at high extraction ratios, nominal safety factors (NSF), calculated using Salamon strength formula and TAT, can become unrealistically low (indicated in Figure 5–1 and Figure 5–2 as "NSF"). However, based on these analyses, it can be deduced that at lower percentage extraction, the tributary area theory gives a reasonable estimation of the actual pillar load. At higher percentage extraction, the theory tends to overestimate the pillar loads by more than 30 per cent. The overestimation of pillar loads calculated with the TAT at high extraction ratios is apparent at both panel width to depth ratios of 1:1 and 2:1.

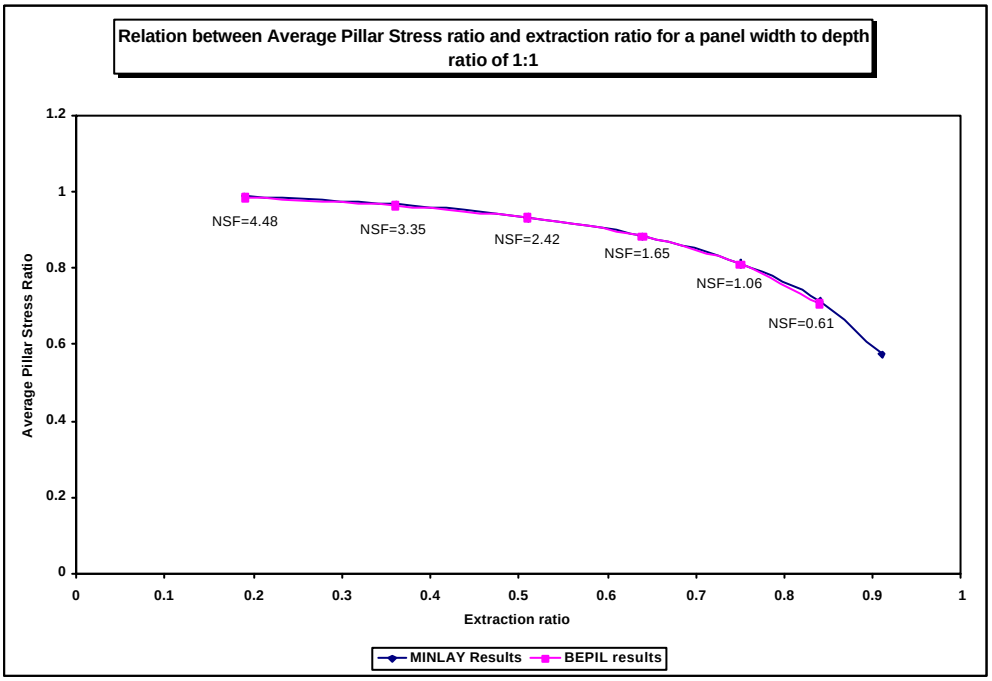


***Figure 5–1 Relationship between APS ratio and extraction for a panel width to depth ratio of 1***

Another important observation made from further analyses is that the modulus ratio tends to influence the pillar load. When both the modulus of the seam and strata are doubled, identical pillar stresses are obtained. In contrast, doubling the panel width and depth whilst keeping all other parameters constant does not produce identical pillar stresses unless the seam height is

also doubled. If the strata modulus is reduced keeping the seam modulus unchanged, the stresses on the pillars increase and tributary area theory becomes increasingly more accurate. At higher panel width to depth ratios, the curves shown in Figure 5–1 and Figure 5–2 would tend to become flatter and lie closer to the value one on the y-axis.

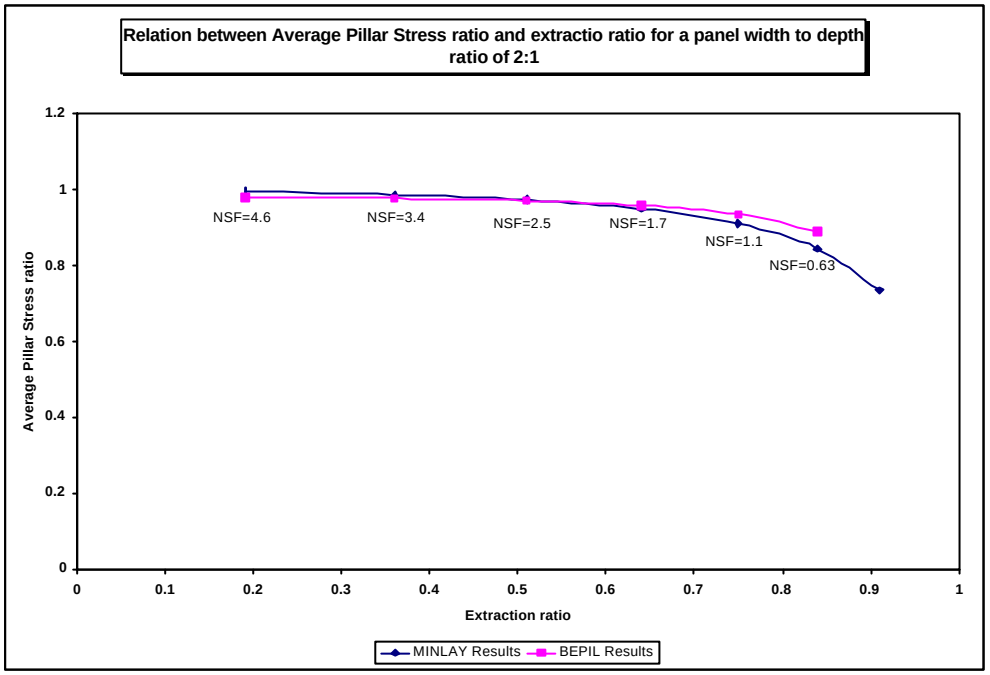


***Figure 5–2 Relationship between APS ratio and extraction for a panel width to depth ratio of 2***

## 5.3 General description of LAMODEL

LAMODEL is a boundary element code which models tabular excavations as displacement discontinuities (DD's). These DD's physically represent cracks, which is appropriate in the gold and coal mining environment where seam height is typically less than one per cent of the maximum dimension of the seam height/mining extent. The region of interest is discretised by regular gridding with a fixed square element size. The geometry of the modelled region is rectangular. Solid and void are specified on the DD plane to model pillars and excavations. A number of mining steps may be simulated by changing elements from solid to void and vice versa when backfill is modelled.

Seam stresses (in the solid) and convergence (in the excavated areas) are the primary outputs of the program. In shallow excavations, the proximity of the surface may influence the stresses and displacements within the seam. LAMODEL models this effect by placing a fictitious seam in space such that a traction-free surface, representing ground level, is created.

LAMODEL is different from continuum boundary element codes in that the overburden is treated as a stack of regularly spaced frictionless laminations. The formulation for this approach is based on the theory of thin plates and it is assumed that the beds are always parallel and that no shear stress or cohesion is present along the contacts. The size of the laminations is user-specified. The effect of this assumption is to reduce the stiffness of the overburden such that convergence is typically higher than for homogenous models. It is also possible to specify symmetry conditions on any edge of the model in LAMODEL, so that infinitely repeating geometries can be modelled.

## 5.4 LAMODEL sensitivity analysis

The aim of this section is to evaluate what effect various parameters within the laminated overburden model have on the pillar stresses. These parameters are as follows:

- Number of laminations
    - The lamination thickness (and therefore the number of laminations for a fixed depth) influences the effective stiffness of the beam overlying the seam. This will influence both pillar stresses and convergence.
- Overburden stiffness
    - This will influence the stiffness of the overlying beam and therefore the pillar stresses and convergence.
- Seam stiffness
    - The compressibility of the seam is expected to effect the roof deflections and the pillar stresses.

## 5.5 Model description

The model is a simple representation of a 100 m wide panel, containing a single row of five 16 m pillars, with 4.0 m bords. 40 m of abutment were modelled on either side of the panel. The boundary element grid size was 1.0 m. Symmetry was applied on two boundaries so that the rows were infinitely repeated in both directions (Figure 5–3). The extraction for this geometry is 36 per cent.

The base material properties were:

$E_{overburnden}$ = 15 GPa

$í_{overburden}$ = 0.3

$E_{seam}$ = 4 GPa

$í_{seam}$ = 0.2

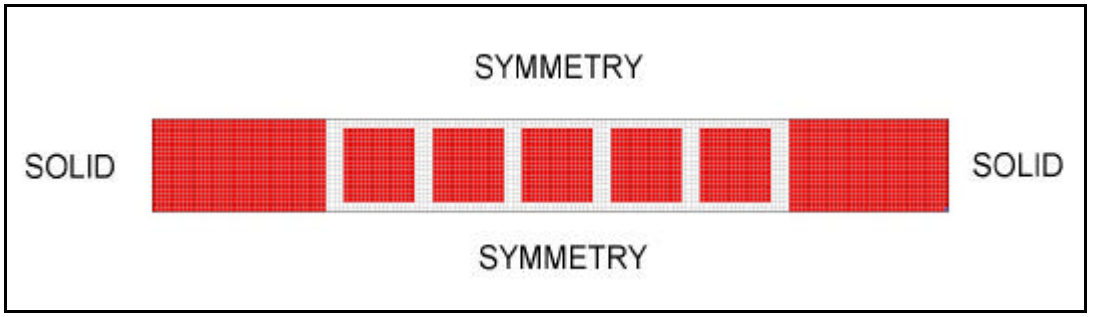


***Figure 5–3 Model geometry for sensitivity analysis***

The overburden density and depth were (respectively) 2500 kg/m$^3$ and 100 m. The seam thickness was 3.0 m. Tributary area theory (TAT) predicts average pillar stresses (APS) of 3.9 MPa. For each run, the stresses in each pillar were averaged to obtain pillar APS. The maximum pillar APS (always in the centre of the panel) is used as a criterion for comparison with the predicted APS according to TAT.

## 5.6 Results

### 5.6.1 Sensitivity to lamination thickness

Figure 5–4 shows the panel APS in relation to the TAT prediction. The maximum difference between modelled pillar stresses and tributary area prediction is less than 0.8 per cent. The trend is for the pillar stress to increase with an increasing number of laminations, as expected. With fewer laminations, the stiffness of the overlying beam is increased. This limits the deformations within the seam, and therefore the stresses on the pillars are lower.

### 5.6.2 Sensitivity to overburden stiffness

Using a lamination thickness of 2 m, corresponding to 50 laminations, analyses were performed with various overburden moduli. The Young's modulus of the seam was set to 4 GPa and the overburden modulus was varied between 4 GPa and 400 GPa (1 to 100 times seam stiffness). The "stiffness ratio" is defined here as the ratio of overburden modulus to seam modulus. The results are presented in Figure 5–5.

It is to be expected that as the overburden stiffness is increased, less load will be carried by the central pillar. The results clearly indicate this trend, but once again differing from TAT by less than one per cent. The greatest difference is evident for an overburden modulus of 400 GPa, which is very unlikely to be encountered in practice. Note that the convergence tolerance had to

be changed from default by a factor of 100 for the high-stiffness analyses to give satisfactory results.

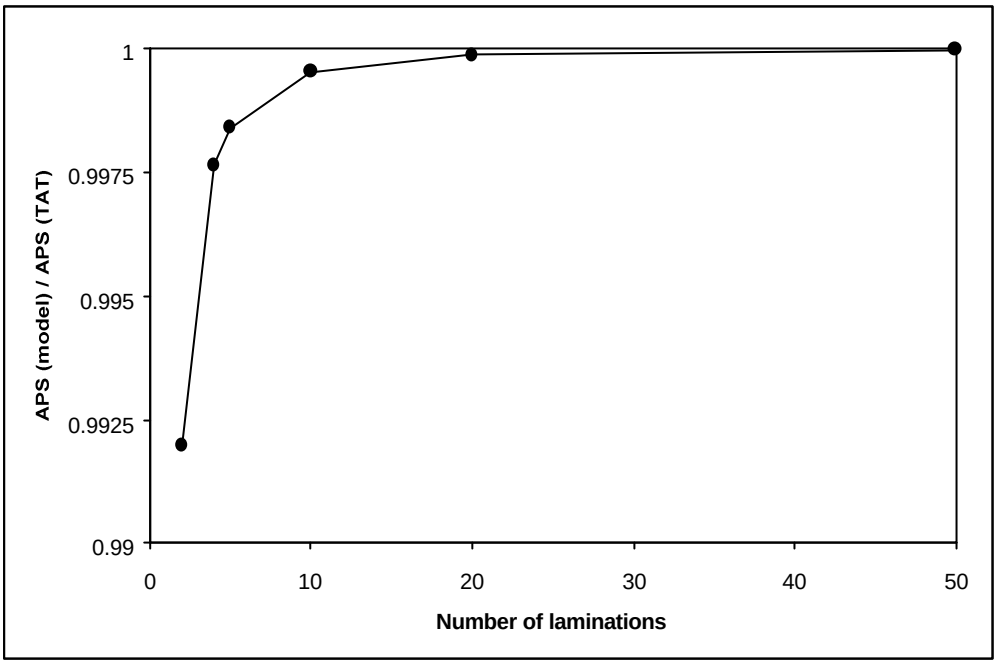


***Figure 5–4 Sensitivity to lamination thickness***

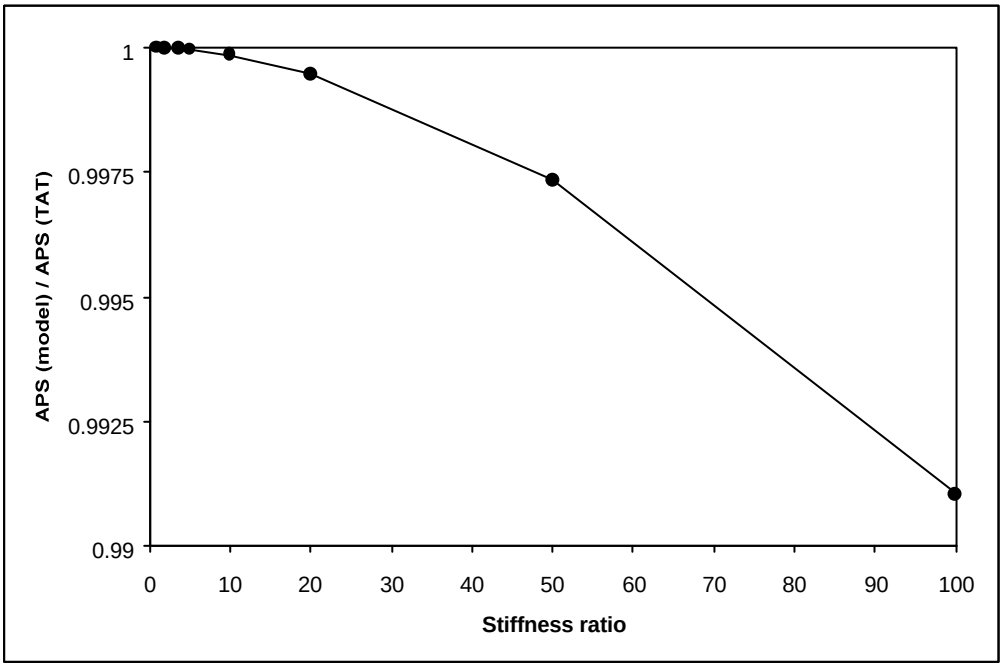


***Figure 5–5 Sensitivity to overburden stiffness***

### 5.6.3 Sensitivity to seam stiffness

For this analysis, the overburden stiffness was set to 15 GPa and a lamination thickness of 2 m was specified. The seam stiffness was varied from 0.15 GPa to 150 GPa. The resultant APS's (relative to TAT) are presented in Figure 5–6. The results vary by less than 0.5 per cent, achieving a maximum stress at the lowest stiffness ratios. Stresses decrease with increasing stiffness ratio (which corresponds to a increasing seam stiffness) as expected. This result is very similar to that obtained while varying overburden stiffness, though the relative magnitudes indicate that the result is less sensitive to seam stiffness than overburden stiffness.

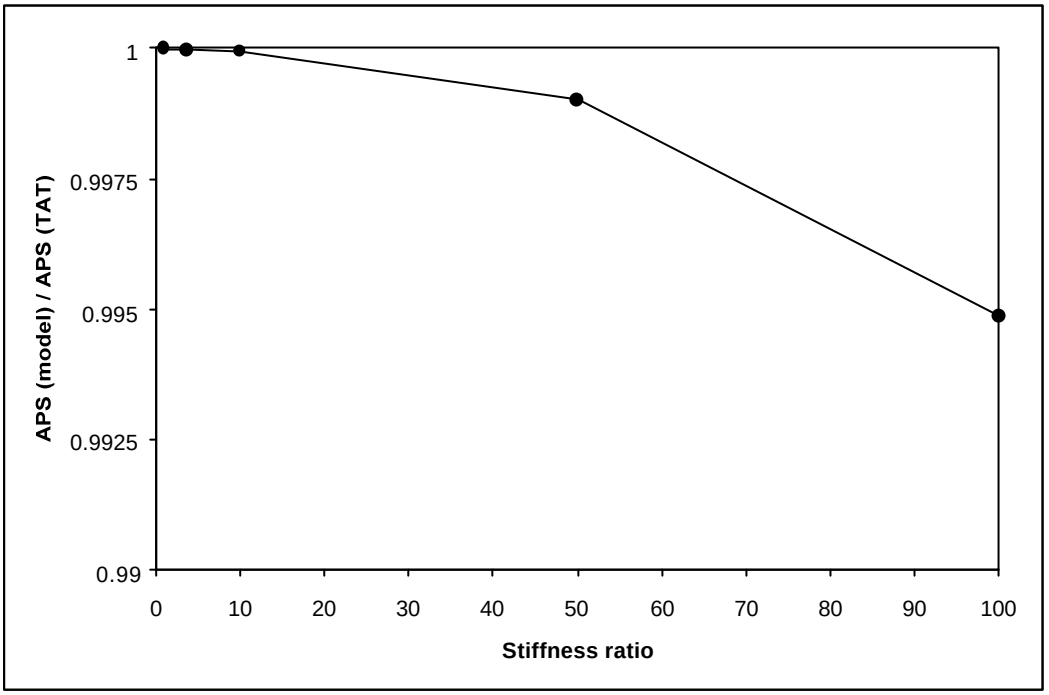


***Figure 5–6 Sensitivity to seam thickness***

## 5.7 The effect of extraction ratio and depth on pillar stresses

The effect of the extraction ratio and depth on maximum pillar stress is discussed next. This work was performed with the LAMODEL code.

### 5.7.1 Model description

The model is essentially the same as that described in section 5.2, except that the extraction ratio is varied by decreasing the sizes of pillars. The extraction is varied from 19 per cent to 91

per cent in 8 steps – three of these steps are illustrated in Figure 5–7. The total dimensions of the model are once again 180 X 20, with a grid size of 1 m.

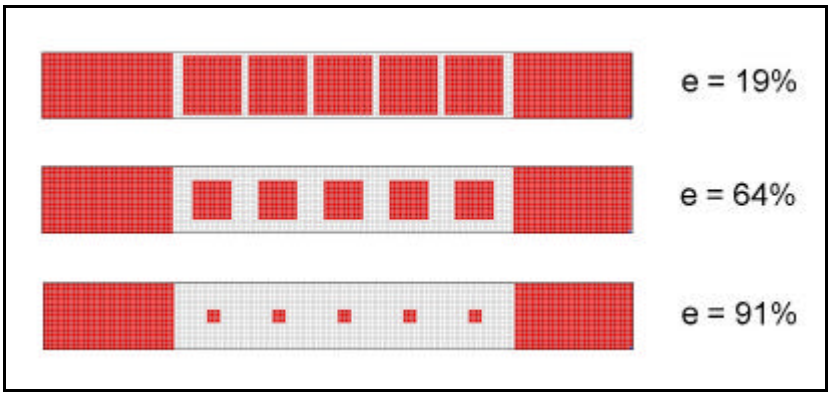


***Figure 5–7 Extraction model***

## 5.7.2 Results

Figure 5–8 shows the relationship between the maximum APS and extraction ratio for two values of lamination thickness. It is evident once again that the model with the stiffer overburden yields lower pillar stresses. The relationship between pillar stresses and extraction shows a steady decrease in stress (relative to TAT) with increased extraction. At high extraction ratios, TAT over-estimates stresses by up to 8 per cent.

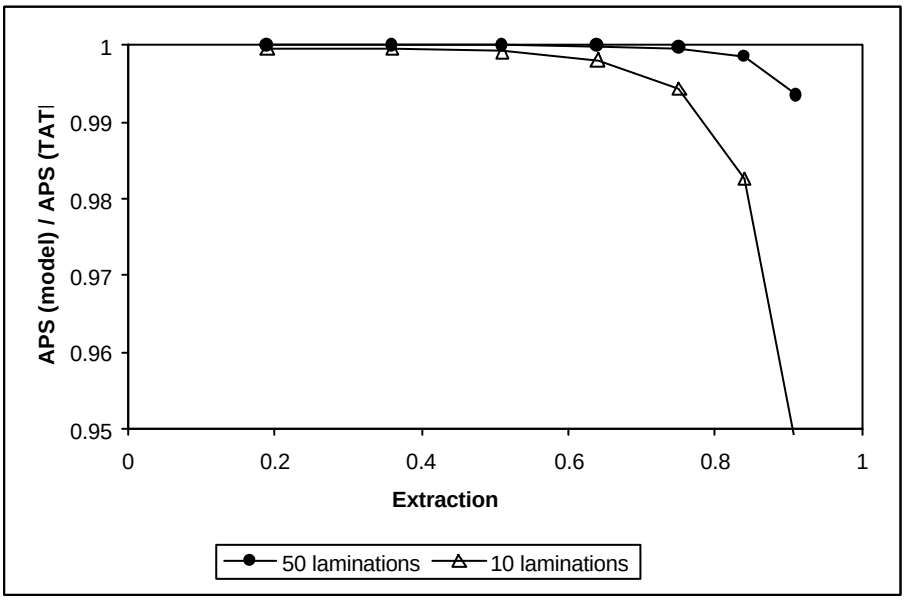


***Figure 5–8 LAMODEL - sensitivity of APS ratio to extraction ratio***

These results differ from those obtained with the BEPIL and MINLAY codes in a number of areas. While the trend for stresses to decrease relative to TAT at higher extraction is evident, in general, the stresses are far closer to TAT in the LAMODEL results. This result can be directly

compared to the BEPIL/MINLAY results for a width-to-depth ratio of 1:1. A maximum deviation from TAT of 8 per cent is observed in LAMODEL, with a maximum deviation of 30 per cent in BEPIL/MINLAY. This comparison demonstrates how the stiffness of the overburden can influence the maximum APS.

The analysis described above was repeated at different depths. All parameters remained the same except for the lamination thickness, which was adjusted so that 10 layers were always present in the overburden. The depth was varied from 25 m to 200 m – note that surface effect was ignored. The LAMODEL results are presented in Figure 5–9.

It was expected that TAT would be closer to the numerical results at depths smaller than the panel width (100 m). This trend is reflected in the results, with the maximum variation from TAT at 25 m depth being less than 4 per cent. The maximum variation at 200 m is 28 per cent. Variation from TAT is once again greatest at the highest extraction ratio. At practical extraction ratios (40 to 60 per cent), the difference between the APS ratios at all depths is less than 0.6 per cent.

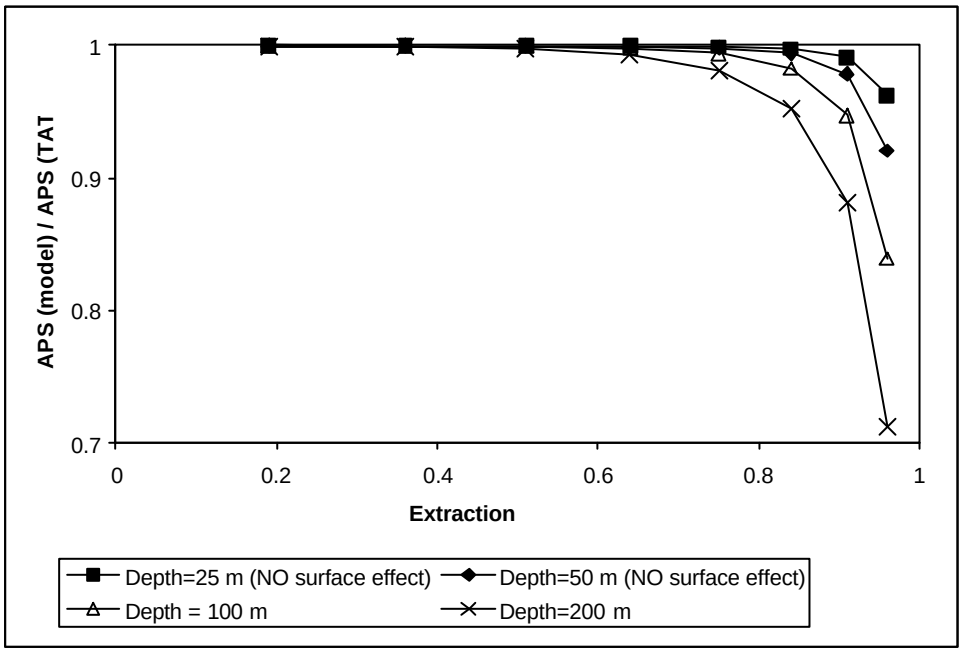


***Figure 5–9 Relationship between APS and extraction at various depths***

The quoted trend for this relationship to “flatten out” at higher width-to-depth ratios can be observed in these results, indicating a qualitative consistency with the BEPIL and MINLAY results.

## 5.8 Inclusion of surface effect

LAMODEL allows for the inclusion of free surface effects as described earlier. The shallow depth analyses in Figure 5–9 (25 m and 50 m) were repeated with this effect activated. The resultant stress ratios are presented (together with the results from Figure 5–9 in Figure 5–10).

The results, which include surface effect, are all greater than the TAT predictions, with the greatest differences evident at the highest extraction ratios, with APS of up to 340 per cent of TAT at 90 per cent extraction at 25 m depth. This is clearly erroneous and this issue is addressed in the following sections.

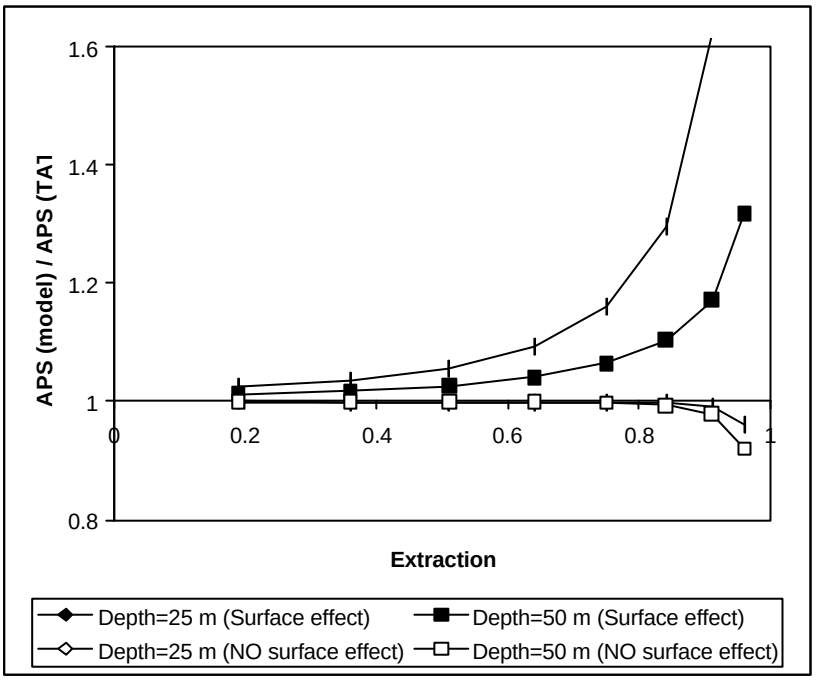


***Figure 5–10 Comparison between analyses at shallow depth with and without free surface effects***

## 5.9 Application of LAMODEL to an irregular geometry

The question is often asked why certain heavily scaled or undersized pillars within a panel do not fail. This question arises because the safety factors for such pillars are calculated based on the dimensions of the individual pillar. Because of the nature of TAT, it only applies for a regular geometry, and the pillars in question are not part of such a regular grid. The case where a single undersized pillar is located within a regular panel is considered in this section.

The geometry for the model consisted of a 7.0 X 7.0 grid of 12 m pillars. The roadways were 6.5 m in width, giving an extraction of 42 per cent. The depth of the panel was 77.3 m, which

gives a TAT stress of 4.59 MPa. The average seam height was 7.0 m, from which a pillar strength of 6.25 MPa is calculated. The nominal safety factor is therefore 1.36. LAMODEL was used to estimate the load on the central pillar. The model was run with 0.5 m elements in a 130 m panel with 20 m abutments. 5 and 10 laminations were included in the overburden for comparison. The results for all analyses are summarized in Table 5–1. The vertical stress distribution is presented in Figure 5–11.

The central pillar was then reduced in size to 9 m X 9 m. The load on this pillar can be estimated as if it were part of the regular geometry described above, giving a TAT pillar stress of 4.59 MPa, as before. The pillar strength is calculated as 5.48 MPa using the Salamon formula, which in this case gives a safety factor of 1.19. If the pillar load is calculated by assuming that all pillars are of these dimensions, a TAT load of 8.17 MPa is obtained. This gives a safety factor of 0.67. LAMODEL was used to analyse this geometry. The vertical stress distribution for this model is presented in Figure 5–12.

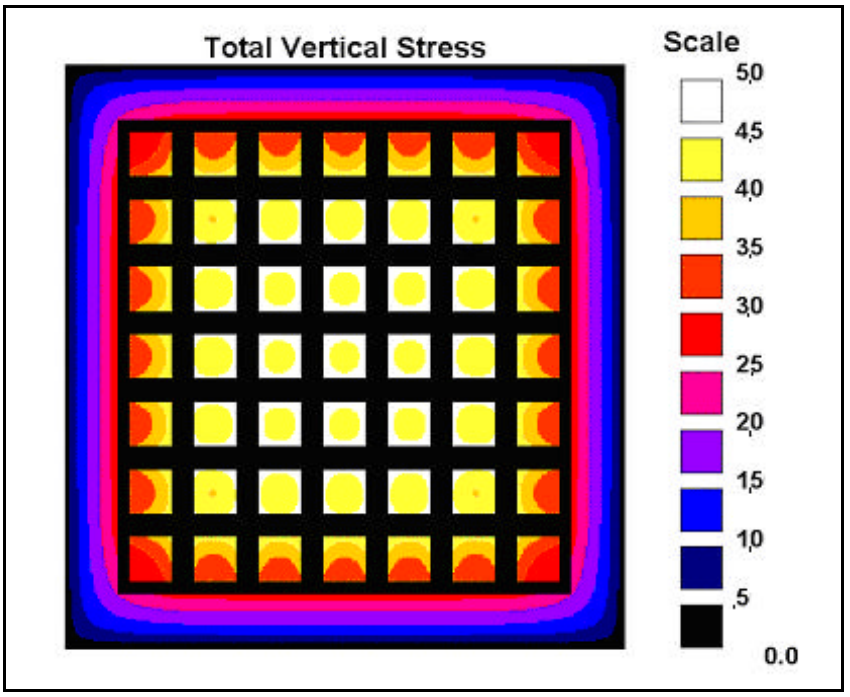


***Figure 5–11 Vertical stress distribution for a regular panel geometry***

The stress distributions clearly show that the stresses on surrounding pillars are increased when the size of the central pillar is reduced. The magnitude of the APS on the central pillar is 4.96 MPa for 5 laminations, and 5.35 MPa for 10 laminations, representing an increase from the regular geometry of 11.6 per cent and 17.1 per cent respectively. This yields safety factors of 1.11 and 1.02. These translate to a maximum deviation from TAT (using a TAT stress based on nominal panel pillar dimensions) of 34 per cent or (using a TAT stress based on the individual pillar dimensions) of 65 per cent.

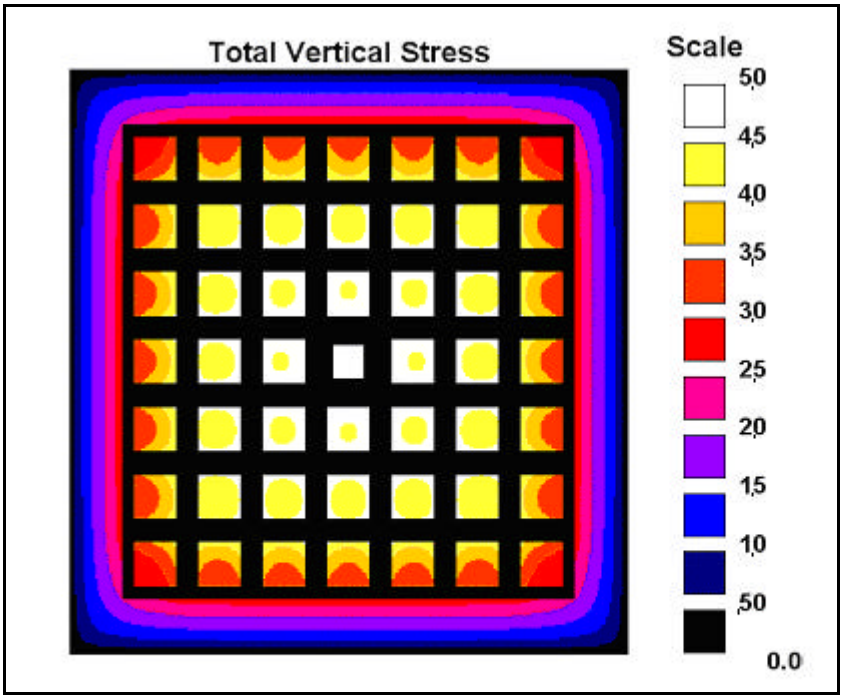


***Figure 5–12 Vertical stress distribution for same geometry with a small central pillar***

An analysis was then conducted with the same regular geometry with a smaller pillar placed at the corner of the model. TAT cannot be used to estimate the stress on this pillar as it resides so close to the abutment that stresses are expected to be much lower than those at the centre of the panel. The APS for the full-size corner pillar in a regular geometry is 2.63 for 5 laminations, and 3.07 for 10 laminations. The stress distribution for the reduced corner pillar geometry is presented in Figure 5–13.

Examination of stresses in the region of interest show that the stresses in the abutment adjacent to the corner pillar are increased slightly. The APS on the small pillar is reduced in the 5 lamination case by 6.6 per cent lower, and in the 10 lamination case, by 0.6 per cent compared to a full size corner pillar.

This exercise has demonstrated how stresses are distributed in a panel with an irregular geometry. Pillars or abutments adjacent to smaller pillars absorb more load in that particular region. The amount of load taken by the adjacent supports is dependent on the overburden stiffness and relative dimensions of the pillars. The resultant distribution may result in the pillar in question seeing less APS than a full size pillar in the same geometry (as seen in the corner pillar model).

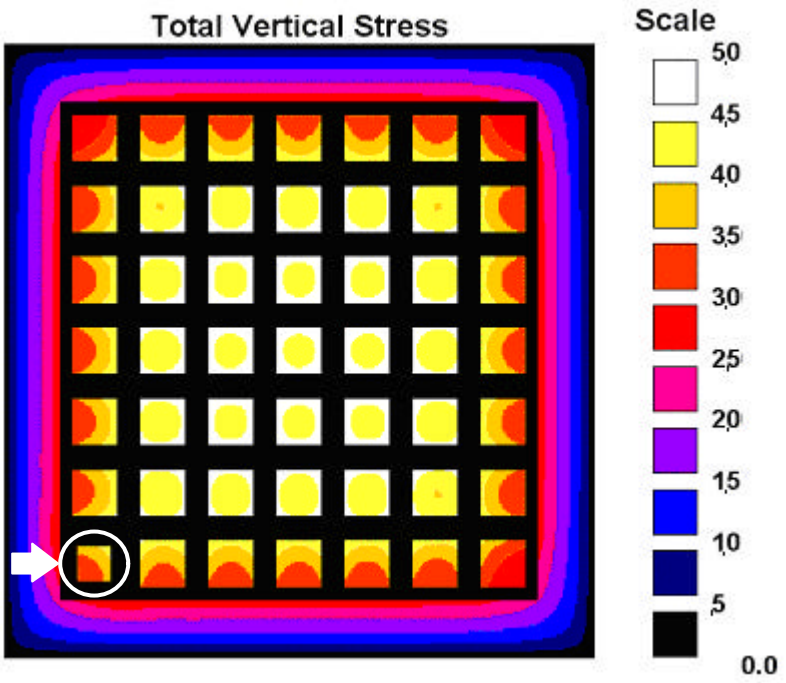


***Figure 5–13 Vertical stress distribution for same geometry with a small corner pillar (indicated)***

***Table 5–1 LAMODEL APS for regular and irregular geometries***

| Model | Maximum APS (Num. Modeling) [MPa] | Safety factor | Difference from regular geometry [%] | APS (model) / APS(TAT) [%] |
|---|---|---|---|---|
| Regular geometry | | | | |
| Central pillar | | | | |
| 5 layers | 4.439 | 1.41 | - | 96.7 |
| 10 layers | 4.569 | 1.37 | - | 99.5 |
| Corner pillar | | | | |
| 5 layers | 2.632 | 2.08 | - | N/A |
| 10 layers | 3.070 | 1.78 | - | N/A |
| Small central pillar | | | | |
| 5 layers | 4.956 | 1.11 | + 11.6 | 108 or 60.7* |
| 10 layers | 5.351 | 1.02 | + 17.1 | 117 or 65.5* |
| Small corner pillar | | | | |
| 5 layers | 2.496 | 2.19 | - 6.6 | N/A |
| 10 layers | 3.049 | 1.80 | - 0.7 | N/A |

* The first TAT estimate is calculated using the panel pillar dimensions, giving a TAT stress of 4.59 MPa. The second is obtained using the individual pillar dimensions, giving a TAT stress of 8.165 MPa.

Comparison with TAT calculations show over-estimation of stress by as much as 34 per cent using pillar dimensions, or an under-estimation of up to 17 per cent using nominal panel

dimension. This indicates that TAT cannot be used to estimate pillar stresses in pillars which deviate in size from the regular geometry. LAMODEL, or any other appropriate numerical modelling code, is the simplest way to estimate pillar loads for such irregular panel geometries.

## 5.10 Comparison between plane strain models and LAMODEL

The relationship between the physical and numerical representation of a laminated overburden is investigated in this section. Plane strain models were generated using the ELFEN and Phase$^2$ finite element programs and an equivalent model was generated using LAMODEL. Various lamination thicknesses were applied to all models.

ELFEN and Phase$^2$ are fundamentally different finite element implementations, however the results were expected to be similar. ELFEN employs discrete element capabilities in an explicit dynamic algorithm. A model is typically made up of a number of elastic or plastic discrete bodies (made up of finite elements) which interact via automatically activated contact laws. Analyses are dynamic, but once a steady state has been achieved, the solution is effectively static. Phase$^2$ is an implicit code. Contact is managed by introducing bi-directional springs between adjacent contacts – no contact searching is employed. The solutions are always steady state and contain no dynamic components, though staging is possible.

### 5.10.1 Model descriptions

The model represents a series of five rib pillars extending infinitely. Pillars and bords were 6.0 m in width. The seam height was 3.0 m and the depth to the centre of the panel was 50 m. In LAMODEL, the ribs extend to the maximum dimension possible (400 grid units at 1.0 m grid size). Symmetry conditions were applied on all four boundaries to ensure consistency with the plane strain models. The model is illustrated in Figure 5–14. The model was run with 5, 10 and 20 laminations in the overburden.

For all analyses, the overburden density was 2500 kg/m$^3$. The extraction ratio for this geometry is simplified to w/C, as the panel “length” is eliminated from the calculation. This yields a 50 per cent extraction. Note that half-bords are modelled at either end of the panel to ensure a regular geometry so that comparison with the TAT prediction is possible.

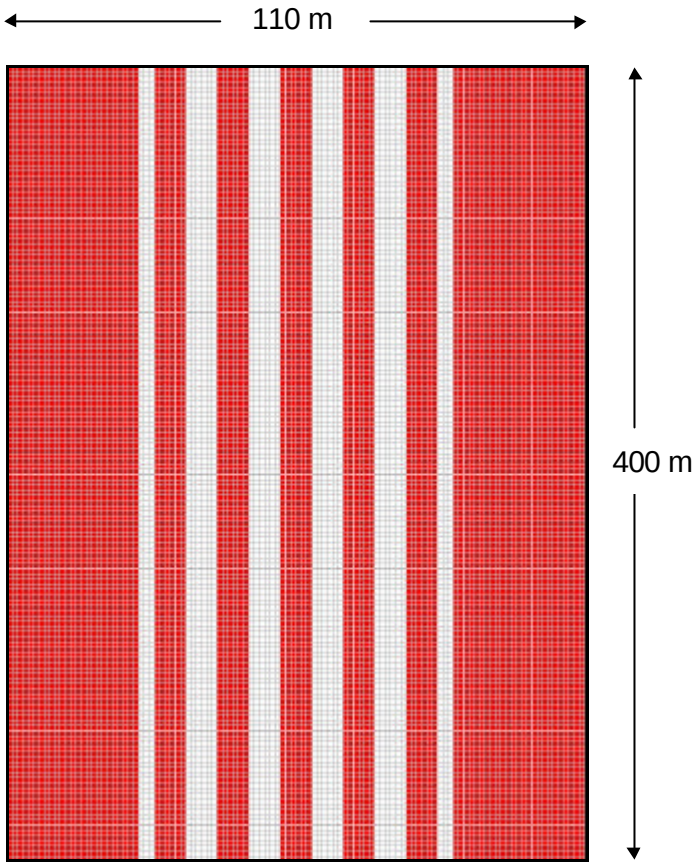


***Figure 5–14 LAMODEL rib pillar model***

The equivalent finite element model (for five laminations) is illustrated in Figure 5–15. The overburden for this particular case was represented by five layers, separated into discrete bodies in the ELFEN analysis, and connected via elastic springs in the Phase$^2$ analysis. The panel was represented by a series of solid and void regions within the coal seam, making up the rib pillars. All features are assumed (due to the plane strain specification) to extend infinitely into the plane. Gravity loading was applied in the vertical direction. Horizontal symmetry conditions were applied along the vertical boundaries.

Models without laminations were also generated to compare laminated and un-laminated results. A single-body model (with no contacts anywhere) was created to simulate a solid overburden or an overburden with infinitely stiff contacts. To further understand the effect of contacts, an additional model was generated with a solid overburden and only two contact planes, located above and below the seam. Models with 10 and 20 laminations in the overburden were also generated. Runs were also conducted with a $30^O$ friction angle applied to the contacts of the 10-lamination model.

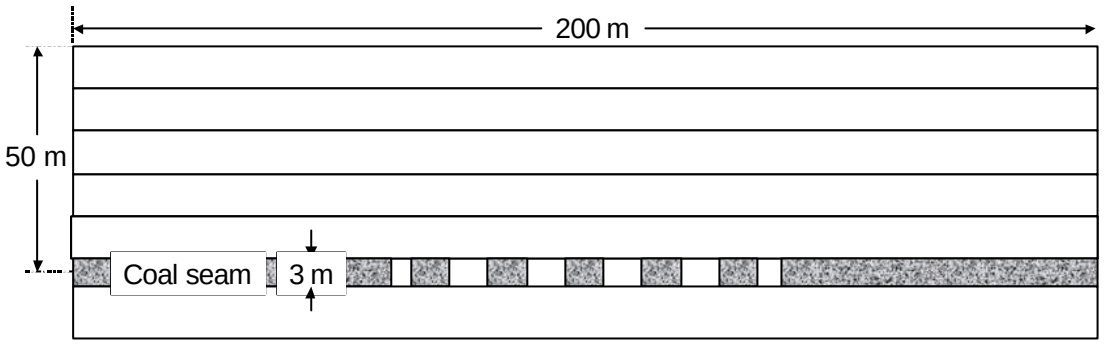


***Figure 5–15 Plane strain rib pillar model***

## 5.10.2 Results

Table 5–2 presents the average pillar stresses for analogous models simulated by LAMODEL, Phase$^2$ and ELFEN.

***Table 5–2 Comparison of APS for different numerical models***

| Number of laminations | Maximum APS (ELFEN) | Maximum APS (Phase$^2$) | Maximum APS (LAMODEL – with surface effect) | Maximum APS (LAMODEL – NO surface effect) |
|---|---|---|---|---|
| None (solid model) | 2.15 | 2.13 | - | - |
| None (seam contact) | 2.01 | 1.97 | - | - |
| 5 | 2.29 | 2.29 | 2.532 | 2.470 |
| 10 | 2.38 | 2.40 | 2.538 | 2.492 |
| 20 | 2.42 | 2.43 | 2.526 | 2.499 |
| 10 with $30^0$ friction | 2.05 | 2.11 | - | - |

Trends are as expected for all models except the LAMODEL results with surface effect activated. In these LAMODEL simulations APSs are greater than tributary area predictions and also the trend for APS to increase with increasing number of laminations is not present – the result for 10 laminations shows the greatest stress, while the lowest is observed for 20 laminations. This is both counter-intuitive and opposite to trends within the plane strain results. The LAMODEL analyses without surface effect show the correct trend, but the stresses are consistently greater than the plane strain results. This discrepancy amounts to less than 8.0 per cent for the same geometries with laminations but is as high as 21 per cent for the same geometries without laminations or with friction included.

Comparing the plane strain analyses, pillar stresses differ by less than 3 per cent for all runs. The largest discrepancy is observed where friction is introduced. Looking more closely at these

results, the distributions of vertical stress along the pillar centre-line are presented for both ELFEN and Phase$^2$ in Figure 5–16 and Figure 5–17 respectively. For all the results where frictionless layers are present, the stress distributions across the pillar are similar both qualitatively and quantitatively with the 20 layer model having the highest stresses. The maximum stress is at the edge of the pillar. Where friction is introduced, and where there are no laminations, the distributions show a change in character. The highest stress in the ELFEN analyses moves from the edge of the pillar to approximately 0.8 m from the pillar edge. Stresses then decrease towards the pillar edge. This effect is even more pronounced in the Phase$^2$ results. The highest stress is recorded at the centre of the pillar, and the lowest stress at the pillar edge. The minimum edge stress is only 16 per cent of the average stress for the solid body model (without laminations).

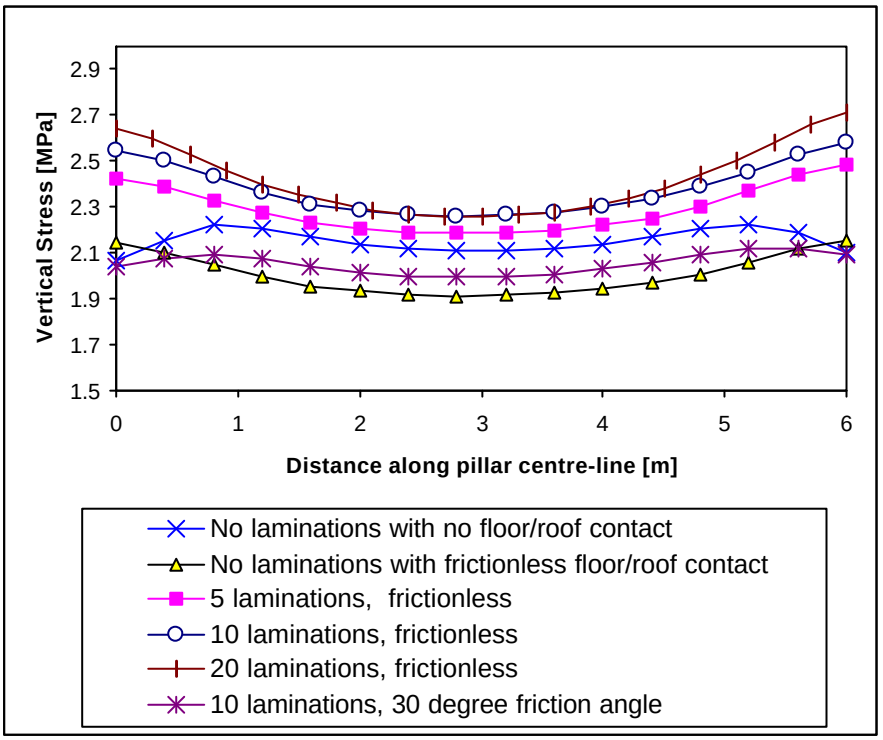


***Figure 5–16 Vertical stress distributions within central pillar for ELFEN analyses***

Vertical stress distributions for LAMODEL are presented in Figure 5–18. The distribution of stresses across the pillars in LAMODEL is parabolic with the maximum stress at the pillar edge as with the other codes. A 2$^{nd}$ order polynomial may be used to approximate the distributions to within a 0.07 per cent error. With decreasing overburden stiffness (increasing number of laminations), the distributions become more concave, varying for 20 laminations by 0.65 MPa, which is much greater than in the other codes, and by 0.175 MPa for 5 laminations.

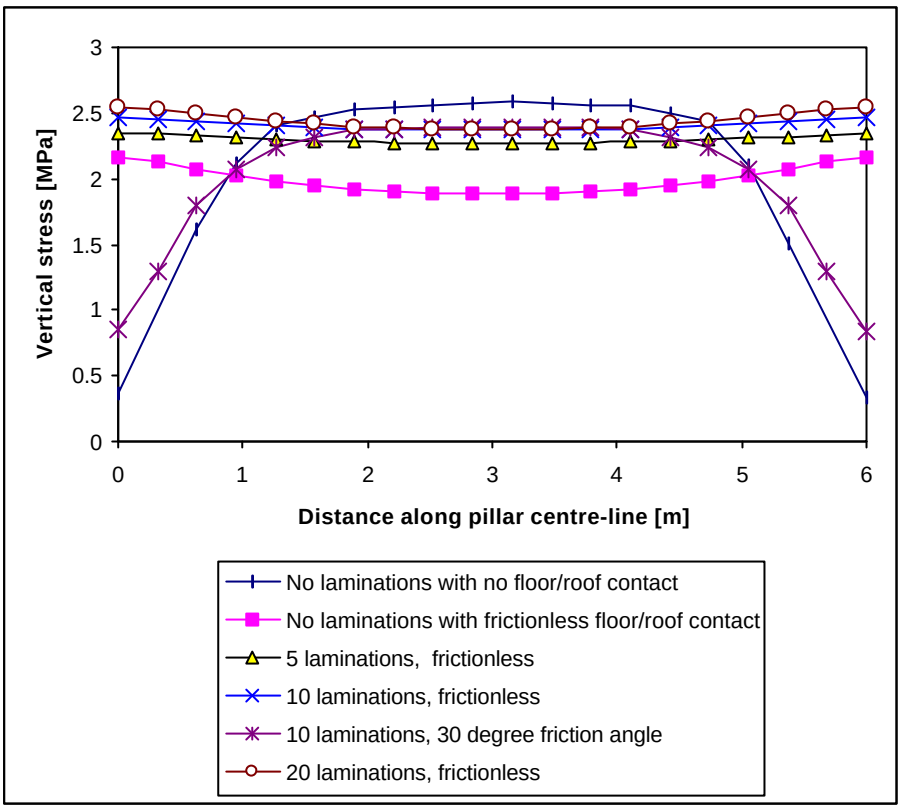


***Figure 5–17 Vertical stress distributions within central pillar for Phase² analyses***

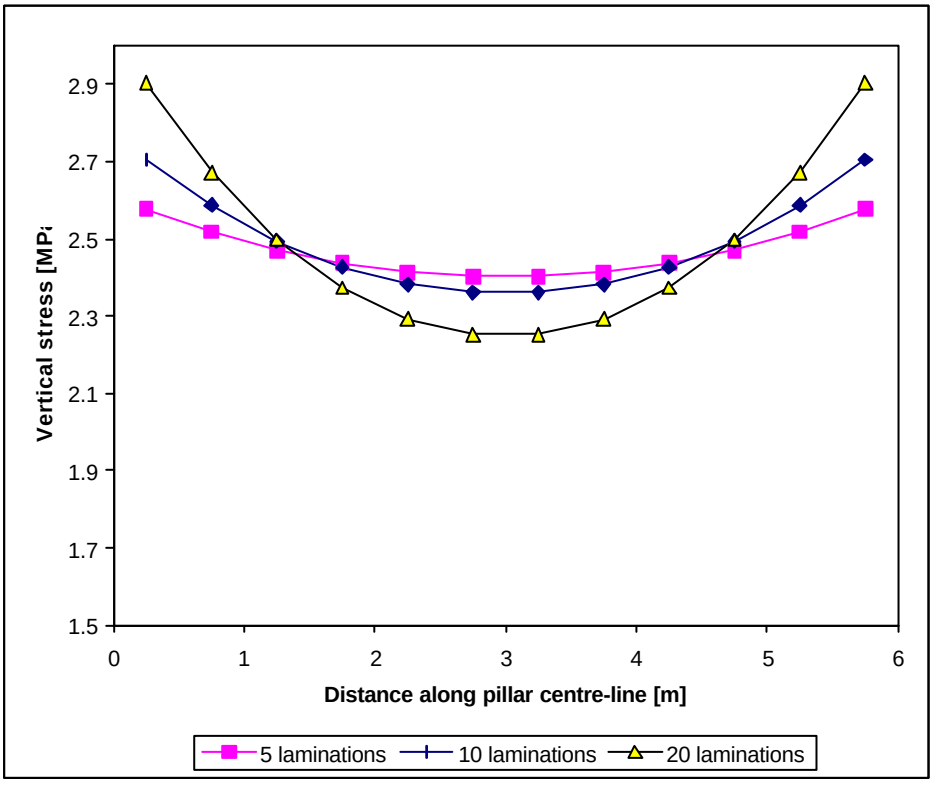


***Figure 5–18 Vertical stress distributions within central pillar for LAMODEL analyses***

Where pillar stresses are increased due to the condition or stiffness of the overburden, it is expected that that the associated abutment stresses will be lower, and vice versa. This tendency was evaluated by calculating the average abutment stress for all models.

The distribution of vertical stresses within the abutments are presented in Figure 5–19 (LAMODEL), Figure 5–20 (Phase$^2$) and Figure 5–21 (ELFEN). Note the different scales along the X-axis. The right-hand side of all the graphs (greatest x value) represents the edge between the abutment and the panel. The LAMODEL stresses were measured in the centre of the panel, i.e. along a horizontal line at 200 m on the vertical scale indicated in Figure 5–14. The ELFEN and Phase$^2$ stresses were measured along the horizontal centre-line of the seam horizon.

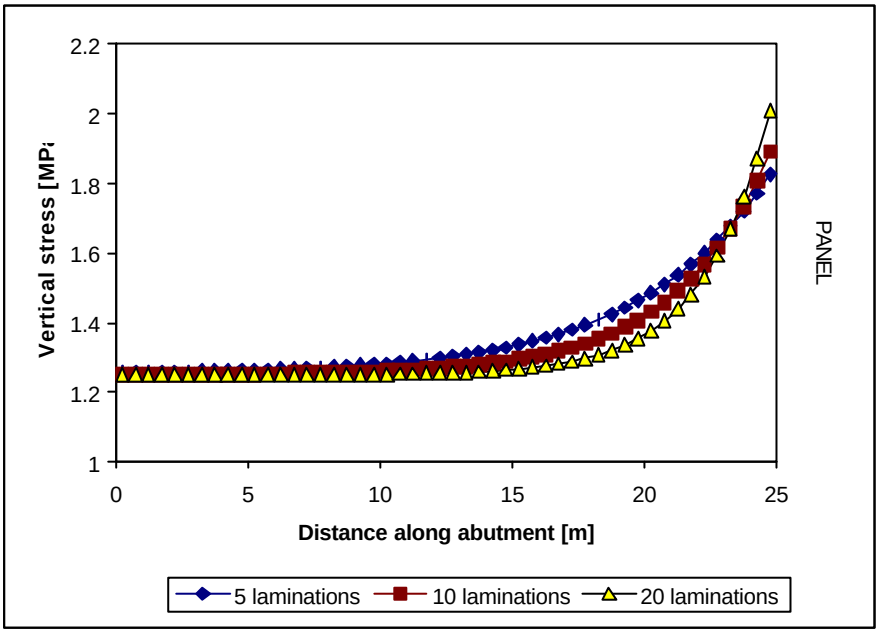


***Figure 5–19 LAMODEL - Vertical stress distribution within abutment***

The ELFEN and LAMODEL analyses show stabilisation of the abutment stress at approximately 15 to 25 m into the abutment. The far-field behaviour of the abutment in the Phase$^2$ analyses was skewed by unexpected movements of unconstrained nodes, hence the reduced trend towards a constant stress value. Despite this apparent inconsistency between models, the distance between the panel and the edge of the model was large enough so that pillar stresses were unaffected.

Distribution of abutment stresses is consistent for most of the frictionless models, but deviates where friction or solid “welded” contacts are introduced. As observed in the in-pillar stress distributions, vertical stresses decrease at the edges of the abutment. This effect is seen extending less than 1.5 m into the ELFEN abutment, and up to 10 m into the Phase$^2$ abutments.

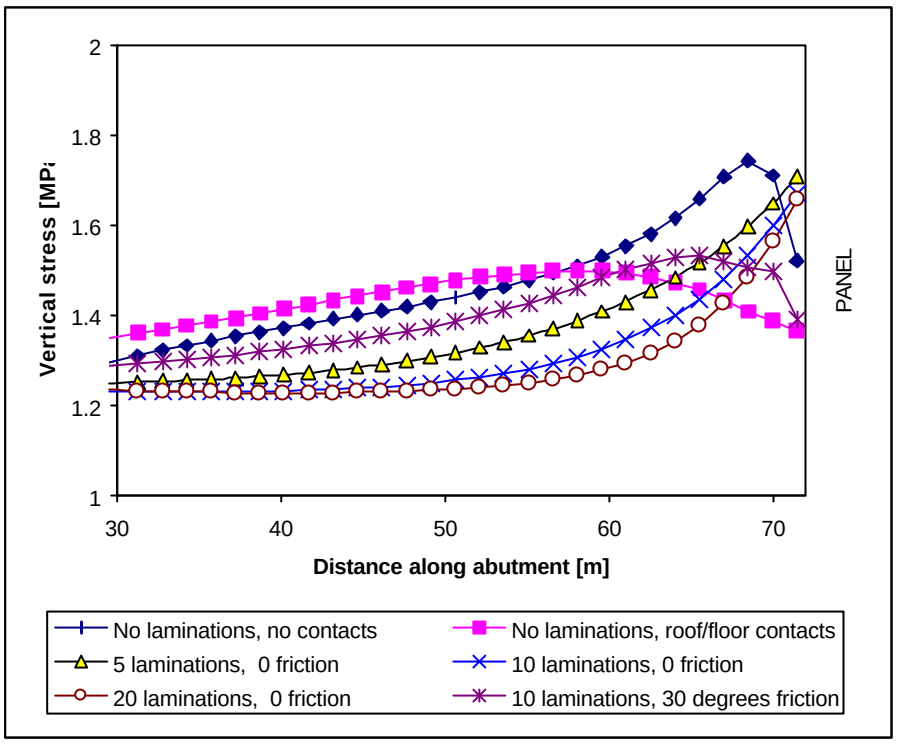


***Figure 5–20 Phase$^2$ - Vertical stress distribution within abutment***

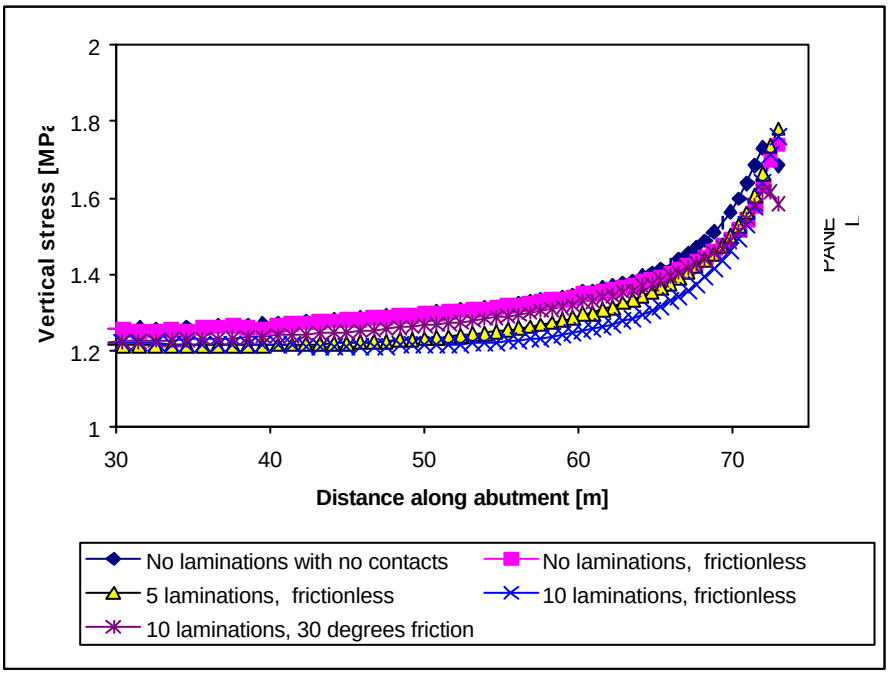


***Figure 5–21 ELFEN - Vertical stress distribution within abutment***

Trends within the abutment stress distributions are investigated by comparing the average abutment stresses, obtained by averaging vertical stress across the entire abutment. These values are presented in Table 5–3. As stated above, it was expected that abutment stresses would decrease with increasing pillar stress (for the same depth and geometry). This trend is

evident in both finite element models and in the LAMODEL results. The appearance of this trend in the LAMODEL results occurs when surface effect is included and is not meaningful, as the pillar stresses do not show the associated trend of increasing pillar stress with decreasing overburden stiffness.

***Table 5–3 Summary of results for all codes***

| Code | Number of laminations | Friction angle | Maximum APS [MPa] | Average abutment stress [MPa] | Maximum tensile stress [MPa] |
|---|---|---|---|---|---|
| ELFEN | None (no con.) | - | 2.15 | 1.33 | 0.45 |
| | None (seam con.) | - | 2.01 | 1.32 | 0.71 |
| | 5 | - | 2.29 | 1.29 | 0.8 |
| | 10 | - | 2.38 | 1.27 | 0.94 |
| | 20 | - | 2.42 | 1.27 | 1.58 |
| | 10 | 30 | 2.05 | 1.30 | 0.67 |
| Phase[2] | None (no con.) | - | 2.13 | 1.34 | - |
| | None (seam con.) | - | 1.97 | 1.40 | - |
| | 5 | - | 2.29 | 1.33 | - |
| | 10 | - | 2.40 | 1.29 | - |
| | 20 | - | 2.43 | 1.28 | - |
| | 10 | 30 | 2.11 | 1.32 | - |
| LAMODEL (with surface effect) | 5 | - | 2.53 | 1.37 | - |
| | 10 | - | 2.53 | 1.35 | - |
| | 20 | - | 2.52 | 1.33 | - |
| LAMODEL (no surface effect) | 5 | - | 2.47 | 1.37 | - |
| | 10 | - | 2.49 | 1.35 | - |
| | 20 | - | 2.49 | 1.33 | - |

With decreased overburden stiffness, it is expected that the roof deflections would increase and that the extent and magnitude of associated tensile stresses over the bords would also

increase. The ELFEN results confirm this; increased maximum tensile stress with decreasing overburden stiffness can be seen in Appendix 1 Distributions of tensile stresses.

Where friction is introduced in the 10-layer model, the overburden stiffness is effectively increased such that the maximum APS is similar to that of the solid model. The main difference between these two models and the frictionless runs is that the pillar stress distribution is altered so that lower stresses are recorded at the edges of the pillars. The reasons for this are related to the nature of the loading and resultant distribution of horizontal stresses.

In the case of the frictionless models, the pillar is effectively being loaded uni-axially. Tangential loads (which manifest as horizontal stresses) cannot be transferred through the frictionless contact. From examination of the shape of the pillars in the different models, (frictionless: Figure 5–22, solid contacts: Figure 5–23), it is evident that the mechanisms by which these pillars are loaded are very different.

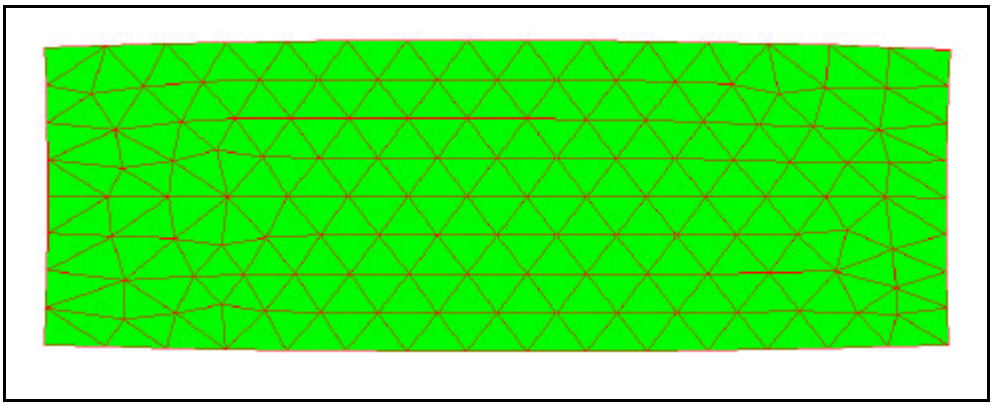

***Figure 5–22 Deformed shape of pillar for model with frictionless floor/roof contact (X 500)***

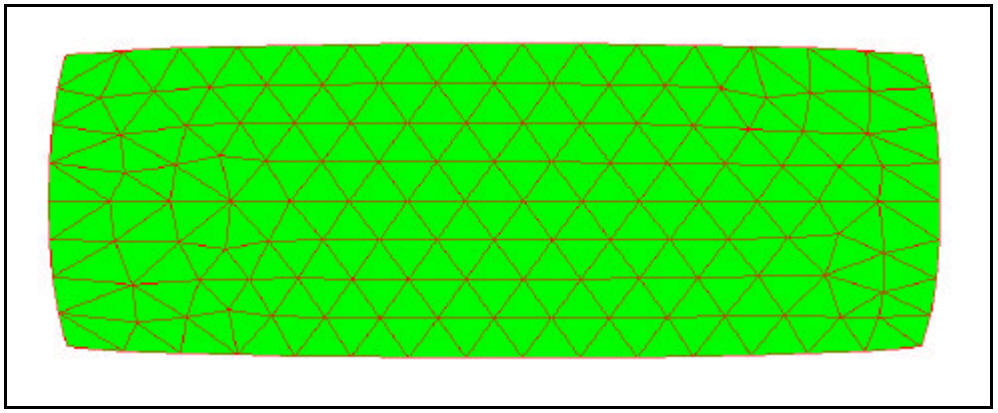

***Figure 5–23 Deformed shape of pillar for model with no contacts (X 500)***

The pillar with frictionless floor and roof contacts has expanded laterally as a result of imposition of vertical stresses. Horizontal stresses therefore arise from the Poisson effect only. The horizontal displacements are greatest where the vertical displacements are greatest, i.e. at the floor and roof contacts, hence the pillar does not bulge convexly in the centre. This lack of "attachment" also reduces the stress concentrations expected at the corners of excavations.

The solid model does show bulging of the pillar, as well as significant stress concentrations at the corners of the pillar. Loads are transferred to the pillar freely, allowing development of stresses within the pillar at any angle relative to the floor and roof plane. This is demonstrated in Figure 5–24 and Figure 5–25, which show the principal stress vectors for the frictionless and solid model respectively. Horizontal stresses (i.e. non-vertical principal stress vectors) within the pillar are visible only in the solid model. In the frictionless contact model, inclined principal stresses above and below the pillar are not transferred into the pillar at all but result in vertical loading only.

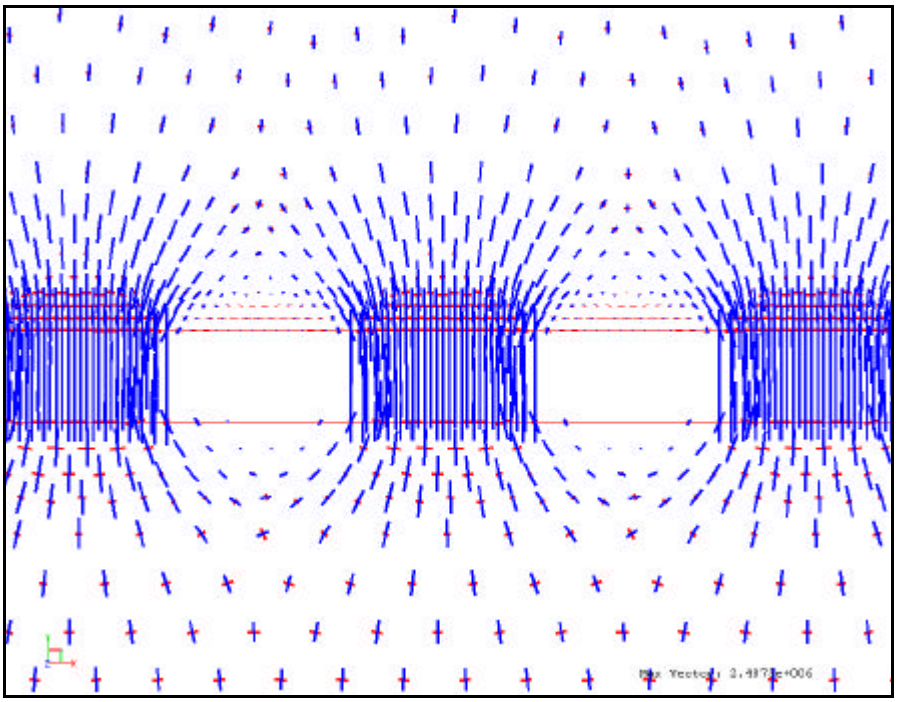

***Figure 5–24 Principal stress vectors for frictionless roof/floor contact***

The horizontal stress distributions along the pillar mid-height lines for these models also show this trend (Figure 5–26). Not only is the distribution more constant for the frictionless models, but the magnitude of stresses is at least an order of magnitude less than for the case with friction, or for the solid model.

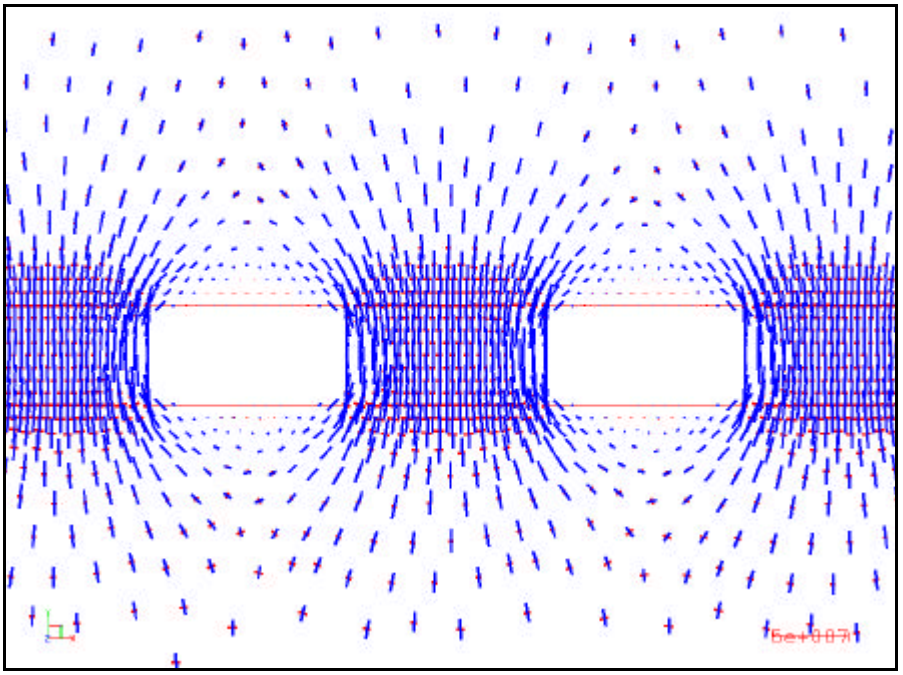

***Figure 5–25 Principal stress vectors for solid model with no contacts***

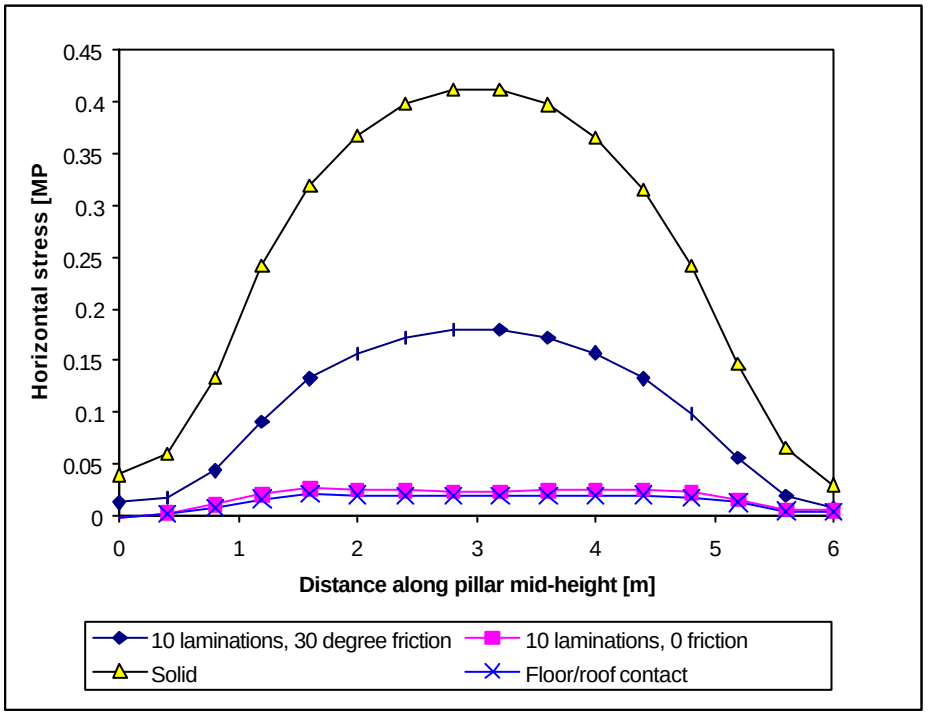


***Figure 5–26 Horizontal stress distributions in ELFEN models with and without friction (and welding).***

The representivity of LAMODEL has also been called into question with regards the assumption that all lamination interfaces are frictionless. This means that slip can occur anywhere within the overburden strata. Where friction is present, it is believed that slip only occurs where possible according to the excess shear stress (ESS) criterion. This criterion is expressed as follows:

$$ESS = \left| t_{xy} \right| - m\, s_{yy} \qquad (5\text{-}1)$$

Where $t_{xy}$ is the shear stress

$ì$ is the coefficient of friction (tangent of the friction angle)

$ó_{yy}$ is stress perpendicular to the laminations (vertical stress)

A positive value of ESS indicates that the incipient shear stress is greater than the frictional resistance to slip. Values of ESS are plotted for the solid overburden model, assuming a friction angle of $30^0$ ($ì$ = 0.57735), in Figure 5–27. Only positive values are contoured, which in this case shows that slip is only possible above the bords and up to 3 m into the roof. This implies that slip is only possible on laminations which lie (at most) 3 m above the seam horizon.

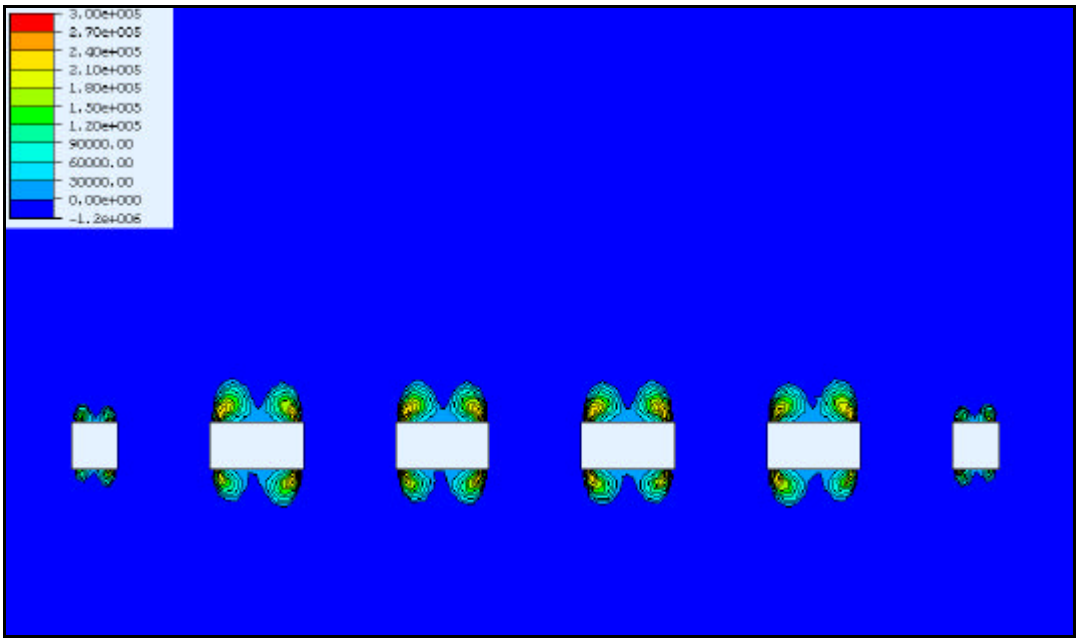


***Figure 5–27 ESS contours for solid overburden model***

The amount of slip was investigated by extracting the relative horizontal displacements along the first lamination interface above the seam for the 10 layer model. This layer is 5 m above the seam horizon, where no slip is expected for the $30^0$ friction model. Relative horizontal displacements indicate the amount of slip along the plane. The resultant amount of slip for both the frictionless and $30^0$ friction model is presented in Figure 5–28. It is clearly evident that the slip in the $30^0$ friction model is negligible in comparison to the slip in the frictionless model, indicating that the ESS criterion is valid for this case.

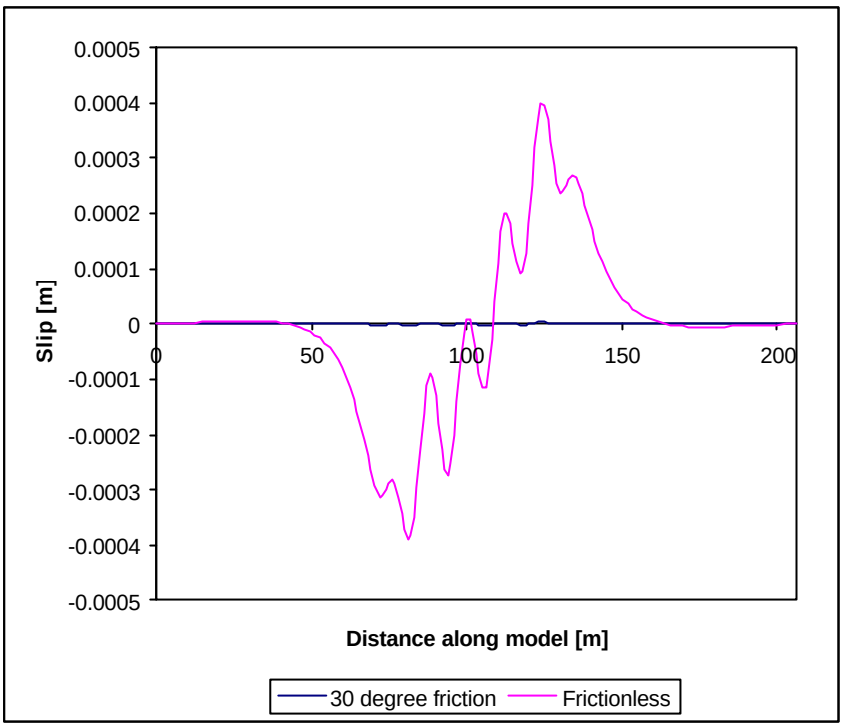


***Figure 5–28 Slip along the first lamination interface above the seam horizon for the 10 layer model***

## 5.11 Three dimensional investigation

A three dimensional model was constructed in ELFEN to assess whether similar trends observed in the previous section are discernible in a model with a bord and pillar configuration. The model is similar to the 2D models in that a 3 m thick seam is modelled at 50 m depth (to mid-height of seam) overlain with 10 frictionless laminations. The five pillars and bords are 6 m with 40 m abutments on all sides. The seam geometry is illustrated in Figure 5–29. The model consists of 113 798 3D linear tetrahedral elements (pyramids), which are standard to the ELFEN suite. TAT predicts a maximum APS of 5 MPa for this geometry.

The stress distributions from the model are presented in Figure 5–30. Compressive stress is negative in this plot. The maximum APS is 4.4 MPa, which is 88 per cent of TAT. An equivalent model was generated in LAMODEL, yielding a maximum APS of 4.78 MPa, or 96 per cent of TAT. The vertical stress distribution is presented in Figure 5–31. The difference between the ELFEN and LAMODEL results is 8 per cent. The stress distributions are qualitatively similar.

This example has demonstrated the applicability of 3D ELFEN models to estimating pillar loads. It should be noted that run times for this model were approximately 6 hours, compared to around 1 minute for LAMODEL analyses.

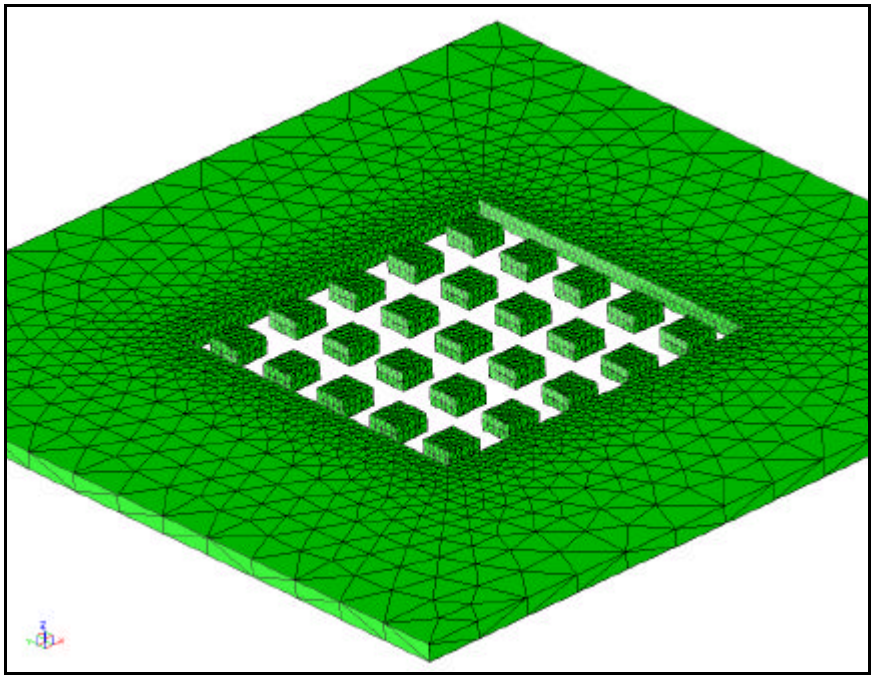

*Figure 5–29 Seam geometry for the 3D model*

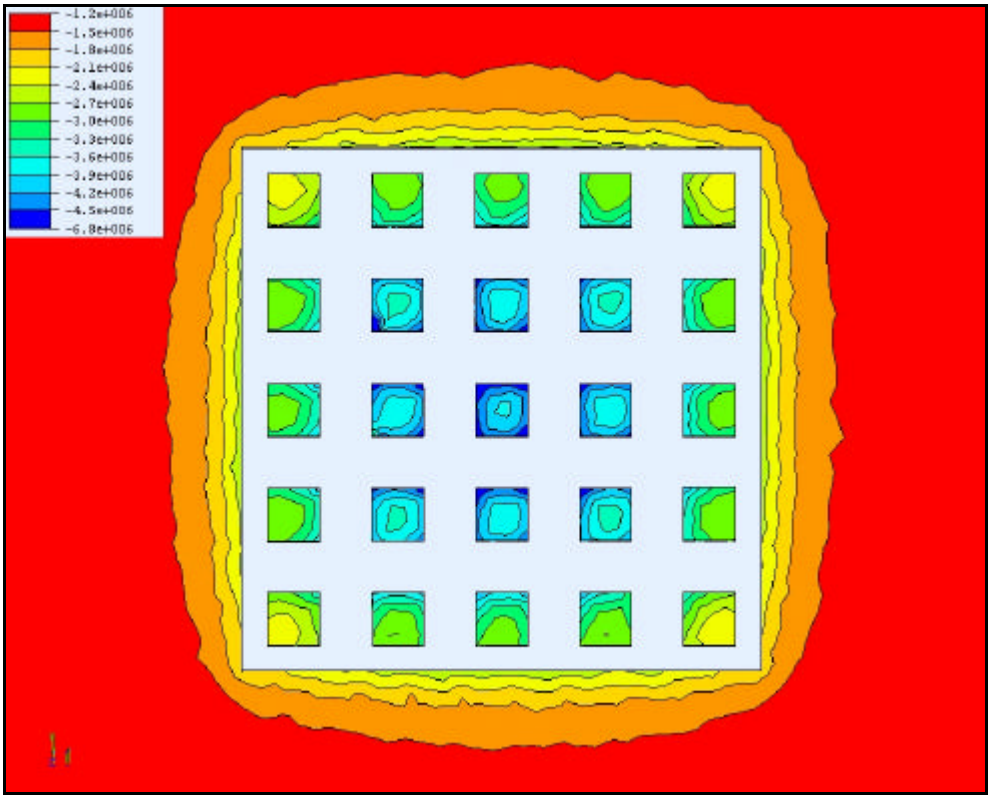


*Figure 5–30 Vertical stress distribution for the 3D model*

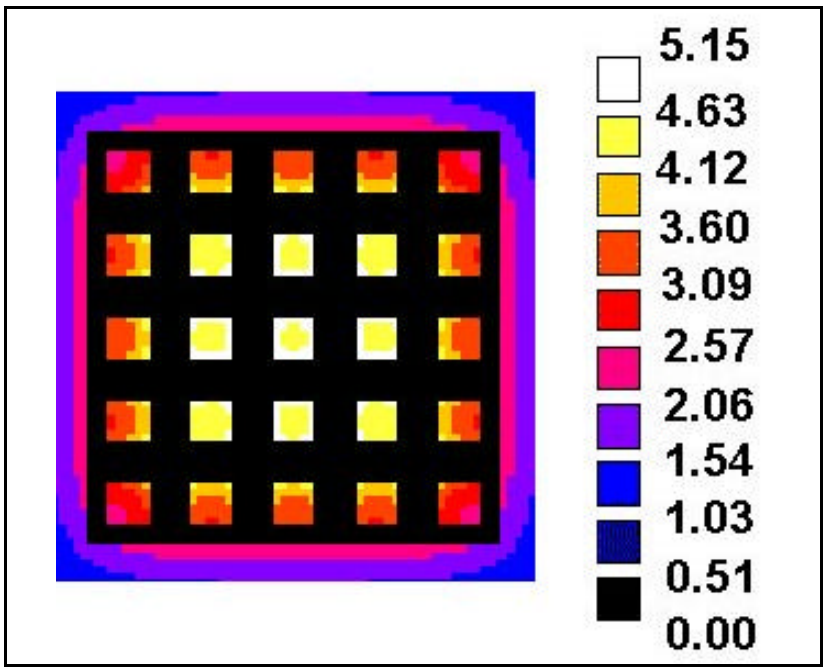


***Figure 5–31 Vertical stress distribution for the LAMODEL equivalent of the 3D model***

## 5.12 Discussion and conclusions

The effectiveness of boundary element codes in modelling tabular excavations has been investigated. Adjustment of the overburden stiffness by introducing a series of frictionless laminations has been studied in this report with the LAMODEL program. Sensitivity analyses showed that a decrease in the stiffness of the overburden results in an increase in the maximum average pillar stress, as expected. The number of laminations in the overburden and the modulus of the overburden both contribute to the overburden stiffness. These parameters were found to influence APS by less than 0.9 per cent. Seam stiffness was found to have an even smaller effect on the pillar stresses – less than 0.5 per cent.

It was only at high extraction ratios, low overburden stiffness and increased depth that the LAMODEL results deviated significantly from TAT prediction. For example, at a depth of 200 m (twice the panel span), an extraction of 0.96 and with 10 laminations in the overburden, the APS was only 72 per cent of TAT. For practical extraction ratios (40 to 60 per cent) the maximum deviation is less than one per cent. This indicates that the use of LAMODEL to better estimate pillar loads *for a regular geometry* is not necessary, as TAT gives a similar estimate. It is proposed that LAMODEL is better suited to estimating pillar loads in panels with irregular pillar sizes and shapes. LAMODEL also has the capability to include surface topography and may be used to estimate subsidence.

The inclusion of free surface effects in the LAMODEL analyses gave incorrect results. All results showed pillar stresses larger than the TAT prediction, with APS's up to 3.4 times greater than those calculated using TAT. The stresses were also found to decrease with decreasing overburden stiffness, contradicting both theory and the other numerical results. It must be assumed that the finite depth option within LAMODEL does not work correctly. Whether this is due to the nature of the numerical formulation for finite depth or due to a program bug has yet to be determined.

The plane strain models confirmed that pillar stresses increase with decreasing overburden stiffness. It was also shown that abutment stresses have an inverse relationship to pillar stresses. The results from the plane strain analyses were comparable, differing by less than 3 per cent for all runs. The physical representivity of LAMODEL was evaluated by comparing results with analogous plane strain results. LAMODEL APS's were between 4 per cent and 8 per cent higher than for the plane strain results. In-pillar and abutment stress distributions were consistent with the plane strain results.

Note that stresses in all analyses did not exceed TAT, except where the surface effect was considered in LAMODEL. Also note that the plane strain models assume that "depth" refers to the depth to the mid-height of the seam – the point at which stresses are measured. In practice, "depth" refers to the distance from surface to the bottom of the seam. The nominal TAT stress for the plane strain models is therefore 2.575 MPa. The information from Table 5–2 is presented in Table 5–3, this time with the APS expressed as a factor of TAT for the nominal (51.5m) and actual (50m) depth.

For the particular geometry in question, and for the most practical case of a laminated overburden with non-zero friction, it is implied that TAT may over-estimate pillar loads by up to 21 per cent. This correlates well with work done on platinum pillars (GAP334), where modelled pillar stresses were found to be as low as 73 per cent of TAT. This result is particularly important as it indicates a significant over-estimation where practical mining parameters are employed in the model. This case also showed a decrease in the maximum vertical stress concentration, and a significant increase in the horizontal stresses within the pillar. At the pillar edges the vertical stress is reduced and the horizontal stress increased (relative to the frictionless case). This indicates that confinement of material within the pillar is increased, which will reduce the probability of localised failure (scaling). Other studies (GAP617) have also shown that the introduction of friction between the pillar and overburden will increase the post-failure stability of pillars.

The question remains whether it is possible to simulate an overburden containing cohesive and/or frictionally bonded layers with a stack of frictionless laminations, as in LAMODEL. It is possible that calibration will allow similar results to be obtained, but the effect of friction-bonded layers, especially in terms of in-pillar stress distribution, cannot be modelled. It has been shown that a significant amount of slip is not possible where, as demonstrated, a $30^0$ friction angle is applied to the contacts. LAMODEL allows slip to occur throughout the model, which is an assumption which cannot be reconciled with the case of friction bonded laminations. It should also be noted that there are mathematical limitations to the thickness of laminations that can be modelled – no less than 2 or 3 times the grid size and no greater than the depth. This means that the variation of overburden stiffness is limited, which may make calibration impossible. To fully answer the questions related to the representivity of LAMODEL, case studies should be undertaken.

***Table 5–4 Average pillar stress in relation to TAT***

| **Code** | **Number of laminations** | **Friction angle** | $\frac{APS_{(model)}}{APS_{(TAT)}}$ **(50m depth)** | $\frac{APS_{(model)}}{APS_{(TAT)}}$ **(51.5m depth)** |
|---|---|---|---|---|
| ELFEN | None (solid) | - | 86.0 | 83.5 |
| | None (seam con.) | - | 80.4 | 78.1 |
| | 5 | - | 91.6 | 88.9 |
| | 10 | - | 95.2 | 92.4 |
| | 20 | - | 96.8 | 94.0 |
| | 10 | 30 | 82.0 | 79.6 |
| Phase[2] | None (solid) | - | 85.2 | 82.7 |
| | None (seam con.) | - | 78.8 | 76.5 |
| | 5 | - | 91.6 | 88.9 |
| | 10 | - | 96.0 | 93.2 |
| | 20 | - | 97.2 | 94.4 |
| | 10 | 30 | 84.4 | 81.9 |
| LAMODEL (no surface effect) | 5 | - | 98.8 | - |
| | 10 | - | 99.7 | - |
| | 20 | - | 99.9 | - |

In summary, the following observations were made. Observed trends were consistent with expectations:

- Pillar stresses increase when the effective stiffness of the overburden is decreased (number of laminations increased).
- Abutment stress decreased with increasing pillar stresses
- Results from both the finite element codes and the boundary element analyses were not identical, but were qualitatively consistent
- Decreasing overburden stiffness and low friction resulted in increased tensile stresses between the laminations
- The introduction of friction in a regularly laminated overburden results in lower pillar stresses than for the frictionless laminations.
- Models with friction or solidly bonded models show a different in-pillar stress distribution to the frictionless models, resulting in lower average stresses.
- TAT is only applicable to regular geometries.

TAT has been shown to over-estimate average pillar stresses by as much as 22 per cent when friction is introduced on the lamination contacts in the models. Analyses with LAMODEL indicated a maximum over-estimation of less than 1 per cent in the practical range. It would seem that friction is a crucial parameter in determining pillar loads, and may have a significant influence in determining pillar strength as well. The practical applicability of this insight is, however, somewhat limited. Estimation of contact parameters in-situ is known to be very difficult. Not only is it difficult to determine these parameters for each contact layer into the roof, but it is also expected that these parameters may vary greatly over relatively short spans. Undulations and irregularities must be accounted for using an averaging process, which degrades the applicability of estimates or corrections of pillar loads based on contact parameters.

# 6.0 Implications for empirically derived strength.

As explained in the introduction to this report, meaningful deviations in real pillar loads as compared to those derived from the tributary area theory, may result in distorted conclusions relating to pillar strength that was derived using the tributary area theory to estimate the loads on failed pillars.

It has now been shown that while the variations in overburden stiffness and the W/H ratio do not result in substantial deviations in load estimates, the percentage extraction can have a meaningful effect if it exceeds 50%.

The extended database of failed pillars was examined to determine the possible deviation in load estimates by using the tributary area theory. The extended data base includes the original Salamon and Munro (1967) data base as well as pillar failures that occurred after 1965.

Figure 6–1 shows the normalised cumulative frequency of percentage extractions of the failed pillars.

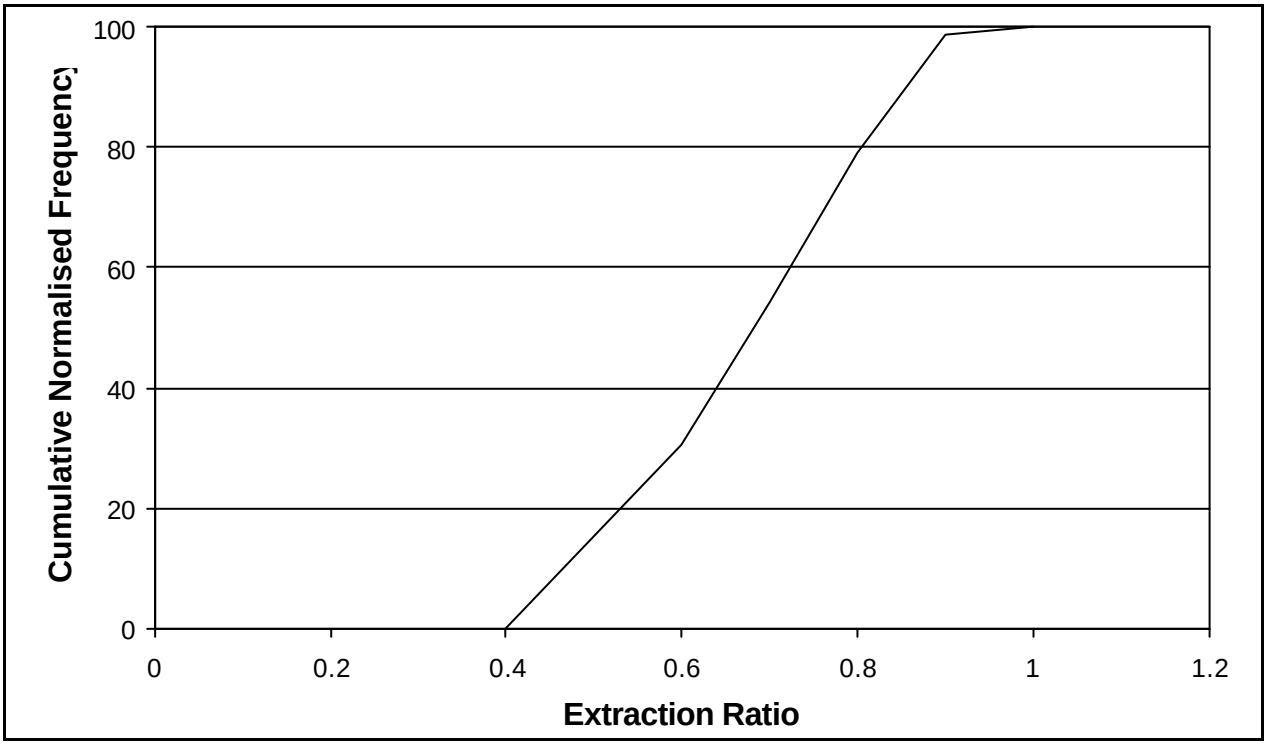


***Figure 6–1 Cumulative normalised frequency of failed pillar cases in the data base.***

The figure shows that 85% of the failed pillars had extraction of more than 50% and that approximately half of the pillars had extraction of more than 75%. This means that there would

be substantial differences between the pillar loads calculated with tributary area theory and those that would be obtained using numerical modelling.

At this stage, however, it is important to realise that the commonly used numerical models all utilise a continuous overburden, even if the constitutive model that is used is not linearly elastic. Before definitive statements regarding the applicability of tributary area theory in this regard can be made, it is necessary to investigate the nature of the overburden during pillar failure at shallow depth.

To supplement the investigation, the amount of overburden flexure necessary to cause pillar failure was investigated. Figure 6–2 shows the effective mining height of the failed pillars. The effective mining height is merely the real pillar height as recorded in the data base, multiplied by the extraction ratio and indicates the amount of subsidence that can occur at the level of the coal seam.

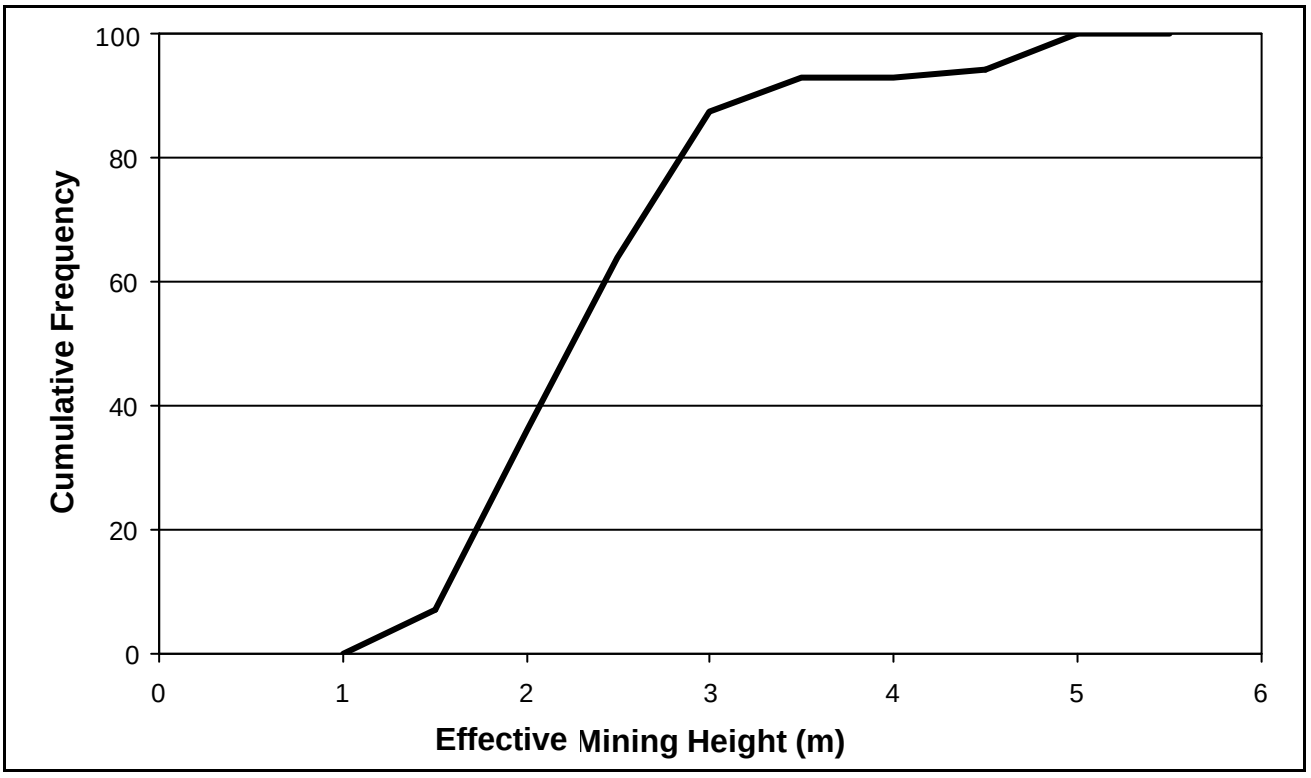


***Figure 6–2 Cumulative normalised frequency of the effective height of the failed pillars in the database***

The figure indicates that the there is a significant potential for subsidence (and therefore the possibility of substantial vertical displacement) at the pillar elevations at the time of failure. It has also been experienced in collieries that when pillars fail at shallow depth (comparable to the cases in the data base), it is accompanied by substantial subsidence of the surface. This is

confirmed by observation underground at the sites of failure that could be entered, where roof sag of more than a metre is commonly observed.

The next question to examine is whether it is possible for sedimentary rocks to deflect elastically to the extent that is required for complete pillar failure.

The following two fundamental equations for the behaviour of clamped beams can assist:

$$\sigma_t = \frac{gL^2}{2t}, \text{ and}$$

$$h = \frac{gL^4}{32Et},$$

where
$\sigma_t$ = tensile stress at edge of beam
$L$ = length of beam (or panel width),
$t$ = thickness of beam
$E$ = Modulus of Elasticity of beam
$h$ = maximum deflection at centre of beam

It can then be seen that

$$h = \frac{\sigma_t L^2}{L16Et}$$

which is an expression that relates the maximum deflection at the centre of the beam to the tensile stress at the end of the beam. Note that this holds true irrespective of the horizontal stress acting on the beam. It can be concluded that once the tensile stress exceeds the tensile strength of the beam, failure will occur and the beam will no longer be continuous. It is thus possible to determine the maximum elastic deflection of the beam prior to failure.

Substituting 8 MPa for $\sigma_t$ and 15 GPa for $E$, the equation can be simplified to

$$h = \frac{L^2}{60t}$$

Figure 6–3 shows the maximum deflections (as a factor of beam thickness) that can be tolerated before the beam fails and consequently beyond which it can no longer be considered as an elastic beam. The beam thickness varied from 5 m to 80 m and the panel spans from 100m to 300 m.

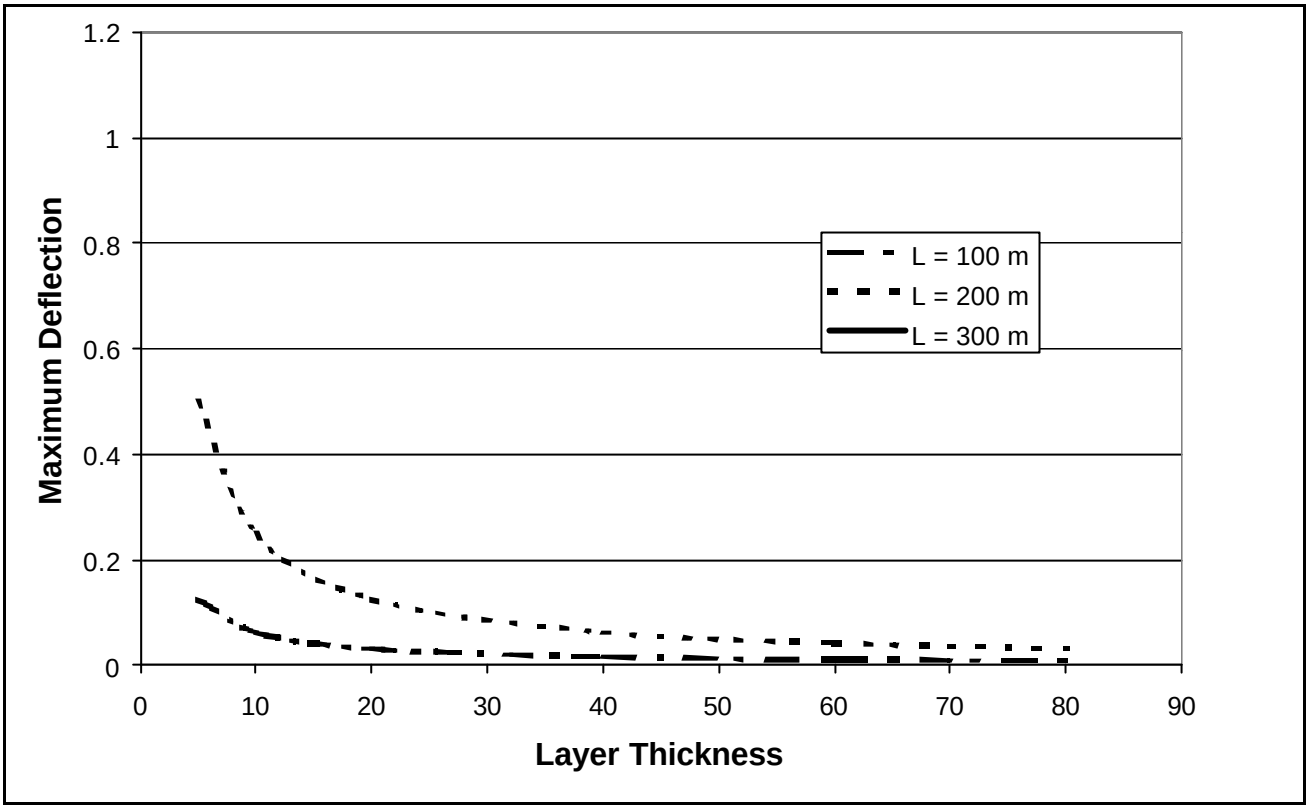


***Figure 6–3 Limits of applicability of elastic behaviour models for different beam thickness and panel spans.***

The figure shows that in the majority of cases, the maximum deflections are less than those, which could be expected in the observed cases of pillar failure.

There thus follows the very important conclusion that the overburden did not behave elastically in the cases where the pillars failed. Therefore, to use the common numerical codes to estimate pillar loads of the failed pillars, is not valid. Furthermore, because the overburden failed, the full overburden load acted on the pillars and consequently tributary area theory is valid for this situation. The only load reduction in this case, could result from the effects of friction of the overburden blocks as they slide down on to the pillars underneath.

For as long as the overburden remains solid, the numerical models probably yield pillar load results that are acceptably accurate. However, as soon as the overburden loses continuity, be it

due to geological factors or because the maximum deflection is exceeded, the numerical model results lose validity.

It is therefore not considered safe to use the pillar loads that are estimated by numerical modelling to calculate pillar safety factors that utilise the empirically derived pillar strengths of either Salamon and Munro (1967) or van der Merwe (1999). The reason is that once the overburden loses continuity, the pillar loads will increase and especially if the extraction ratio is high, the increase in pillar loads will be substantial. This is especially the case where Partial High Extraction such as pillar splitting or checker board stooping is done.

Models can still be used to estimate pillar loads for comparative purposes but not to calculate safety factors.

.

# 7.0 Conclusions

Literature review highlighted that previous work concentrated on coal pillar strength formulae, and little effort went into investigation of loading environment. The few that focused on coal pillar loads mostly applied the tributary area method. Other methods that have been proposed for the determination of pillar loads included the application of beam theory, analytical methods and photo-elastic modelling. These methods have not found much application in coal pillar design. The literature review also highlighted that despite its limitations, the tributary area theory is the most widely used for determining coal pillar loads. The main limitations of the tributary area theory and the conditions under which the method is valid have been presented in the text. It has been deduced that in addition to the panel width to depth ratio, the percentage extraction and the stiffness of the surrounding strata influence the validity of the tributary area method.

An underground test was conducted to assess the magnitude of changes in pillar stress. Various stress measurement devices were installed in test pillars just prior to mining. The stress changes were monitored and compared with numerical modelling results. It was found that stresses increased by between 0.3 MPa and 0.5 MPa and that the stresses stabilised after the final splits were cut. The numerical modelling codes using different codes showed similar trends, with an increase of between 0.5 MPa and 1 MPa.

Numerical modelling was employed to determine the influence of mining parameters on pillar loads. The overburden stiffness and seam stiffness were varied using the LAMODEL boundary element code. It was found that pillar loads decreased with increasing overburden stiffness. It was observed that abutment loads increase as pillar loads decrease. The greatest deviations from TAT were observed at large depths, high extraction and low overburden stiffness. However, it was noted that, for typical mining parameters, the deviation from TAT was less than one per cent. This indicates that LAMODEL is better suited to modelling irregular geometries, as the pillar loads are so close to TAT. The application of LAMODEL to irregular geometries was investigated. It was revealed that under-sizing of pillars may lead to a decrease of stress on that pillar and an increase on surrounding pillars, depending on the position of the pillar within the panel.

Finite element models were generated to assess the representivity of the LAMODEL boundary element code, which assumes no friction on stratigraphic parting. Friction was introduced in the overburden contacts in the Finite Element (FE) models, which resulted in APS's up to 21 per cent lower than estimated using LAMODEL, for a 50 per cent extraction. It was noted that

contact conditions, both along seam contacts and into the roof, can greatly influence pillar loads and the confinement within the pillar.

A formula for calculating pillar load was determined through a numerical modelling procedure. The formula contains overburden stiffness and the panel width-to-depth ratio as parameters.

In light of the observed over-estimation of pillar loads using TAT, the implications for the Salamon safety factor formula were examined. Analysis of the roof showed that failure of the immediate roof beam occurred in nearly all failed cases in the database. The resulting discontinuous beam results in full load distribution to individual pillars, exactly the conditions required by tributary area theory. This implies that pillar load estimations were accurate and that the safety factor formula, as it stands, is valid.

In conclusion from the results presented above it is obvious that pillar loading is a function of many parameters. These may be divided into two categories; those relating to the micro, and macro environments. Each one of these categories contains a number of parameters that have a significant effect on pillar loading.

Parameters which effect pillar loading in the micro environment are as follows:

- Pillar width, bord width, depth below surface and unit weight of overburden. The effects of these parameters are well known from the tributary area theory. However, there are also other factors which can effect pillar stresses. The most important of these is the contact friction between the pillar and the immediate roof.

In the macro-environment, the important parameters are:

- panel width, barrier pillar width, ratio of depth below surface to panel width, as well as the distribution of competent strata in the overburden.

The large number of parameters prohibits the use of an algebraic formula to estimate pillar loads. Estimates of pillar load, which do consider all of these parameters, can only be based on numerical modelling. The tributary area theory considers the worst-case scenario and is therefore the simplest and also the most conservative way of calculating pillar loads.

It should also be emphasized that when the safety factor concept was developed by Salamon and Munro (1967), the strength of collapsed and intact pillars was calculated by applying the likelihood function, and the load was calculated using tributary area theory. This indicates that

the “load” side of the safety factor equation is not accurate, which reflects on the accuracy of the calculated safety factor. It may be suggested that the data could be re-analysed to obtain more accurate estimates of load, however the available data is somewhat limited. Not all of the parameters listed above are available in the data. A more accurate estimate of pillar load is therefore not possible based on the data set.

It is therefore strongly recommended that for cases where an accurate estimate of pillar load is required, numerical modelling should be conducted using input parameters from the laboratory and an appropriate failure criterion for strength, such as Mohr-Coulomb.

Another important recommendation applies to irregular geometries. Tributary area theory should not be used to calculate the loading on irregular pillars, or on pillars within an irregular layout. Numerical modelling should be conducted and results should be used for a comparative evaluation. If accurate results are required and accurate input parameters are available then pillar loads can be determined quantitatively. In fact, numerical modelling is recommended as the best way to obtain accurate pillar stress estimates.

It was proposed that conservative estimates of pillar loads provided by the tributary area theory would result in an over-estimation of the strength of failed pillars in the Salamon database. Investigation of the roof integrity has shown that failure of the immediate roof beam occurred in nearly all failed cases in the Salamon database. This resulted in a discontinuous beam overlying the pillars, which would result in load distribution exactly described by tributary area theory. This leads to the very important conclusion that the load calculations in the database are accurate and that the safety factor formula is therefore valid.

# 8.0 References

**Brady, B. H. G. and Brown, E. T. (1993).** Rock Mechanics For Underground Mining, published by Chapman and Hall, London, pp 354-356.

**Dunnicliff, J. 1993**. Geotechnical instrumentation for monitoring field performance. John Wiley and Sons. New York.

**Geokon 2000.** Instruction manual. Vibrating wire readout. Geokon. Inc. Lebanon. U.S.A.

**Jaeger, J.C. and Cook, N.G.W. 1979**. Fundamentals of Rock Mechanics. Chapman and Hall. London.

**Jeremic, M. L. (1985)**. Strata Mechanics in Coal Mining. A. A. Balkema Publishers, Rotterdam, Netherlands, pp244-261.

**Mindata, 2001.** Yoke gauge instruction manual. Mindata. Seaford. Australia.

**Salamon, M. D. G. and Oravecz, K. I. (1976).** Rock Mechanics in Coal Mining. Chamber of Mines of South Africa, P.R.D. Series No. 198, 1976.

**Sheory, P. R. and Singh, B. (1974).** Estimation of Pillar Loads in Single and Continuous Seam Workings, Int. J. Rock Mech. Min. Sci., 11 : 97-102.

**Van Heerden, W.L**. Stress distribution in coal pillars. CSIR Restricted contract report for the coal mining research controlling council. Report MEG 798. CSIR.

**Van der Merwe, J. N. (1998).** Practical Coal Mining Strata Control. Second Edition, published by Itasca Africa (Pty) Ltd, Johannesburg.

**Wagner, H (1980).** Pillar design in coal mines. Journal of the South African Institute of Mining Metallurgy. January. pp 37-45.

**Wardle, L.J. and McNabb, K.E. 1985.** Stress monitoring during wongawilli extraction in 3 North panel, Laleham No. 1 Colliery, South Blackwater, Queensland. CSIRO report no. 59. CSIRO Australia.

# Appendix 1 Distributions of tensile stresses

Maximum tensile stress = 0.71 MPa

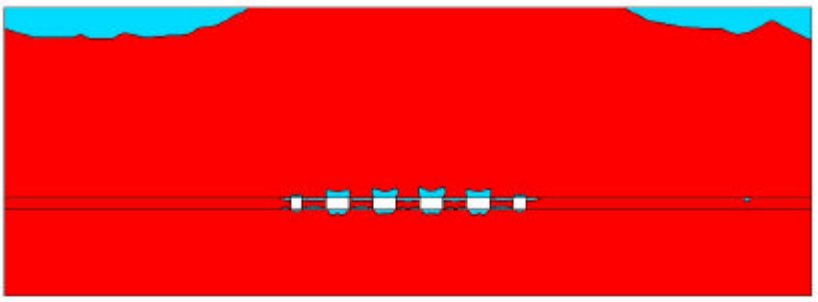

**No laminations Frictionless**

Maximum tensile stress = 0.8 MPa

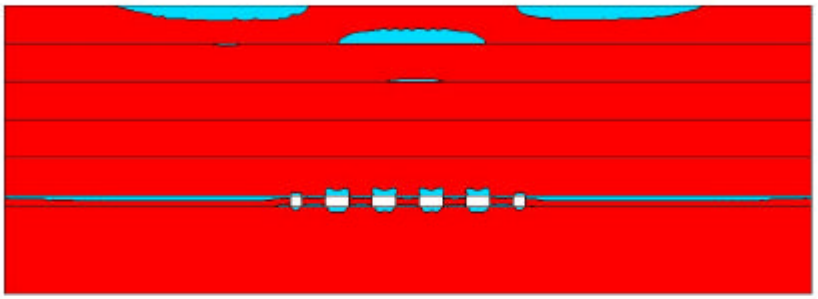

**Frictionlesss 5 layers**

Maximum tensile stress = 0.94 MPa

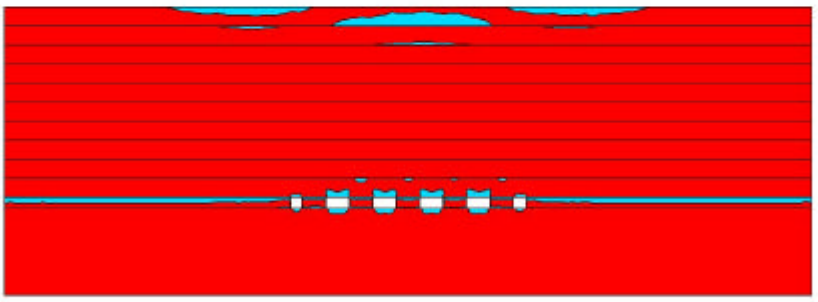

**Frictionless 10 layers**

Maximum tensile stress = 1.58 MPa

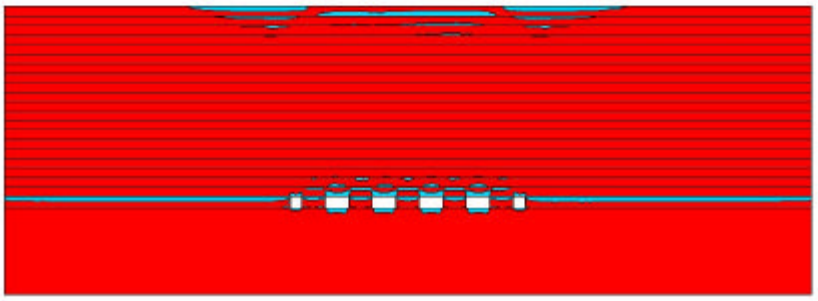

**Frictionless 20 layers**

***Distribution of tensile stresses in ELFEN frictionless models***

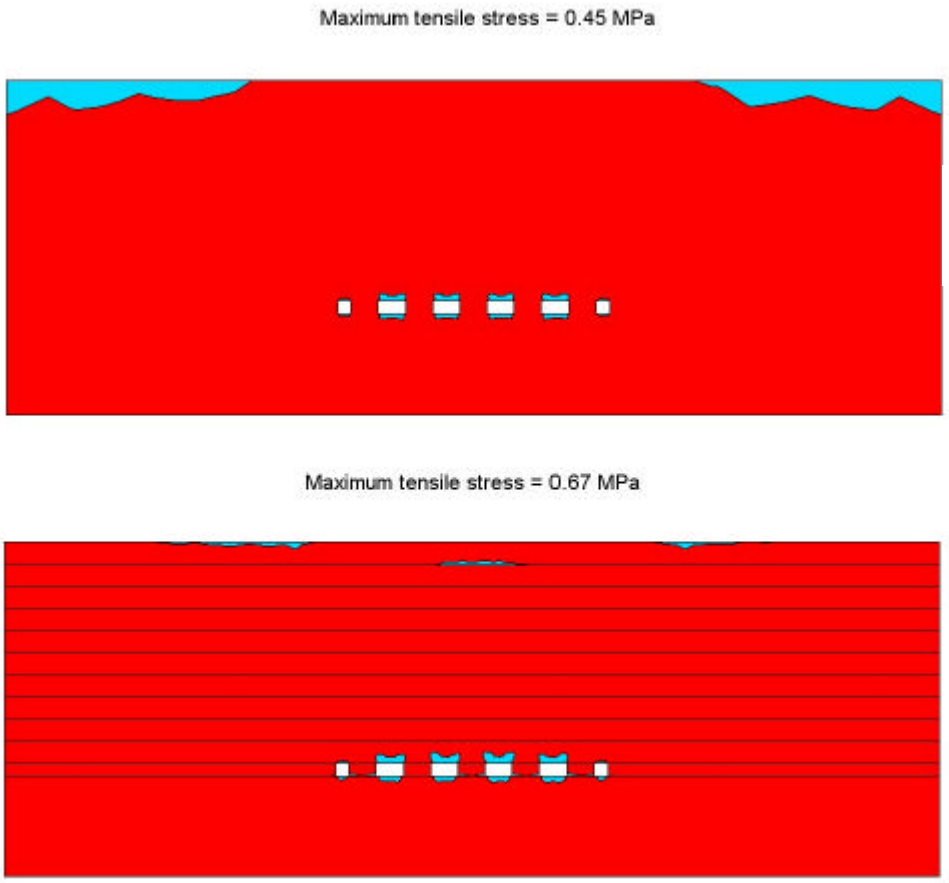


***Distribution of tensile stresses in ELFEN models with friction and without contacts***